RUI YANG

LDPC-coded Modulation for Transmission over AWGN and Flat Rayleigh Fading Channels

Mémoire présenté
à la Faculté des études supérieures de l'Université Laval
dans le cadre du programme de maîtrise en génie électrique
pour l'obtention du grade de Maître ès Sciences (M. Sc.)

FACULTÉ DES SCIENCES ET DE GÉNIE
UNIVERSITÉ LAVAL
QUÉBEC

2010

Abstract

Coded modulation is a bandwidth-efficient scheme that integrates channel coding and modulation into one single entity to improve performance with the same spectral efficiency compared to uncoded modulation. Low-density parity-check (LDPC) codes are the most powerful error correction codes (ECCs) and approach the Shannon limit, while having a relatively low decoding complexity. Therefore, the idea of combining LDPC codes and bandwidth-efficient modulation has been widely considered.

In this thesis, we study a power and bandwidth-efficient coded modulation scheme based on LDPC codes, with the advantages of excellent BER performance and low implementation complexity, which is embodied by using only one fast encoder, one low complexity decoder, and no bit interleaving. The performance of this proposed system transmitted over both additive white Gaussian noise (AWGN) and flat Rayleigh fading channels are evaluated via simulations. Numerical results show that this coded modulation scheme with M-ary quadrature amplitude modulation (M-QAM) can achieve excellent performance while having various spectral efficiencies.

Another contribution of this thesis is a simple adaptive LDPC-coded modulation scheme for transmission over flat slowly-varying Rayleigh fading channels. In this scheme, six combinations of encoding and modulation pairs are employed for frame by frame adaptation and the average spectral efficiency varies between 0.5 and 5.0 bits/symbol/Hz during data transmission. Simulation results show that adaptive LDPC-coded modulation has the benefit of offering better spectral efficiency while maintaining an acceptable error performance.

Résumé

La modulation codée est une technique de transmission efficace en largeur de bande qui intègre le codage de canal et la modulation en une seule entité et ce, afin d'améliorer les performances tout en conservant la même efficacité spectrale comparé à la modulation non codée. Les codes de parité à faible densité (low-density parity-check codes, LDPC) sont les codes correcteurs d'erreurs les plus puissants et approchent la limite de Shannon, tout en ayant une complexité de décodage relativement faible. L'idée de combiner les codes LDPC et la modulation efficace en largeur de bande a donc été considérée par de nombreux chercheurs.

Dans ce mémoire, nous étudions une méthode de modulation codée à la fois puissante et efficace en largeur de bande, ayant d'excellentes performances de taux d'erreur binaire et une complexité d'implantation faible. Ceci est réalisé en utilisant un encodeur rapide, un décoder de faible complexité et aucun entrelaceur. Les performances du système proposé pour des transmissions sur un canal additif gaussien blanc et un canal à évanouissements plats de Rayleigh sont évaluées au moyen de simulations. Les résultats numériques montrent que la méthode de modulation codée utilisant la modulation d'amplitude en quadrature à M niveaux (M-QAM) peut atteindre d'excellentes performances pour toute une gamme d'efficacité spectrale.

Une autre contribution de ce mémoire est une méthode simple pour réaliser une modulation codée adaptative avec les codes LDPC pour la transmission sur des canaux à évanouissements plats et lents de Rayleigh. Dans cette méthode, six combinaisons de paires encodeur modulateur sont employées pour une adaptation trame par trame. L'efficacité spectrale moyenne varie entre 0.5 et 5 bits/s/Hz lors de la transmission. Les résultats de simulation montrent que la modulation codée adaptative avec les codes LDPC offre une meilleure efficacité spectrale tout en maintenant une performance d'erreur acceptable.

Acknowledgements

This thesis has been a tough but enriching and improving experience for me. I would like to acknowledge a lot of people who helped me during the course of this work.

First and foremost, my deepest appreciation and gratitude must go to my supervisor, Dr. Paul Fortier for his time devoted to my thesis completion and constant guidance, patience and support throughout my research. His way of thinking and extensive knowledge in the field of wireless communications were valuable resources for my graduate studies.

I would also like to thank Dr. Jean-Yves Chouinard and Dr. Leslie Ann Rusch for their excellent courses of Théorie et pratique des codes correcteurs, Communications numériques, Théorie de l'information and Processus aléatoires: méthodes d'étude et applications.

I wish to thank the examiners of my thesis, Dr. Jean-Yves Chouinard and Dr. Sébastien Roy for their valuable time spent on evaluating my thesis.

Besides, I am grateful to my colleagues at Laboratoire de Radiocommunications et de Traitement du Signal (LRTS) for their friendship and numerous fruitful discussions, especially Dr. Zhiyong He; thanks for his helpful suggestions regarding this thesis.

Lastly, my greatest gratitude is dedicated to my parents, Xiuhai Yang and Yan Wang, and my wife, Na Dong for their love and understanding. They provided me not only great moral support but also financial support for my Master's studies. Without them, this thesis could not have been done.

Contents

List of Tables

List of Figures

Acronyms

3G: Third Generation Mobile Communication Systems

4G: Fourth Generation Mobile Communication Systems

ACM: Adaptive Coded Modulation

AWGN: Additive White Gaussian Noise

BER: Bit Error Rate

BICM: Bit Interleaved Coded Modulation

BP: Belief Propagation

BF: Bit Flipping

BPSK: Binary Phase Shift Keying

DVB-S2: Second Generation Satellites for Digital Video Broadcasting

ECC: Error Correction Code

FEC: Forward Error Coding

IEEE: Institute of Electrical and Electronic Engineers

LDPC: Low-density Parity-check Codes

LLR: Logarithmic Likelihood Ratio

MAN: Metropolitan Area Network

MIMO: Multiple Input Multiple Output

ML: Maximum Likelihood

MLC: Multilevel Coded Modulation

OFDM: Orthogonal Frequency Division Multiplexing

OFDMA: Orthogonal Frequency Division Multiple Access

PSK: Phase Shift Keying

QAM: Quadrature Amplitude Modulation

QoS: Quality of Service

QPSK: Quadrature Phase Shift Keying

SNR: Signal to Noise Ratio

TCM: Trellis Coded Modulation

WiFi: Wireless Fidelity

WiMAX: Worldwide Interoperability for Microwave Access

Chapter 1

Introduction

During the last decades, wireless communications have advanced at an incredible pace. The first example which changes our life-style is the mobile phone. Mobile phones have evolved from the simple phones for voice-calling in 1970s to present smart-phones with computer-like functionality. The International Telecommunication Union estimated that mobile cellular subscriptions worldwide reached approximately 4.6 billion by the end of 2009. The second example is wireless local area networks (WLAN), the so-called WiFi. Equipped with a WLAN device, a laptop or desktop computer can connect easily to the Internet without the use of wires. As of 2010 WLAN devices have been installed in many personal computers, video game consoles, mobile phones, printers, and other peripherals, and virtually all laptop or palm-sized computers. The third example is the Global Positioning System (GPS), a space-based global navigation satellite system which provides reliable location and time information in all weather and at all times and anywhere on or near the Earth. With the navigation of GPS, we can drive easily in any cities. GPS has become a useful tool for map-making, land surveying, commerce, scientific uses, tracking and surveillance, and hobbies such as geo-caching and way-marking.

To achieve reliable and high data transmission in modern communication systems, error correction coding (ECC) techniques are used usually combined with bandwidth-efficient modulation schemes. Especially, with effective iterative decoding algorithms, turbo codes and low-density parity-check (LDPC) codes are two powerful coding techniques.

In this chapter, we briefly review basic digital communication systems and their main conditions for performance. Then, we introduce advances in ECC technologies, especially LDPC codes. Finally, the motivation and the contributions of this thesis are given.

1.1 Digital communication systems

Fig. 1.1 illustrates a general block diagram for a digital communication system. In this diagram, digital data from a source are encoded and modulated for transmission over a channel. At the other side, the data are extracted by demodulation, decoding, and then sent to a sink. The encoder can be divided into two blocks, namely the source encoder and the channel encoder. In this thesis, we only consider the channel encoder and refer to it simply as the encoder.

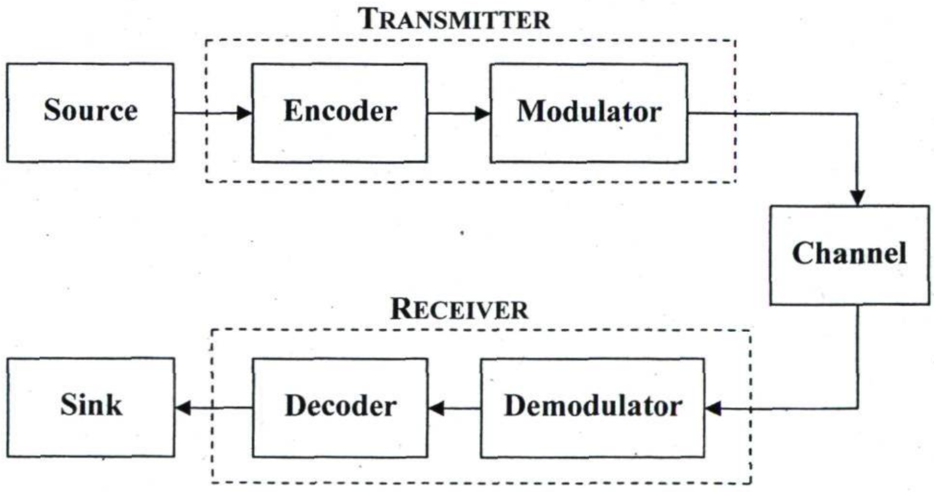

Figure 1.1: Block diagram of a digital communication system.

In some digital communication systems, channel coding and modulation are combined together; this is called coded modulation. In general, there are two main constraints in communication systems, the available spectrum (or bandwidth) and the power required for data transmission. The bandwidth is becoming a rare commodity with the demand of high-speed and high quality of service (QoS) for wireless communications. In this thesis, a coded modulation system based on LDPC codes and *M*-ary phase shift keying (*M*-PSK) or *M*-ary quadrature amplitude modulation (*M*-QAM) modulation is studied for improving BER performances and spectral efficiency.

1.2 Overview of low-density parity-check (LDPC) codes

1.2.1 Evolution of error correction coding (ECC) techniques

In 1948, in his landmark work "A mathematical theory of communication" [1], C. E. Shannon proved that there exists a code such that the error probability can be made arbitrarily small if the rate of transmission is less than channel capacity. Since then, researchers began to develop channel coding systems (error correction coding techniques) to reach this capacity.

One of the first coding techniques was Hamming codes [2]. After that, a class of convolutional codes [3] which have better error performance was developed in 1955, and an efficient decoding technique for these codes was invented by Viterbi [4] in 1967. The Viterbi algorithm was used in many practical applications in the following three decades. Simultaneously, Reed Solomon (RS) codes [5] were proposed and found in some practical applications ranging from compact disc players to deep-space applications [6]. Trellis coded modulation (TCM) [7], proposed by Ungerböeck in 1982, proved that a high performance gain can be obtained by joining a coding and a modulation scheme in a single entity.

The next key point in the field of coding theory was the discovery of Turbo codes [8] by Berrou, Glavieux and Thitimajshima in 1993. Turbo codes were able to approach the Shannon limit within 0.5 dB with iterative decoding techniques.

LDPC codes were rediscovered [9] in 1996. First created in 1962 by Gallager [10], [11], these codes were forgotten because of their impractical encoding and decoding at the time. It was demonstrated that LDPC codes are also able to reach the Shannon limit just as Turbo codes, but with lower complexity [12].

1.2.2 Advances in LDPC codes

Low-density parity-check (LDPC) codes are a class of linear block error correction codes (ECC). They have a simple decoding mechanism and exhibit very good performance in data transmission. LDPC codes have several advantages compared to other channel coding codes. First, LDPC codes can use hard or soft decision decoding.

Second, the error performance of LDPC codes does not always exhibit an error floor due to the good Hamming distance spectra of these codes. This is an important advantage over the other powerful ECCs, in particular Turbo codes. Another advantage of LDPC codes is the iterative decoding scheme based on a graph model, for which one can implement parallel decoders. The iterative decoding scheme is essentially a belief propagation (BP) [13] method on factor graph, which was shown in Gallager's paper in 1963. It is possible to decode large LDPC codes using the BP algorithm, which leads to relatively simple decoding strategies. This is the key contributing factor to the success of LDPC codes. Furthermore, LDPC codes are more flexible in their construction in terms of the code rate and other parameters.

Currently, LDPC codes are considered the best ECCs to allow data transmission rates close to the theoretical Shannon limit. The best known class of these codes over AWGN channels is a class of irregular LDPC codes [12] whose empirical performance achieves a bit error rate (BER) of 10^{-6} within 0.04 dB of the Shannon limit with a code length of 10^{7}.

Theoretically, the code threshold is within 0.0045 dB of the Shannon limit; this can be reached when the code length tends to infinity.

1.2.3 LDPC codes in current wireless communication systems

Duo to their advantages mentioned above, LDPC codes have been proposed for several state-of-the-art wireless standards, such as worldwide interoperability for microwave access (WiMAX) [14], wireless fidelity (WiFi) [15] and second generation satellites for digital video broadcasting (DVB-S2) [16]. Also, they constitute an important option for forward error coding (FEC) in fourth generation (4G) wireless communication systems. We briefly introduce two important wireless standards, WiMAX and 4G, in the following.

WiMAX

WiMAX is an industry consortium with the goal of promoting technologies based on the IEEE 802.16 standard for the transmission of wireless data over long distances. The standard can operate with single carrier modulation, orthogonal frequency division multiplexing (OFDM) or orthogonal frequency division multiple access (OFDMA). It is designed to accommodate both fixed and mobile data networks. Mobile WiMAX (IEEE 802.16e) was created in December 2005 and is an amendment to the fixed WiMAX standard (IEEE 802.16d-2004). It is aimed at delivering “last mile” broadband wireless access as an alternative to digital subscriber loop (DSL) solutions.

Compared to Wi-Fi and 3G, the WiMAX standard has some improved characteristics. It defines a selectable bandwidth of 1.25 to 20 MHz and is developed to establish non-line-of-sight (NLoS) connectivity between a base station and a subscriber in the licensed and unlicensed bands in the 2 to 11 GHz frequency range. This provides for less expensive service rates for a larger number of customers but does hurt transfer rates. WiMAX has capabilities of transmitting with a range of up to 31 miles. The transmit data rate of WiMAX is also an improvement, being up to 75 megabits per second (Mbps). Capacity can be improved by using smart adaptive coded modulation (ACM) and multiple input multiple output (MIMO) technology.

4G

Up to now, there is no formal definition for what 4G is. However, there are certain objectives that are projected for 4G, including that 4G will be a fully IP-based integrated system and be able to provide much higher data rates between 100 Mbps and 1 Gbps with optimum quality and high security [17]. It is likely to use a combination of 3G, WiMAX and WiFi technologies.

1.3 Thesis motivation

The main goal in designing a communication system is to achieve reliable data transmission with as small a transmission power as possible, in other words, a power efficient system with the lowest error probability (bit error rate or frame error rate). Moreover, a higher data rate with a constraint on available bandwidth is another target.

LDPC codes can be selected as an excellent coding scheme to achieve the highest reliability transmission. On the other hand, in terms of efficient use of bandwidth while having a high data rate, we can use bandwidth-efficient modulation techniques, since a larger number of bits are transmitted over one signal duration.

Therefore, motivated by the development of a power and bandwidth-efficient wireless communication system, the combination of LDPC coding and bandwidth-efficient modulation is studied in this thesis. Furthermore, due to the time-variability of fading channels in wireless communications, an adaptive coded modulation (ACM) system is evaluated.

1.4 Thesis contributions and outline

1.4.1 Thesis contributions

This thesis is devoted to the study of bandwidth-efficient communication systems based on code rate and length-flexible WiMAX LDPC codes. The thesis contributions are the following:

- The analysis and evaluation of the properties and performances of the LDPC codes specified in the WiMAX standard.
- A bandwidth-efficient LDPC-coded modulation scheme is proposed for transmission over both AWGN and flat uncorrelated Rayleigh fading channels. Specifically, the LDPC-coded M-ary quadrature amplitude modulation (M-QAM) scheme with various spectral efficiencies is evaluated for transmission over an AWGN channel.
- The performance of LDPC-coded modulation schemes with square QAMs, i.e., QPSK, 16-QAM and 64-QAM transmitted over the uncorrelated Rayleigh fading channel is investigated.
- A simple adaptive LDPC-coded modulation system for transmission over flat slowly-varying Rayleigh fading channels is designed using the method presented in [18]. In this scheme, six combinations of encoding and modulation pairs are employed for frame by frame adaptation with various spectral efficiencies ranging between 0.5 and 5.0 bits/s/Hz. The adaptive coded modulation scheme is a promising idea for the next generation wireless systems, i.e., WiMAX and 4G wireless systems under a relatively slowly-varying fading environment.

1.4.2 Thesis outline

This thesis is organized in six chapters. In the current chapter, a brief introduction to digital communication systems and LDPC codes is presented, as well as the contributions and the outline of the thesis.

Chapter 2 presents the basics for the study and use of LDPC codes, including their definition, classical construction schemes, encoding methods and an iterative decoding algorithm. Moreover, to enhance the understanding of the process for LDPC codes, numerical results comparing different decoding algorithms are given.

The LDPC codes defined in the current WiMAX standard are studied in Chapter 3. These codes are also the main codes we use for the proposed coded modulation systems. In particular, we discuss the construction and encoding of these codes. Furthermore, the performance of WiMAX LDPC codes for transmission over additive white Gaussian noise (AWGN) and uncorrelated Rayleigh fading channels is evaluated and discussed via simulations in the last section of Chapter 3. A summary of the advantages and main applications of these codes for the next generation of communication systems is presented.

Chapter 4 is the core of this thesis, in which two kinds of LDPC-coded modulation communication systems are studied. Our aim is to use LDPC codes in conjunction with multi-level modulation schemes to achieve both power and bandwidth efficiency for wireless communication systems. We first review the bandwidth-efficient modulation schemes and several typical coded modulation systems. Then, we present the first system model for transmission over both AWGN and uncorrelated Rayleigh fading channels. Finally, an adaptive coded modulation (ACM) scheme with LDPC coding for flat slowly-varying Rayleigh fading is proposed.

In Chapter 5, numerical simulation results using MATLAB according to our proposed coded modulation systems are depicted and discussed in details.

Finally, conclusions are given in Chapter 6, as well as suggestions for future studies.

Chapter 2

Low-density parity-check (LDPC) codes

Low-density parity-check (LDPC) codes are a class of linear block error correction codes (ECC) which provide near-capacity performance. They were invented by Robert Gallager in 1962 [10], [11]. However, these codes were neglected for more than 30 years, since the hardware at that time could not attain the requirements needed by the encoding process. With the increased capacity of computers and the development of relevant theories such as the belief propagation algorithm and Turbo codes, LDPC codes were rediscovered by Mackay and Neal in 1996 [9]. In the last decade, researchers have made great progress in the study of LDPC codes.

This chapter provides the basics for the study and practice of LDPC codes. We start with the concept of linear block codes and LDPC codes, as well as their representation, classification and degree distribution. Then, we briefly review construction techniques and an efficient encoding method for LDPC codes. Finally, the iterative decoding of LDPC codes which provides near-optimal performance and low decoding complexity is presented via simulation results.

2.1 Basics of LDPC codes

2.1.1 Linear block codes

Assume that the message to be encoded is a k-bit block constituting a generic message $\boldsymbol{m} = (m_1, m_2, \cdots, m_k)$, that is one of 2^k possible messages. The encoder takes this message and generates a codeword $\boldsymbol{c} = (c_1, c_2, \cdots, c_n)$, where $n > k$; that is, redundancy is added. Besides block coding, convolutional coding is also a mechanism for adding redundancy in error correcting coding (ECC) techniques.

Definition of linear block codes: A block code $\boldsymbol{c}$ is a linear code if the codewords form a vector subspace of the vector space $\boldsymbol{V}^n$; there will be k linearly independent vectors that in turn are codewords, such that each possible codeword is a linear combination of them [19].

This definition means that the set of 2^k codewords constitutes a vector subspace of the set of words of n bits. A linear code is characterized by the fact that the sum of any two codewords is also a codeword.

Generator matrix

Let $\boldsymbol{c}(n, k)$ be a linear block code and let $(\boldsymbol{g}_1, \boldsymbol{g}_2, \dots, \boldsymbol{g}_k)$ be k linearly independent vectors. Each codeword is a linear combination of them:

$$\boldsymbol{c} = m_1 \cdot \boldsymbol{g}_1 + m_2 \cdot \boldsymbol{g}_2 + \cdots + m_k \cdot \boldsymbol{g}_k \tag{2.1}$$

Unless stated otherwise, all vector and matrix operations are modulo 2. These linearly independent vectors can be arranged in a matrix called the generator matrix $\mathbf{G}$:

$$\mathbf{G} = \begin{bmatrix} \boldsymbol{g}_1 \\ \boldsymbol{g}_2 \\ \vdots \\ \boldsymbol{g}_k \end{bmatrix} = \begin{bmatrix} g_{1,1} & g_{1,2} & \cdots & g_{1,n} \\ g_{2,1} & g_{2,2} & & g_{2,n} \\ & \vdots & \ddots & \vdots \\ g_{k,1} & g_{k,2} & \cdots & g_{k,n} \end{bmatrix} \tag{2.2}$$

For a given message vector $\boldsymbol{m} = (m_1, m_2, \cdots, m_k)$, the corresponding codeword is obtained by matrix multiplication:

$$\boldsymbol{c} = \boldsymbol{m} \cdot \mathbf{G} = (m_1, m_2, \cdots, m_k) \cdot \begin{bmatrix} \boldsymbol{g}_1 \\ \boldsymbol{g}_2 \\ \vdots \\ \boldsymbol{g}_k \end{bmatrix} = m_1 \cdot \boldsymbol{g}_1 + m_2 \cdot \boldsymbol{g}_2 + \cdots + m_k \cdot \boldsymbol{g}_k \qquad (2.3)$$

Parity-check matrix

The parity-check matrix $\mathbf{H}$ is an $(n-k) \times n$ matrix with $(n-k)$ independent rows. It is the dual space of the code $\boldsymbol{c}$, i.e. $\mathbf{GH}^T = 0$.

$$\mathbf{H} = \begin{bmatrix} \boldsymbol{h}_1 \\ \boldsymbol{h}_2 \\ \vdots \\ \boldsymbol{h}_{n-k} \end{bmatrix} = \begin{bmatrix} h_{1,1} & h_{1,2} & \cdots & h_{1,n} \\ h_{2,1} & h_{2,2} & & h_{2,n} \\ \vdots & & \ddots & \vdots \\ h_{n-k,1} & h_{n-k,2} & \cdots & h_{n-k,n} \end{bmatrix} \qquad (2.4)$$

It can also be verified that the parity-check equations can be obtained from the parity-check matrix $\mathbf{H}$, i.e. $\boldsymbol{c}\mathbf{H}^T = 0$. Hence, this matrix also specifies completely a given block code.

2.1.1.1 Block codes in systematic form

The structure of a codeword in systematic form is shown in Fig. 2.1. In this form, a codeword consists of k message bits followed by $(n-k)$ parity-check bits.

***k* message bits**	**$(n-k)$ parity-check bits**

Figure 2.1: Systematic form of a codeword of a block code.

Thus, a systematic linear block code $\boldsymbol{c}(n,k)$ can be specified by the following generator matrix:

$$\mathbf{G} = \left[\begin{array}{cccc|cccc} 1 & 0 & \cdots & 0 & p_{1,k+1} & p_{1,k+2} & \cdots & p_{1,n} \\ 0 & 1 & \cdots & 0 & p_{2,k+1} & p_{2,k+2} & \cdots & p_{2,n} \\ \vdots & & \ddots & \vdots & \vdots & & \ddots & \vdots \\ 0 & 0 & \cdots & 1 & p_{k,k+1} & p_{k,k+2} & \cdots & p_{k,n} \end{array}\right] \tag{2.5}$$

$$\begin{array}{cc} \textbf{Identity matrix} & \textbf{Parity-check matrix} \\ \mathbf{I}_{k\times k} & \mathbf{P}_{k\times(n-k)} \end{array}$$

which, in a compact notation, is $\mathbf{G} = [\,\mathbf{I}_{k\times k} \quad \mathbf{P}_{k\times(n-k)}]$. The corresponding parity-check matrix is given by $\mathbf{H} = \left[\,\mathbf{P}^{T}_{(n-k)\times k} \quad \mathbf{I}_{(n-k)\times(n-k)}\right]$.

2.1.1.2 Decoding of linear block codes

We can observe from Fig. 2.2 that as a consequence of its transmission through a noisy channel, a codeword could be received containing some errors. The received vector can therefore be different from the corresponding transmitted codeword, and it will be denoted as $\boldsymbol{r} = (r_1, r_2, \cdots, r_n)$. An error event can be modeled as an error vector or error pattern $\boldsymbol{e} = (e_1, e_2, \cdots, e_n)$ where $\boldsymbol{e} = \boldsymbol{r} + \boldsymbol{c}$.

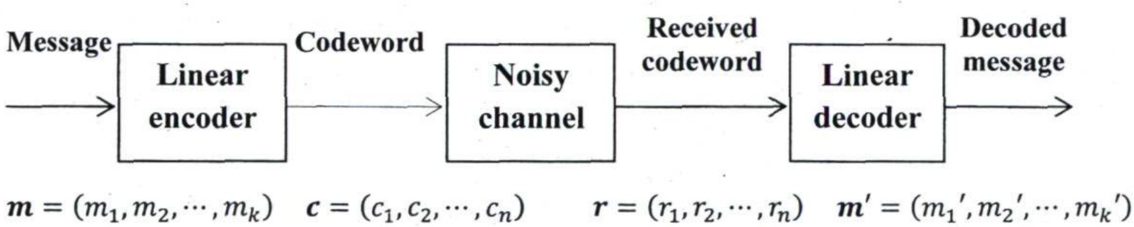

Figure 2.2: Diagram of a block coding system.

To detect the errors, we use the fact that any valid codeword should obey the condition $\boldsymbol{c}\mathbf{H}^T = 0$. An error-detection mechanism is based on the above expression, which adopts the following form: $\boldsymbol{s} = \boldsymbol{r}\mathbf{H}^T$, where $\boldsymbol{s} = (s_1, s_2, \cdots, s_n)$ is called the syndrome vector. The detecting operation is performed over the received vector:

- If $\boldsymbol{s}$ is the all-zero vector, the received vector is a valid codeword.

- Otherwise, there are errors in the received vector. The syndrome array is checked to find the corresponding error pattern $\boldsymbol{e}_j$ for $j = 1, 2, \dots, n$, and the decoded message is obtained by $\boldsymbol{m}' = \boldsymbol{r} + \boldsymbol{e}_j$.

2.1.2 Definition of LDPC codes

LDPC codes are linear block codes that can be denoted as (n, k) or (n, w_c, w_r), where n is the length of the codeword, k is the length of the message bits, w_c is the column weight (i.e. the number of nonzero elements in a column of the parity-check matrix), and w_r is the row weight (i.e. the number of nonzero elements in a row of the parity-check matrix).

There are two obvious characteristics for LDPC codes:

- **Parity-check**: LDPC codes are represented by a parity-check matrix **H**, where **H** is a binary matrix that must satisfy $\boldsymbol{c}\mathbf{H}^T = 0$, where **c** is a codeword.
- **Low-density**: **H** is a sparse matrix (i.e. the number of '1's is much lower than the number of '0's). It is the sparseness of **H** that guarantees the low computing complexity.

2.1.3 Tanner graphs

Besides the general expression as an algebraic matrix, LDPC codes can also be represented by a bipartite Tanner graph, which was proposed by Tanner in 1981 [20].

The Tanner graph consists of two sets of vertices: n vertices for the codeword bits (called variable nodes), and k vertices for the parity-check equations (called check nodes). An edge joins a variable node and a check node if that bit is included in the corresponding parity-check equation and so the number of edges in the Tanner graph is equal to the number of ones in the parity-check matrix.

Cycle

A cycle (loop) in a Tanner graph is a sequence of connected vertices which starts and ends at the same vertex in the graph, and which contains other vertices no more than once. The length of a cycle is the number of edges it contains. Since Tanner graphs are bipartite, every cycle will have even length [21].

Girth

The girth is the minimum length of the cycles in their Tanner graph.

We will illustrate the cycle and girth by a simple example. Let **H** be the parity-check matrix of an irregular (10, 5) LDPC code:

$$\mathbf{H} = \begin{bmatrix} 1 & 1 & 0 & 0 & 0 & 1 & 0 & 1 & 0 & 1 \\ 0 & 1 & 1 & 0 & 0 & 1 & 0 & 0 & 1 & 0 \\ 0 & 0 & 1 & 1 & 0 & 0 & 1 & 1 & 0 & 1 \\ 0 & 0 & 0 & 1 & 1 & 1 & 0 & 0 & 1 & 0 \\ 1 & 0 & 0 & 0 & 1 & 0 & 1 & 0 & 1 & 0 \end{bmatrix} \tag{2.6}$$

The corresponding Tanner graph is illustrated in Fig. 2.3. For the LDPC code defined above, the path $(p_1 \rightarrow v_8 \longrightarrow p_3 \rightarrow v_{10} \rightarrow p_1)$ with the black bold lines is a cycle of length 4. This cycle is also the girth of this graph since it is the smallest cycle length.

This structure is crucial for the performance of LDPC codes. LDPC codes use an iterative decoding algorithm based on the statistical independence of message transitions between the different nodes. When there exists a cycle, the message generated from one node will be passed back to itself, thus negating the assumption of independence, so that the decoding accuracy is impacted. Therefore, it is desirable to obtain matrices with high girth values.

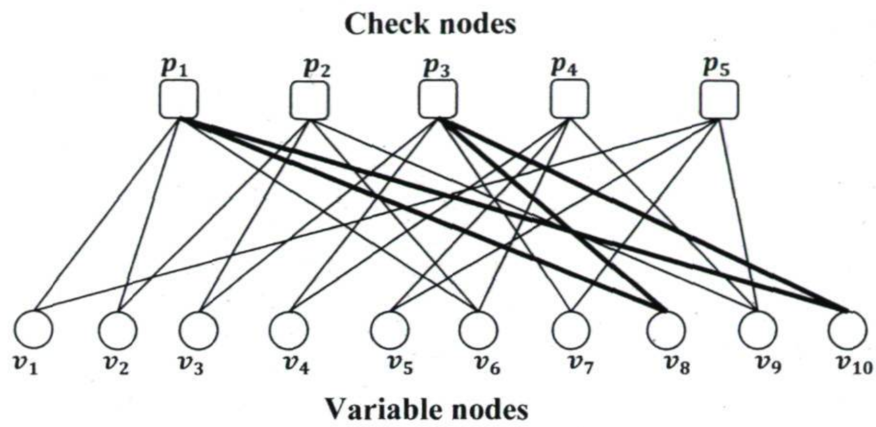

Figure 2.3: Tanner graph corresponding to the parity check matrix **H** in (2.6).

2.1.4 Regular and irregular LDPC codes

2.1.4.1 Regular codes

The conditions to be satisfied in the construction of the parity-check matrix **H** of a binary regular LDPC code are:

- The corresponding parity-check matrix **H** should have a fixed column weight w_c.
- The corresponding parity-check matrix **H** should have a fixed row weight w_r.
- The number of "1"s between any two columns is no greater than 1.
- Both w_c and w_r should be small numbers compared to the code length n and the number of rows in **H**.

Normally, the code rate of LDPC codes is $R = 1 - w_c/w_r$.

2.1.4.2 Irregular codes

An irregular LDPC code has a parity-check matrix **H** that has a variable w_c or w_r. In general, the bit error rate (BER) performance of irregular LDPC codes is better than that of regular LDPC codes [22].

2.1.4.3 Degree distribution

In general, we want the length L of each cycle to satisfy $L \geq 4$, and L is a multiple of 2 [21]. The basic structure of an LDPC code is defined by its degree distribution [23], which are two polynomials that give the fraction of edges in the graph that are connected to the check-nodes and the variable-nodes, respectively. We call them degree distribution polynomials, denoted by $\gamma(x)$ and $\rho(x)$, respectively.

$$\gamma(x) = \sum_{i=1}^{d_v} \gamma_i x^{i-1} \tag{2.7}$$

where γ_i corresponds to the fraction of edges connected to variable nodes and d_v denotes the maximum variable node degree. Similarly,

$$\rho(x) = \sum_{i=1}^{d_c} \rho_i x^{i-1} \tag{2.8}$$

where ρ_i corresponds to the fraction of edges connected to check nodes and d_c denotes the maximum check node degree.

For the example in Fig. 2.3, the corresponding degree distribution polynomials are $\gamma(x) = 0.8x + 0.2x^2$ and $\rho(x) = 0.6x^3 + 0.4x^4$.

2.2 Construction of LDPC codes

The most obvious method for the construction of LDPC codes is via constructing a parity-check matrix with the properties described in the previous section. A larger number of construction designs have been researched and introduced in the literature, for example, see [10], [11] and [24]. LDPC code construction is based on different design criteria to implement efficient encoding and decoding, in order to obtain near-capacity performance.

Several methods for constructing good LDPC codes can be summarized into two main classes: random and structural constructions. Normally, for long code lengths, random constructions [22], [23] of irregular LDPC codes have been shown to closely approach the theoretical capacity limits for the additive white Gaussian noise (AWGN) channel. Generally, these codes outperform algebraically constructed LDPC codes. But because of their long code length and the irregularity of the parity-check matrix, their implementation becomes quite complex.

On the other hand, for short or medium-length LDPC codes, the situation is different. Irregular constructions are generally not better than regular ones, and graph-based or structured constructions can outperform random ones [26].

Structured constructions of LDPC codes can be decomposed into two main categories. The first category is based on finite geometries [24], while the second category is based on circulant permutation matrices. In this thesis, we will focus on the second category and study a fast efficient encoding algorithm based on a matrix having an approximate triangular form [27], [28], which has been adopted in the WiMAX standard.

2.2.1 Gallager codes

The original LDPC codes presented by Gallager [10], [11] are regular LDPC codes and are defined by a banded structure in $\mathbf{H}$. Let

$$\mathbf{H} = \begin{bmatrix} \mathbf{H}_1 \\ \mathbf{H}_2 \\ \vdots \\ \mathbf{H}_{w_c} \end{bmatrix} \tag{2.9}$$

where the submatrix $\mathbf{H}_i$ has the following structure: for any integers μ and w_r that are greater than 1, each submatrix $\mathbf{H}_i$ is $\mu \times \mu w_r$ with row weight w_r and column weight 1. For submatrix $\mathbf{H}_1$, the i^{th} row ($i = 1, 2, \dots, \mu$) contains all of its w_r 1's in columns $(i-1)w_r + 1$ to iw_r. The other sub-matrices are simply column permutations of $\mathbf{H}_1$. It is easy to show that $\mathbf{H}$ is regular with fixed row and column weights w_r and w_c, respectively. The absence of 4 cycles in **H** is not guaranteed, but they can be avoided via computer design of **H** [10], [29].

2.2.2 Quasi-cyclic (QC) LDPC codes

Compared with randomly constructed LDPC codes, the quasi-cyclic (QC) LDPC codes are a category of structured constructions with girth of at least 6 which can be encoded in linear time with shift registers. QC-LDPC codes are well known for their low encoding complexity and low memory requirement, while preserving a high error correcting performance [30].

The QC-LDPC codes are characterized by their parity-check matrix consisting of small square blocks which are zero matrices or circulant permutation matrices [28], [30]. Assume that a QC-LDPC code has column-size n and row-size m that are multiples of an integer q. Let $\mathbf{P}^i$ be the $q \times q$ circulant permutation which shifts the identity matrix $\mathbf{I}$ to the right i times for any integer i, $0 \leq i < q$. For simplicity of notation, $\mathbf{P}^\infty$ denotes the all-zero matrix.

Let the parity-check matrix **H** be the $mq \times nq$ matrix defined by

$$\mathbf{H} = \begin{bmatrix} \mathbf{P}^{a_{11}} & \mathbf{P}^{a_{12}} & \cdots & \mathbf{P}^{a_{1(n-1)}} & \mathbf{P}^{a_{1n}} \\ \mathbf{P}^{a_{21}} & \mathbf{P}^{a_{22}} & \cdots & \mathbf{P}^{a_{2(n-1)}} & \mathbf{P}^{a_{2n}} \\ \vdots & \vdots & \cdots & \vdots & \vdots \\ \mathbf{P}^{a_{m1}} & \mathbf{P}^{a_{m2}} & \cdots & \mathbf{P}^{a_{m(n-1)}} & \mathbf{P}^{a_{mn}} \end{bmatrix} \tag{2.10}$$

where $a_{ij} \in \{0, 1, \cdots q-1, \infty\}$. **H** has full rank, its codeword size is $N = nq$ and information bit size is $M = (n-m)q$. Therefore, its code rate is given by

$$R = \frac{qn - qm}{qm} = \frac{n-m}{n} = 1 - \frac{m}{n} \tag{2.11}$$

Thus, we can obtain larger size block LDPC codes by increasing the size of the circulant permutation matrices $\boldsymbol{P}^i$ which are element matrices of **H**. Hence, this method enables an efficient implementation of the encoder. The required memory for storing the parity-check matrix of the QC-LDPC codes can be reduced by a factor $1/q$, as compared to randomly constructed LDPC codes.

2.3 Encoding of LDPC codes

Regardless of their many advantages, the encoding of LDPC codes can be an obstacle for their commercial applications, since they have high encoding complexity and encoding delay. The encoding for LDPC codes basically comprises two tasks:

- Construct a sparse parity-check matrix;
- Generate codewords using this matrix.

2.3.1 Conventional encoding based on Gauss-Jordan elimination

The conventional encoding algorithm is based on Gauss-Jordan elimination and re-ordering of columns to calculate the codeword.

Similar to the general method of encoding linear block codes, Neal has proposed a simple scheme [31]. For a given codeword $\boldsymbol{c}$ and an $m \times n$ irregular parity-check matrix $\mathbf{H}$, we partition the codeword $\boldsymbol{c}$ into message bits, $\boldsymbol{x}$, and check bits, $\boldsymbol{p}$.

$$\boldsymbol{c} = [\boldsymbol{x}|\boldsymbol{p}] \tag{2.12}$$

After Gauss-Jordan elimination, the parity-check matrix $\mathbf{H}$ is converted to systematic form and then divided into an $m \times (n-m)$ matrix $\mathbf{A}$ on the left and an $m \times m$ matrix $\mathbf{B}$ on the right.

$$\mathbf{H} = [\mathbf{A}|\mathbf{B}] \tag{2.13}$$

From the condition that for all codewords $\boldsymbol{c}\mathbf{H}^T = 0$, we have

$$\boldsymbol{A}\boldsymbol{x}^T + \boldsymbol{B}\boldsymbol{p}^T = \mathbf{0} \tag{2.14}$$

Hence,

$$p^T = \mathbf{B}^{-1}\mathbf{A}x^T \tag{2.15}$$

So (2.15) can be used to compute the check bits as long as **B** is non-singular and not just when **A** is an identity matrix (**H** in a systematic form). In general, the parity-check matrix **H** will not be sparse after the pre-processing. Thus the complexity of conventional methods for the encoding of LDPC codes is high.

2.3.2 Efficient encoding based on approximate lower triangulation

The complexity of conventional encoding algorithms is essentially proportional to the square of the code length and becomes a significant problem when dealing with long code lengths. To solve this problem, Richardson and Urbanke [27] proposed an efficient encoding algorithm for LDPC codes. We will give a detailed description for this encoding algorithm in the following.

The idea is to do a transformation of the parity-check matrix using only row and column permutations so as to keep **H** sparse. Any arbitrary sparse matrix can be converted into the desired parity check matrix **H** with an approximate lower triangular form as shown in Fig. 2.4.

$$\mathbf{H} = \begin{bmatrix} \mathbf{A} & \mathbf{B} & \mathbf{T} \\ \mathbf{C} & \mathbf{D} & \mathbf{E} \end{bmatrix} =$$

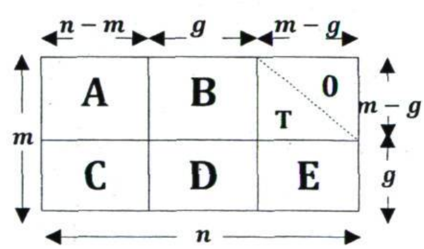

$$c = [\ x \quad p_1 \quad p_2\ ]$$

Figure 2.4: Parity-check matrix **H** in approximate lower triangular form.

Richardson-Urbanke encoding algorithm [27]

1) Perform row and column permutation to bring $\mathbf{H}$ into an approximate lower triangular form

$$\mathbf{H} = \begin{bmatrix} \mathbf{A} & \mathbf{B} & \mathbf{T} \\ \mathbf{C} & \mathbf{D} & \mathbf{E} \end{bmatrix} \tag{2.16}$$

where $\mathbf{A}$ is $(m-g)\times(n-m)$, $\mathbf{B}$ is $(m-g)\times g$, $\mathbf{T}$ is an $(m-g)\times(m-g)$ lower triangular matrix, $\mathbf{C}$ is $g\times(n-m)$, $\mathbf{D}$ is $g\times g$ and finally $\mathbf{E}$ is $g\times(m-g)$. The g rows of $\mathbf{H}$ are called the gap of the approximate representation, and the smaller g is, the lower is the encoding complexity for LDPC codes.

2) Once the upper triangular format of $\mathbf{T}$ is obtained, we use Gauss elimination to clear $\mathbf{E}$ which is equivalent to the following pre-multiplication:

$$\begin{bmatrix} \mathbf{I} & \mathbf{0} \\ -\mathbf{E}\mathbf{T}^{-1} & \mathbf{I} \end{bmatrix}\begin{bmatrix} \mathbf{A} & \mathbf{B} & \mathbf{T} \\ \mathbf{C} & \mathbf{D} & \mathbf{E} \end{bmatrix} = \begin{bmatrix} \mathbf{A} & \mathbf{B} & \mathbf{T} \\ -\mathbf{E}\mathbf{T}^{-1}\mathbf{A}+\mathbf{C} & -\mathbf{E}\mathbf{T}^{-1}\mathbf{B} & \mathbf{0} \end{bmatrix} = \begin{bmatrix} \mathbf{A} & \mathbf{B} & \mathbf{T} \\ \hat{\mathbf{C}} & \hat{\mathbf{D}} & \mathbf{0} \end{bmatrix} \tag{2.17}$$

where we denote

$$\hat{\mathbf{C}} = -\mathbf{E}\mathbf{T}^{-1}\mathbf{A} + \mathbf{C} \tag{2.18}$$

$$\widehat{\mathbf{D}} = -\mathbf{E}\mathbf{T}^{-1}\mathbf{B} + \mathbf{D} \tag{2.19}$$

3) Encoding

Consider the codeword $\boldsymbol{c}$ consisting of a systematic part $\boldsymbol{x}$ and two parity parts $\boldsymbol{p}_1$ and $\boldsymbol{p}_2$, with lengths g and $(m-g)$, respectively. Because the codeword $\boldsymbol{c} = [\boldsymbol{x} \quad \boldsymbol{p}_1 \quad \boldsymbol{p}_2]$ must satisfy the parity-check equation $\mathbf{H}\boldsymbol{x}^T = \mathbf{0}^T$, we have

$$\mathbf{A}\boldsymbol{x}^T + \mathbf{B}\boldsymbol{p}_1^T + \mathbf{T}\boldsymbol{p}_2^T = 0 \tag{2.20}$$

$$\hat{\mathbf{C}}\boldsymbol{x}^T + \widehat{\mathbf{D}}\boldsymbol{p}_1^T + 0\boldsymbol{p}_2^T = \hat{\mathbf{C}}\boldsymbol{x}^T + \widehat{\mathbf{D}}\boldsymbol{p}_1^T = 0 \tag{2.21}$$

Assume that $\widehat{\mathbf{D}}$ is invertible, $\boldsymbol{p}_1$ can be found from (2.20):

$$\boldsymbol{p}_1^T = -\widehat{\mathbf{D}}^{-1}\hat{\mathbf{C}}\boldsymbol{x}^T = -\widehat{\mathbf{D}}^{-1}(-\mathbf{E}\mathbf{T}^{-1}\mathbf{A} + \mathbf{C})\,\boldsymbol{x}^T \tag{2.22}$$

where the sparseness of **A**, **B** and **T** can be employed to keep the complexity of this operation low; since **T** is upper triangular, $\boldsymbol{p}_2$ can be found using back substitution.

$$\boldsymbol{p}_2^T = -\mathbf{T}^{-1}(\mathbf{A}\boldsymbol{x}^T + \mathbf{B}\boldsymbol{p}_1^T) \tag{2.23}$$

Hence, once the $g \times (n-m)$ matrix $\widehat{\mathbf{D}}^{-1}\widehat{\mathbf{C}}\boldsymbol{x}^T$ has been pre-computed, the determination of $\boldsymbol{p}_1$ can be accomplished with complexity $O(g^2)$ simply by performing a multiplication with this matrix as shown in Table 2.1. The corresponding complexity of $\boldsymbol{p}_2$ is $O(n)$ as shown in Table 2.2 [27].

Table 2.1: Efficient computation of $\boldsymbol{p}_1^T = -\widehat{\mathbf{D}}^{-1}(-\mathbf{E}\mathbf{T}^{-1}\mathbf{A} + \mathbf{C})\,\boldsymbol{x}^T$.

Operations	Comments	Complexity
Ax^T	Multiplication by sparse matrix	$O(n)$
$T^{-1}Ax^T$	$T^{-1}Ax^T = y^T \Leftrightarrow Ax^T = Ty^T$	$O(n)$
$-E\,T^{-1}Ax^T$	Multiplication by sparse matrix	$O(n)$
Cx^T	Multiplication by sparse matrix	$O(n)$
$-E\,T^{-1}Ax^T + Cx^T$	Addition	$O(n)$
$-\widehat{D}^{-1}(-E\,T^{-1}Ax^T + Cx^T)$	Multiplication by dense $g \times g$ matrix	$O(g^2)$

Table 2.2: Efficient computation of $\boldsymbol{p}_2^T = -\mathbf{T}^{-1}(\mathbf{A}\boldsymbol{x}^T + \mathbf{B}\boldsymbol{p}_1^T)$.

Operations	Comments	Complexity
Ax^T	Multiplication by sparse matrix	$O(n)$
Bp_1^T	$T^{-1}Ax^T = y^T \Leftrightarrow Ax^T = Ty^T$	$O(n)$
$Ax^T + Bp_1^T$	Multiplication by sparse matrix	$O(n)$
$-T^{-1}(Ax^T + Bp_1^T)$	$-T^{-1}(Ax^T + Bp_1^T) = y^T$ $\Leftrightarrow -(Ax^T + Bp_1^T) = Ty^T$	$O(n)$

This method is the most popular one for encoding LDPC codes and it has been adopted by the IEEE 802.11n and IEEE 802.16e standards. The advantage of these codes is their construction which is made in a systematic way that decreases encoding complexity and lowers memory requirement. The code and the encoding method defined in the WiMAX standard [14] will be studied in this thesis.

2.4 Iterative decoding of LDPC codes

Decoding is a crucial factor for the performance of channel coding techniques. In the groundbreaking work on LDPC codes by Gallager [10], [11], a decoding algorithm was also provided that is typically near optimal. It can be viewed as an iterative message-passing (MP) algorithm since its operation can be explained by the passing of messages iteratively along the edges of a Tanner graph.

In general, the MP algorithms can be decomposed into two classes: bit-flipping (BF) algorithm and belief-propagation (BP) algorithm. The difference between the BF and the BP algorithms is that the messages are binary bits in the BF algorithm, while the messages are probabilities which represent the belief about each bit in the BP algorithm. Furthermore, the BP algorithm was shown to achieve near-capacity performance [13] with a higher implementation complexity, while the BF algorithm has a lower complexity, but with worse decoding performance.

2.4.1 Notation

To describe the iterative decoding algorithms for LDPC codes, we will use the notation of Table 2.3.

Consider an (n, k) LDPC code with an $(n-k) \times n$ parity-check matrix $\mathbf{H}$. Let $R = k/n$ denote the code rate. Suppose that the LDPC-coded bits are BPSK modulated and then transmitted over an AWGN channel. Let $\boldsymbol{c} = (c_1, c_2, \cdots, c_n)$ denote a codeword. It is then mapped to bipolar format $\boldsymbol{t} = (t_1, t_2, \cdots, t_n)$ by $t_j = 2c_j - 1$ before transmission. At the receiver, we get the received vector $\boldsymbol{r} = (r_1, r_2, \cdots, r_n)$, where $r_j = t_j + w_j$, $j = 1, \cdots, n$. w_j is a zero-mean additive Gaussian noise with variance $\sigma^2 = N_0/2 = (2R \cdot E_b/N_0)^{-1}$, where the average bit energy E_b is 1. Let $\mathbf{z} = (z_1, z_2, \cdots, z_n)$ be the binary hard-decision vector obtained from $\boldsymbol{r}$, i.e. $z_j = \mathrm{sign}(r_j)$, where $\mathrm{sign}(r) = 1$, if $r \geq 0$ and $\mathrm{sign}(r) = 0$, if $r < 0$.

Table 2.3: Notation of iterative message-passing LDPC decoders.

s	$s = \mathbf{z}\mathbf{H}^T$
E_j	The highest flipping metric in the BF decoding algorithm.
p_j^a	A priori probability of transmitted codeword $c_j = a$ where a is 0 or 1.
f_j^a	A posteriori probability (APP) of $q_j^a = Pr(c_j = a \mid r_j)$.
$l(c_j)$	Log-likelihood ratio (LLR), $\log(f_j^0/f_j^1)$.
$M(j)$	The set checks in which bit j participates as $M(j) \equiv \{\, i: h_{ij} = 1 \,\}$.
$N(i)$	The set of bits j that participate in check i by $N(i) \equiv \{\, j: h_{ij} = 1 \,\}$.
$N(i)\backslash j$	The set $N(i)$ with bit j excluded.
$M(j)\backslash i$	The set $M(j)$ with check node i excluded.
q_{ij}^a	The probability that bit j of x is a, given the information obtained via checks other than check i.
r_{ij}^a	The probability of check i being satisfied if bit j of $\boldsymbol{x}$ is considered fixed at a, and other bits have a separable distribution given by the probabilities $q_{ij'}$: $j' \in N(i)\backslash j$.

2.4.2 Belief-propagation (BP) decoding algorithm

The belief-propagation (BP) decoding can be conducted either in the probabilistic [9] or logarithmic domain [10], [11]. The advantage of using logarithmic probabilities is that a product of several messages will be converted to a sum. This will decrease the complexity of the decoding process since a sum is more convenient to implement in hardware. The two decoding algorithms have almost equal bit error rate (BER) performances.

2.4.2.1 Probabilistic BP decoding algorithm

Input: A posteriori probability (APP) f_j^0 and f_j^1 for each bit c_j for an AWGN channel.

$$f_j^1 = P(c_j = 1|r_j) = \frac{1}{1 + \exp\left(-\frac{2r_j}{\sigma^2}\right)} \tag{2.24}$$

$$f_j^0 = 1 - f_j^1 \tag{2.25}$$

Initialization: The variables q_{ij}^0 and q_{ij}^1 are initialized to the values f_j^0 and f_j^1. Set the loop counter and maximum number of iterations i_{max}.

Iterative processing:

1) **Row operation**

   Define $\delta q_{ij} = q_{ij}^0 - q_{ij}^1$ and compute for each i, j:

$$\delta r_{ij} = \prod_{j' \in N(i) \setminus j} \delta r_{ij'}^{a} \tag{2.26}$$

   then set $r_{ij}^0 = \frac{1}{2}(1 + \delta r_{ij})$ and $r_{ij}^1 = \frac{1}{2}(1 - \delta r_{ij})$.

2) **Column operation**

   For each j and i and $a = 0, 1$, update:

$$q_{ij}^a = \alpha_{ij} f_j^a \prod_{j' \in N(i) \setminus j} r_{i'j}^a \tag{2.27}$$

   where α_{ij} is chosen such that $q_{ij}^0 + q_{ij}^1 = 1$.

3) **Decision**

   We update the 'pseudo posterior probabilities' q_j^0 and q_j^1 given by

$$q_j^a = \alpha_j f_j^a \prod_{i \in M(j)} r_{ij}^a \tag{2.28}$$

$$\hat{c}_j = \begin{cases} 1, & q_j^1 > q_j^0 \\ 0, & \text{elsewhere} \end{cases}$$

4) **Parity check**

   If $\hat{\mathbf{c}}\mathbf{H}^T = \mathbf{0}$, output $\hat{\mathbf{c}}$ and stop the algorithm.

5) **Iteration counter**

   Stop if the number of iterations exceeds the limit. Otherwise, go to step **1)**.

2.4.2.2 Logarithmic BP decoding algorithm

The logarithmic BP decoding algorithm [10] is an enhanced version of the probabilistic BP algorithm, introducing logarithmic likelihood ratios (LLR) which reduce most multiplications to additions. We first define:

$$l(c_j) = \log(f_j^0/f_j^1) \tag{2.29}$$

$$l(r_{ij}) = \log(r_{ij}^0/r_{ij}^1) \tag{2.30}$$

$$l(q_{ij}) = \log(q_{ij}^0/q_{ij}^1) \tag{2.31}$$

$$l(q_j) = \log(q_j^0/q_j^1) \tag{2.32}$$

Input: the prior logarithmic likelihood ratio (LLR) $l(c_j)$ for each bit x_j, $j = 1, \cdots, n$.

Initialization: $l(q_{ij}) = l(c_j) = 2r_j/\sigma^2$ for an AWGN channel.

Iterative processing:

1) **Row operation**

   From the rearrangement of step **1)** in the probabilistic BP algorithm, we have

$$1 - 2r_{ij}^1 = \prod_{j' \in N(i) \setminus j} \left(1 - 2q_{ij'}^1\right) \tag{2.33}$$

   Using the fact $\tanh\left[\frac{1}{2}\log(f_j^0/f_j^1)\right] = f_j^0 - f_j^1 = 1 - 2f_j^1$, (2.33) is transformed into

$$\tanh\left(\frac{1}{2}l(r_{ji})\right) = \prod_{j' \in N(i) \backslash j} \tanh\left(\frac{1}{2}l(q_{ij'})\right) \tag{2.34}$$

2) Separate $l(q_{ij})$

To remove the products in (2.34), we define

$$l(q_{ij}) = \alpha_{ij}\beta_{ij} \tag{2.35}$$

$$\alpha_{ij} = \text{sign}[l(q_{ij})] \tag{2.36}$$

$$\beta_{ij} = |l(q_{ij})| \tag{2.37}$$

Thus

$$\tanh\left(\frac{1}{2}l(r_{ji})\right) = \prod_{j' \in N(i) \backslash j} \alpha_{ij'} \cdot \prod_{j' \in N(i) \backslash j} \tanh\left(\frac{1}{2}\beta_{ij'}\right) \tag{2.38}$$

Then define $\phi(x) = -\tanh[\log(x/2)] = \log\left(\frac{e^x+1}{e^x-1}\right)$. We have

$$l(r_{ij}) = \prod_{j' \in N(i) \backslash j} \alpha_{ij'} \cdot \phi\left(\sum_{j' \in N(i) \backslash j} \phi(\beta_{ij'})\right) \tag{2.39}$$

3) Column operation

For the j^{th} column, update l

$$l(q_{ij}) = l(c_j) + \sum_{j' \in N(i) \backslash j} l(r_{i'j}) \tag{2.40}$$

4) Decision

$$l(q_j) = l(c_j) + \sum_{j \in N(i)} l(r_{ij}) \tag{2.41}$$

$$\hat{c}_j = \begin{cases} 1, & l(q_j) < 0 \\ 0, & \text{elsewhere} \end{cases}$$

5) Parity check

If $\hat{\boldsymbol{c}}\mathbf{H}^T = \mathbf{0}$, output $\hat{\boldsymbol{c}}$ and stop the algorithm.

6) Iteration counter

Stop if the number of iterations exceeds the limit. Otherwise, go to step **1)**.

In the procedure of the Log-BP algorithm, the derivation of (2.39) is as follows:

$$\begin{aligned} l(r_{ij}) &= \prod_{j'} \alpha_{ij'} \cdot 2\tanh^{-1}\left(\prod_{j'} \tanh\left(\tfrac{1}{2}\beta_{ij'}\right)\right) \\ &= \prod_{j'} \alpha_{ij'} \cdot 2\tanh^{-1}\log^{-1}\log\left(\prod_{j' \in N(i)\setminus j} \tanh\left(\tfrac{1}{2}\beta_{ij'}\right)\right) \\ &= \prod_{j'} \alpha_{ij'} \cdot 2\tanh^{-1}\log^{-1}\sum_{j'} \log\left(\tanh\left(\tfrac{1}{2}\beta_{ij'}\right)\right) \\ &= \prod_{j' \in N(i)\setminus j} \alpha_{ij'} \cdot \phi\left(\sum_{j' \in N(i)\setminus j} \phi(\beta_{ij'})\right) \end{aligned} \tag{2.42}$$

2.4.3 Bit-flipping (BF) decoding algorithm

A simple BF decoding algorithm was first devised in the early 1960s by Gallager as a message passing algorithm with hard decision inputs [10], [11] as follows.

Input: hard decision z_j about each received bit r_j

Iterative processing

1) Compute the parity-check sums (syndrome bits): $\boldsymbol{s} = \mathbf{z}\mathbf{H}^T$. If all the parity-check equations are satisfied (i.e., $\boldsymbol{s} = \mathbf{0}$), stop decoding.
2) Find the number of unsatisfied parity-check equations for each code bit position, denoted $\boldsymbol{u} = \boldsymbol{s}\mathbf{H}$, where regular vector-matrices multiplication is used.
3) Identify the set of bits for which u_j is the largest i.e. $\max_j(u_j)$ and then flip the bits in this set.
4) Repeat steps **1)** to **3)** until all the parity-check equations are satisfied or a predefined maximum number of iterations is reached.

Example

With the LDPC code with the parity-check matrix given by (2.6), code length $n = 10$ and $k = 5$, suppose the received vector after hard decision is $\mathbf{z} = [0\ 0\ 0\ 0\ 0\ 0\ 0\ 0\ 1\ 0]$. Thus, the syndrome is $\boldsymbol{s} = \mathbf{z}\mathbf{H}^T = [0\ 1\ 0\ 1\ 1\ ]$; $\boldsymbol{s} \neq \mathbf{0}$ means there is at least one error in the received vector. Thus, we compute the $\boldsymbol{u} = \boldsymbol{s}\mathbf{H} = [1\ 1\ 1\ 1\ 2\ 2\ 1\ 0\ 3\ 0]$ and $\max_j(\boldsymbol{u}) = u_9 = 3$, so we flip z_9 to have $\mathbf{z} = [0\ 0\ 0\ 0\ 0\ 0\ 0\ 0\ 0\ 0]$; the first iteration is completed. Then repeating the above steps, we find that the new syndrome is $\boldsymbol{s} = 0$, and the decoding is successful.

Among the BF decoding algorithms discovered so far, there are some efficient algorithms which can attain better performances than the simple BF decoding described above, such as the weighted bit-flipping (WBF) algorithm [24] or the improved WBF (IWBF) algorithm [32]. In the following section, we will study an efficient BF decoding algorithm based on the WBF algorithm, called the reliability ratio weighted bit-flipping (RRWBF) decoding algorithm [33].

2.4.3.1 Reliability ratio weighted bit-flipping (RRWBF) decoding algorithm

For the AWGN channel, a simple measure of the reliability of a received symbol r_j is its magnitude $|r_j|$ [24]. The larger the magnitude is, the larger the reliability of the hard decision digit z_j is. We first introduce a quantity designated the reliability ratio (RR) defined as follows:

$$v_{ij} = \beta \frac{|r_j|}{|r_i^{max}|} \tag{2.43}$$

where $|r_i^{max}|$ is used to denote the highest soft magnitude of all the variable nodes participating in the i^{th} check. The variable β is a normalisation factor introduced to ensure that we have $\sum_{j \in N(i)} v_{ij} = 1$.

Decoding steps:

1) Find the syndrome vector $\boldsymbol{s}$, i.e. $\boldsymbol{s} = \mathbf{z}\mathbf{H}^T$. If $\boldsymbol{s} = \mathbf{0}$, the decoder will declare successful decoding and the iterations will be terminated. If not, go on to the next step.
2) Identify the most unreliable variable node associated with each individual check node by computing v_{ij} as in (2.43).
3) Calculate the error term E_j for each variable node as follows:

$$E_j = \sum_{i \in M(j)} (2s_i - 1)/v_{ij} \tag{2.44}$$

where s_i is the syndrome bit associated with the i^{th} check node. The variable s_i will take the value of 1 if the i^{th} check is violated, or 0 otherwise.

4) Invert the value of the bit associated with the highest E_j. Afterwards, steps **1)**, **3)** and **4)** will be repeated, until a valid codeword has been found or the predefined maximum number of iterations has been reached.

2.4.3.2 Performance over the AWGN channel

We use a class of irregular pseudo random LDPC codes which were proposed by Neal [31] to simulate the error performance over an AWGN channel. The code length is $N = 400$ bits, the code rate $R = 1/2$, the average column weight $w_c = 4$ or 8 and the average row weight $w_r = 8$ or 12. The maximum number of iterations for the BF and BP decoders are set to 10 and 50, respectively.

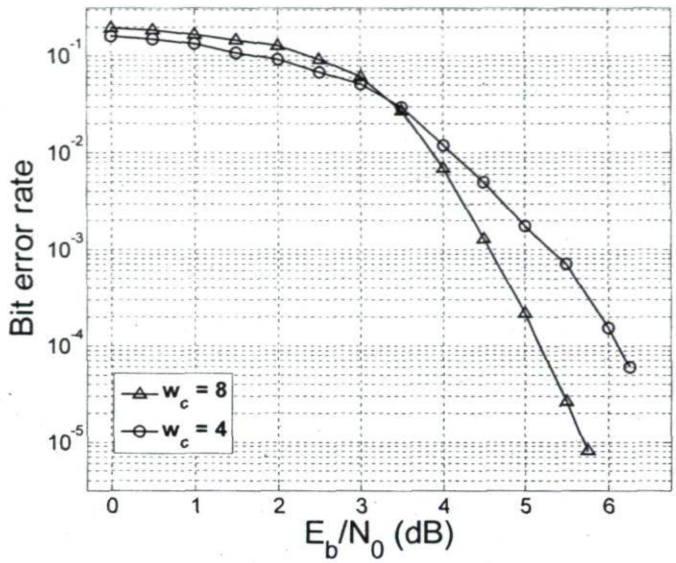

Figure 2.5: BER performance of an irregular random LDPC code with code length $N = 400$ bits and code rate $R = 1/2$ over an AWGN channel via BPSK modulation. The maximum number of iterations for the RRWBF algorithm is 50.

From Fig. 2.5, we can observe that by using a higher average column weight ($w_c = 8$), the distance properties of the LDPC code are improved, which leads to better performances when $E_b/N_0 > 3.5$ dB. The reason for this phenomenon is that the RRWBF algorithm calculates the reliability ratio using w_r channel outputs r_j. For these types of irregular random LDPC codes, when the column weight w_c increases, the row weight w_r increases accordingly. Hence, the RRWBF algorithm is capable of calculating the reliability ratio with more information. Statistically speaking, a higher number of values will always results in a more accurate prediction. Therefore, the RRWBF algorithm can obtain a better performance over the AWGN channel as the column weight increases for this class of LDPC codes.

2.4.4 Comparison of BF and BP decoding algorithms

We now discuss the comparison of the BF and BP decoding algorithms using the LDPC code indicated above with an average column weight $w_c = 8$ and an average row weight $w_r = 12$. The signal is modulated using BPSK and transmitted over an AWGN channel. The maximum number of iterations for the BP algorithm is set to 10, while the RRWBF decoder uses a maximum number of 50 iterations.

2.4.4.1 Comparison of the decoding complexity

As shown in (2.44), the E_j term has to be updated. However, since BF decoding aims to only change the state of a particular bit, only w_c syndrome bits s_i are flipped at each iteration. Consequently, since every check node is associated to w_c message bits, there is an overall maximum of $w_r \cdot w_c$ message nodes requiring the recalculation of the error term. Equation (2.44) requires w_c additions. Hence, during each iteration, the maximum decoding complexity will be $w_c \cdot w_r \cdot w_c$ additions. Since the average column weight w_c is 8 and the row weight w_r is 12 in this case, the required decoding complexity per iteration is upper bounded by $w_c \cdot w_r \cdot w_c = 8 \times 12 \times 8 = 768$ additions. Moreover, the maximum number of iterations is set to 50 for the RRWBF decoder, thus the overall decoding complexity is $50 \times 768 = 38400$ additions.

By contrast, the BP algorithm requires $N(3w_c + 1)$ additions and $N(11w_c - 9)$ multiplications per iteration [34]. For this case, the code length is 400 bits with a maximum of 10 iterations. Thus, the required number of arithmetic operations is $400\times(3\times8+1)\times10 = 100000$ additions and $400\times(11\times8-9)\times10 = 316000$ multiplications. This shows the advantage of BF decoding over the BP algorithm as far as computational complexity is concerned.

2.4.4.2 Performance comparison

As seen in Fig. 2.6, the performance of the BP decoding algorithm with a maximum of 10 iterations is 1.5 dB better at a BER of 10^{-5} than that of the RRWBF algorithm with a maximum of 50 iterations. This clearly shows that the BP decoding algorithm can achieve excellent error performance with a low number of iterations compared to the BF decoding.

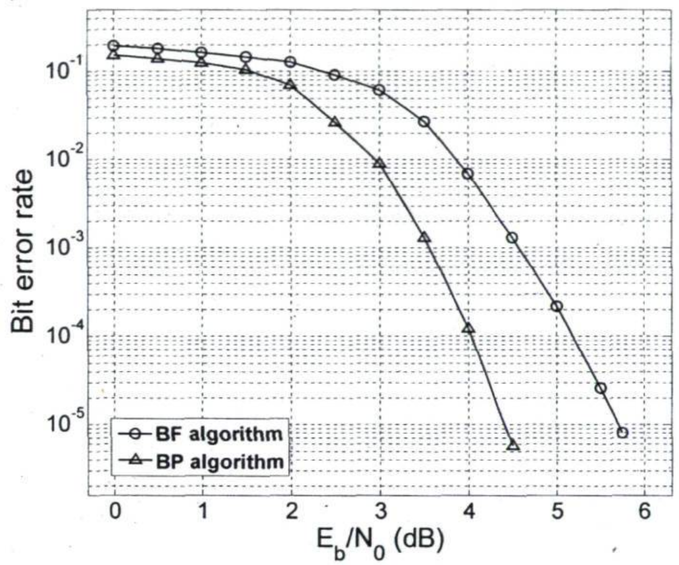

Figure 2.6: Performance comparison of the LDPC codes decoded by the BP (maximum of 10 iterations) and RRWBF (maximum of 50 iterations) algorithms when transmitting over an AWGN channel using BPSK modulation.

Moreover, with the efforts on reducing the decoding complexity of the BP algorithm such as the min-sum algorithm [26], most of the research on LDPC decoder design has focused on the BP algorithm. BP decoding is the decoder for LDPC codes that is used in the next generation of communications systems such as WiMAX [25], [35], [36]. Therefore, in this thesis, the decoder in the simulations is the logarithmic BP algorithm, which is also easily implemented in MATLAB.

Chapter 3

LDPC codes for the WiMAX standard

Due to their excellent error correcting capacity, low-density parity-check (LDPC) codes have been adopted as an optional error correction coding (ECC) scheme by several new communication systems such as WiMAX (IEEE 802.16e) [14], WiFi (IEEE 802.11n standard) [15] and DVB-S2 (satellite video broadcasting standard) [16].

In this chapter, we focus on the LDPC codes specified in the current WiMAX standard, in particular we discuss the construction and encoding of these codes. The WiMAX LDPC codes flexibly support different code lengths for each code rate through the use of an expansion factor [28], and the protocol proposes four types of code rates, i.e. 1/2, 2/3, 3/4, and 5/6. Furthermore, the performance of WiMAX LDPC codes over additive white Gaussian noise (AWGN) and uncorrelated Rayleigh fading channels is evaluated and analyzed via numerical simulations in the last section.

3.1 Construction and encoding of WiMAX LDPC codes

LDPC codes have been selected for forward error correction (FEC) in the WiMAX standard, a reliable broadband metropolitan area wireless technology [14]. In the WiMAX standard, the LDPC codes are a set of systematic linear block codes which are built from a special class of QC-LDPC codes from circulant matrices [30] and the Richardson-Urbanke encoding algorithm [27] presented in Chapter 2. Furthermore, we add the condition that the parity-check matrix is not only in an approximate lower triangular form but also exhibits a dual diagonal structure. The parity-check matrix with this constraint guarantees that the LDPC codes can be linearly encodable regardless of the size of the circulant permutation matrices (also called cyclic-shift matrices) [28].

3.1.1 Definition of the base-matrix

We consider an $m \times n$ parity-check matrix $\mathbf{H}$, where n is the codeword length and m is the parity-check bits length. Thus, the parity-check matrix $\mathbf{H}$ is defined as:

$$\mathbf{H} = \begin{bmatrix} \mathbf{P}^{a_{1,1}} & \mathbf{P}^{a_{1,2}} & \cdots & \mathbf{P}^{a_{1,n_b}} \\ \mathbf{P}^{a_{2,1}} & \mathbf{P}^{a_{2,2}} & & \mathbf{P}^{a_{2,n_b}} \\ \vdots & & \ddots & \vdots \\ \mathbf{P}^{a_{m_b,1}} & \mathbf{P}^{a_{m_b,2}} & \cdots & \mathbf{P}^{a_{m_b,n_b}} \end{bmatrix} \tag{3.1}$$

where $\mathbf{P}^{a_{ij}}$ represents a $z \times z$ right cyclic-shift matrix [11], a_{ij} is the shifting coefficient with $a_{ij} \in \{-1, 0, \cdots, z-1\}$ and z is called the expansion factor. $\mathbf{P}^{-1}$ represents the zero matrix and $\mathbf{P}^{0}$ represents the identity matrix, respectively.

In addition, the parity-check matrix $\mathbf{H}$ is also expanded from a compact form which is called the base-matrix $\mathbf{H}_b$ of size $m_b \times n_b$. Hence, $n = z \times n_b$ and $m = z \times m_b$. The base-matrix $\mathbf{H}_b$ can be represented by the shifting coefficient a_{ij} below:

$$\mathbf{H}_b = \begin{bmatrix} a_{1,1} & a_{1,2} & \cdots & a_{1,n_b} \\ a_{2,1} & a_{2,2} & & a_{2,n_b} \\ \vdots & & \ddots & \vdots \\ a_{m_b,1} & a_{m_b,2} & \cdots & a_{m_b,n_b} \end{bmatrix} \tag{3.2}$$

We denote that the base-matrix $\mathbf{H}_b$ is expanded by replacing each $a_{ij} = -1$ with a $z \times z$ zero matrix, each $a_{ij} = 0$ with a $z \times z$ identity matrix, and each positive number $a_{ij} = \{1, \cdots, z-1\}$ by a right cyclic-shift $z \times z$ identity matrix.

3.1.2 Construction of the parity-check matrix

As shown in tables 2.1 and 2.2, the Richardson-Urbanke encoding algorithm has an encoding complexity upper-bounded by $O(n) + O(g^2)$, where n is the code length and g is the gap measuring the "distance" between a given parity-check matrix and a lower triangular matrix. Therefore, it may be possible to reduce the encoding complexity if we can reduce the gap g. We can transform the matrix $\widehat{\mathbf{D}}$ which is responsible for the $O(g^2)$ encoding complexity term to a special form, e.g. $\widehat{\mathbf{D}} = \mathbf{I}$, where $\mathbf{I}$ is the identity matrix [28].

Because the WiMAX LDPC codes are systematic linear block codes, the parity-check matrix $\mathbf{H}$ can be divided into two parts: the information part $\mathbf{H}_i$ and the parity-check part $\mathbf{H}_p$, where $\mathbf{H}_i$ contains the systematic bits. Thus, $\mathbf{H} = [\,\mathbf{H}_i \mid \mathbf{H}_p\,]$. Moreover, as in the efficient encoding method in [28], we restrict the parity part $\mathbf{H}_p$ to an almost lower triangular matrix with additional constraints, i.e., put the parity-check part $\mathbf{H}_p$ in an approximate dual-diagonal form, $\mathbf{H}_p = [\,\mathbf{H}_{p'} \mid \mathbf{H}_{dual}\,]$. Hence, we define the parity-check matrix $\mathbf{H}$ with size $n \times m = (z \times n_b) \times (z \times m_b)$ as follows:

$$\mathbf{H} = [\,\mathbf{H}_i \mid \mathbf{H}_p\,] = [\,\mathbf{H}_i \mid \mathbf{H}_{p'} \mid \mathbf{H}_{dual}\,]$$

$$= \left[\begin{array}{c|c|cccccc} & \mathbf{P}^{b_1} & \mathbf{I} & 0 & & & 0 & 0 \\ & 0 & \mathbf{P}^{b_2} & \mathbf{I} & \cdots & & 0 & 0 \\ & \vdots & 0 & \mathbf{P}^{b_3} & & & 0 & 0 \\ \mathbf{H}_i & \mathbf{P}^{y} & & \vdots & \ddots & & \vdots & \\ & \vdots & 0 & 0 & & & \mathbf{I} & 0 \\ & 0 & 0 & 0 & \cdots & & \mathbf{P}^{b_{m_b-1}} & \mathbf{I} \\ & \mathbf{P}^{x} & 0 & 0 & & & 0 & \mathbf{P}^{b_{m_b}} \end{array}\right] \tag{3.3}$$

where, as mentioned previously, $\mathbf{P}$ is the $z \times z$ right cyclic-shift matrix and $\mathbf{P}^y$ is located in the l^{th} row block for an integer $l \neq 1$ or m, $\mathbf{P}^x$ is located in the last row block and b is the shifting coefficient for each sub-matrix $\mathbf{P}$. We also explain the dual-diagonal matrix in the following.

Dual-diagonal matrix

A dual-diagonal matrix $\mathbf{C}_{dual}$ is defined as a matrix that has a main diagonal of '1's like the identity matrix, and a second diagonal of '1's on the left of the main diagonal, as shown in (3.4). In other words, $\mathbf{C}_{dual}(i,j) = 1$, for $(i = j$ and $j+1)$, $\mathbf{C}_{dual}(i,j) = 0$, elsewhere.

$$\mathbf{C}_{dual} = \begin{bmatrix} 1 & & & & \\ 1 & 1 & & \cdots & 0 \\ & 1 & 1 & & \\ & \vdots & & \ddots & \vdots \\ & 0 & & \cdots\ 1 & \\ & & & 1 & 1 \end{bmatrix} \tag{3.4}$$

On the other hand, based on the Richardson-Urbanke method [27], the parity-check matrix $\mathbf{H}$ is divided into six sub-matrices shown in Fig. 3.1.

$$\mathbf{H} = \left[\begin{array}{c|cc} \mathbf{A} & \mathbf{B} & \mathbf{T} \\ \mathbf{C} & \mathbf{D} & \mathbf{E} \end{array}\right] =$$

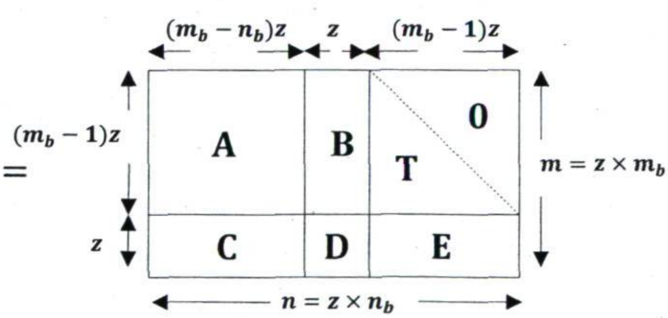

Figure 3.1: Systematic parity-check matrix $\mathbf{H}$ in an approximate lower triangular form.

where $\mathbf{A}$ is $(m_b-1)z \times k_b z$, $\mathbf{B}$ is $(m_b-1)z \times z$, $\mathbf{T}$ is a $(m_b-1)z \times (m_b-1)z$, $\mathbf{C}$ is $z \times k_b z$; $\mathbf{D} = \mathbf{P}^x$ is $z \times z$, $\mathbf{E}$ is $z \times (m_b-1)z$ and $n_b = m_b + k_b$. As defined in (3.3), we have

$$\mathbf{H} = [\ \mathbf{H}_i \ | \mathbf{H}_{p'} \ | \mathbf{H}_{dual}\ ] = \left[\begin{smallmatrix} \mathbf{A} \\ \mathbf{C} \end{smallmatrix} \middle| \begin{smallmatrix} \mathbf{B} \\ \mathbf{D} \end{smallmatrix} \middle| \begin{smallmatrix} \mathbf{T} \\ \mathbf{E} \end{smallmatrix} \right] \tag{3.5}$$

Now, we recall the computation of $\boldsymbol{p}_1$ in (2.22),

$$\boldsymbol{p}_1^T = -\widehat{\mathbf{D}}^{-1}\widehat{\mathbf{C}}\boldsymbol{x}^T = -\widehat{\mathbf{D}}^{-1}(-\mathbf{E}\mathbf{T}^{-1}\mathbf{A} + \mathbf{C})\,\boldsymbol{x}^T$$

and

$$\widehat{\mathbf{D}} = \mathbf{E}\mathbf{T}^{-1}\mathbf{B} + \mathbf{D}$$

Because matrix $\widehat{\mathbf{D}}^{-1}$ is not sparse in general, the overall complexity of computing $\boldsymbol{p}_1$ is $O(n) + O(z^2)$. So if $\widehat{\mathbf{D}}$ can be chosen as the identity matrix, then the encoding complexity may be linearly scaled. The key idea is to choose the matrix $\widehat{\mathbf{D}}$ as the identity matrix by a suitable selection of $\mathbf{P}^x$ and $\mathbf{P}^y$ in (3.3). Therefore, the overall complexity of computing $\boldsymbol{p}_1$ can be reduced to $O(n)$ regardless of the size of cyclic-shift matrices.

In order to compute $\widehat{\mathbf{D}}$, consider $\mathbf{H}$ given in (3.3) and (3.5). We get,

$$\begin{bmatrix} \mathbf{B} \\ \mathbf{D} \end{bmatrix} = \begin{bmatrix} \mathbf{P}^{b_1} \\ 0 \\ \vdots \\ \mathbf{P}^y \\ \vdots \\ 0 \\ \mathbf{P}^x \end{bmatrix} \quad \text{and} \quad \begin{bmatrix} \mathbf{T} \\ \mathbf{E} \end{bmatrix} = \begin{bmatrix} \mathbf{I} & 0 & & 0 & 0 \\ \mathbf{P}^{b_2} & \mathbf{I} & \cdots & 0 & 0 \\ 0 & \mathbf{P}^{b_3} & & 0 & 0 \\ \vdots & & \ddots & & \vdots \\ 0 & 0 & & \mathbf{I} & 0 \\ 0 & 0 & \cdots & \mathbf{P}^{b_{m_b-1}} & \mathbf{I} \\ 0 & 0 & & 0 & \mathbf{P}^{b_{m_b}} \end{bmatrix}$$

Therefore, according to (3.3), $\mathbf{D} = \mathbf{P}^x$ and

$$\mathbf{B}^T = [\ \mathbf{P}^{b_1 T} \quad \mathbf{0} \quad \cdots \quad \mathbf{P}^{yT} \quad \cdots \quad \mathbf{0}\ ] \tag{3.6}$$

$$\mathbf{E} = [\,\mathbf{0} \quad \mathbf{0} \quad \cdots \quad \mathbf{0} \quad \mathbf{P}^{b_{m_b}}\,] \tag{3.7}$$

$$\mathbf{T} = \begin{bmatrix} \mathbf{I} & 0 & & 0 & 0 \\ \mathbf{P}^{b_2} & \mathbf{I} & \cdots & 0 & 0 \\ 0 & \mathbf{P}^{b_3} & & 0 & 0 \\ \vdots & & \ddots & \vdots & \\ 0 & 0 & & \mathbf{I} & 0 \\ 0 & 0 & \cdots & \mathbf{P}^{b_{m_b-1}} & 0 \end{bmatrix} \tag{3.8}$$

Then we have,

$$\mathbf{E}\mathbf{T}^{-1}\mathbf{B} = \mathbf{P}^{\left(\sum_{i=1}^{m_b} b_i\right)} + \mathbf{P}^{\left(\sum_{i=l+1}^{m_b} b_i\right)}\mathbf{P}^{y} \tag{3.9}$$

where $\mathbf{P}^{y}$ is located in the l^{th} row block of $\mathbf{B}$. Since we are pursuing that $\widehat{\mathbf{D}} = \mathbf{I}$, i.e.,

$$\widehat{\mathbf{D}} = \mathbf{E}\mathbf{T}^{-1}\mathbf{B} + \mathbf{D} = \mathbf{P}^{\left(\sum_{i=1}^{m_b} b_i\right)} + \mathbf{P}^{\left(\sum_{i=l+1}^{m_b} b_i\right)}\mathbf{P}^{y} + \mathbf{P}^{x} = \mathbf{I}$$

Matrix $\widehat{\mathbf{D}}$ becomes the identity matrix if x and y are chosen such that

$$x = \sum_{i=1}^{m_b} b_i \bmod z \text{ and } y = -\sum_{i=l+1}^{m_b} b_i \bmod z$$

or

$$\sum_{i=1}^{m_b} b_i = 0 \bmod z \text{ and } x = y + \sum_{i=l+1}^{m_b} b_i \bmod z \tag{3.10}$$

Example

As an example, the parity-check matrix for the WiMAX LDPC code with a code rate of $1/2$ is given in shifting coefficient form as:

$$\mathbf{H} = [\,\mathbf{H}_i \mid \mathbf{H}_p\,] = [\,\mathbf{H}_i \mid \mathbf{H}_{p'} \mid \mathbf{H}_{dual}\,]$$

$$= \left[\begin{array}{cccccccccccc|cccccccccccc}
 & 94 & 73 & & & & & & 55 & 83 & & & 7 & 0 & & & & & & & & & & \\
 & 27 & & & & 22 & 79 & 9 & & & & 12 & & 0 & 0 & & & & & & & & & \\
 & 1 & & 24 & 22 & 81 & & 33 & & & & 0 & & & 0 & 0 & & & & & & & & \\
61 & & 47 & & & & & & 65 & 25 & & & & & & 0 & 0 & & & & & & & \\
 & & 39 & & & & 84 & & & 41 & 72 & & & & & & 0 & 0 & & & & & & \\
 & & & & 46 & 40 & & 82 & & & & 79 & 0 & & & & & 0 & 0 & & & & & \\
 & & 95 & 53 & & & & & & 14 & 18 & & & & & & & & 0 & 0 & & & & \\
 & 11 & 73 & & & & 2 & & & 47 & & & & & & & & & & 0 & 0 & & & \\
12 & & & & 83 & 24 & & 43 & & & & 51 & & & & & & & & & 0 & 0 & & \\
 & & & & & 94 & & 59 & & & 70 & 72 & & & & & & & & & & 0 & 0 & \\
 & & 7 & 65 & & & & & 39 & 49 & & & & & & & & & & & & & 0 & 0 \\
43 & & & & & 65 & & 41 & & & & 26 & 7 & & & & & & & & & & & 0
\end{array}\right] \tag{3.11}$$

where unmarked positions are zero matrices, "0" (0 shifted) is the identity matrix and a number represents a right cyclic-shift $z \times z$ identity matrix by this number.

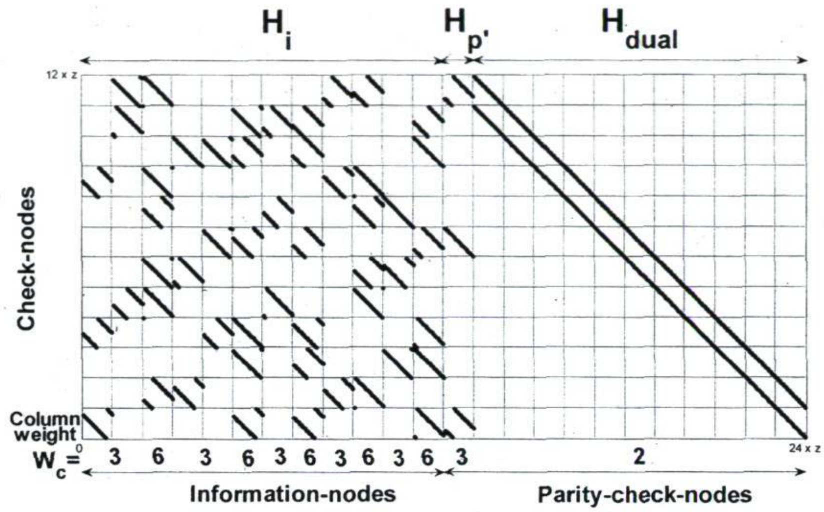

Figure 3.2: Structure of the parity-check matrices **H** for the WiMAX LDPC codes with code rates of 1/2 and code length $n = 576$ ($z = 24$), where the bold lines represent elements '1' in **H**.

From (3.5), $\mathbf{D} = [7]$. The structure of this parity check matrix **H** according to the LDPC codes with code rate 1/2 is shown in Fig. 3.2 with code length 576. Each square is a cyclic-shift sub-matrix, the expansion factor $z = z_1 = 24$ and the dual-diagonal matrix $\mathbf{H}_{dual}$ has size $12z \times 11z = 276 \times 264$.

Hence, we re-compute the information message parts of the codeword, $\boldsymbol{p_1}$ and $\boldsymbol{p_2}$ being based on (2.22) and (2.23). The encoder architecture for these codes in the WiMAX standard is shown in Fig. 3.3.

$$\boldsymbol{p}_1^T = (-\mathbf{E}\mathbf{T}^{-1}\mathbf{A} + \mathbf{C})\ \boldsymbol{x}^T \tag{3.12}$$

$$\boldsymbol{p}_2^T = \mathbf{T}^{-1}(\mathbf{A}\boldsymbol{x}^T + \mathbf{B}\boldsymbol{p}_1^T) \tag{3.13}$$

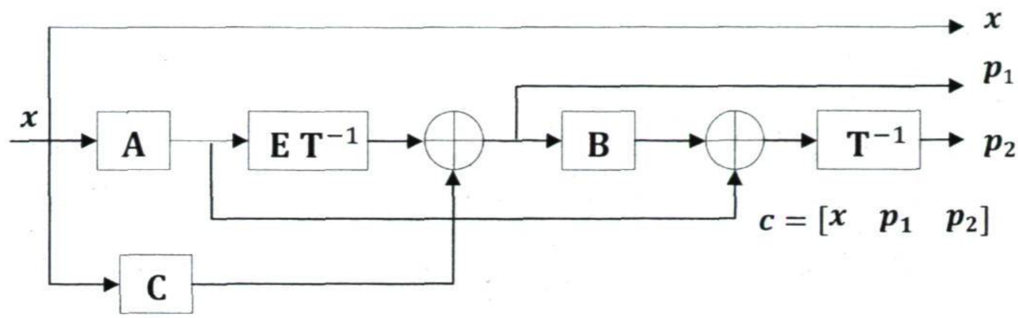

Figure 3.3: Block diagram of the encoder architecture for the LDPC codes in WiMAX.

3.2 Characteristics of the WiMAX LDPC codes

Based on the analysis of their construction discussed previously, the WiMAX LDPC codes offer four flexible code rates: 1/2, 2/3, 3/4 and 5/6 and the base-matrices $\mathbf{H}_b$ for these code rates are defined by systematic LDPC codes with size 12 × 24, 8 × 24, 6 × 24 and 4 × 24, respectively [14].

3.2.1 Various code rates and code lengths

In the WiMAX system, the sub-matrices size are determined by the expansion factor z_f, where z_f is defined as $n/24$ for code length n, and varies from 24 to 96 with increments of 4, i.e. $\{24, 28, 32, 36, 40, 44, 48, 52, 56, 60, 64, 68, 72, 76, 80, 84, 88, 92, 96\}$. Here, f is the index of the code length for a given code rate, i.e. $f = \{1, 2, \ldots 18, 19\}$. Thus the parity-check matrix size is based on both code rate and expansion factor z_f. Accordingly, there are 19 different code lengths, ranging from the minimal code length ($n_{min} = z_1 \times 24 = 24 \times 24 = 576$ bits) to the maximum code length ($n_{max} = z_{19} \times 24 = 96 \times 24 = 2304$ bits).

3.2.2 Degree distribution of the WiMAX LDPC codes

The WiMAX standard consists of six different code rate classes with different variable-nodes and check-nodes distributions: 1/2, 2/3A, 2/3B, 3/4A, 3/4B and 5/6. Among them, there are classes of codes with the same code rates, i.e. 2/3A vs. 2/3B and 3/4A vs. 3/4B. It is obvious from their base matrices (see Appendix A) that 2/3A is quite irregular with column weight 2, 3 and 6, and uniform row weight 10, while 2/3B is moderately irregular with maximum column weight 4 and row weights 10 and 11. The only difference between code rates 3/4A and 3/4B is that the maximum column weight increases from 4 to 6. Accordingly, the error rate performance will be improved with increasing column weight. This will be shown via simulations in section 3.3.3.1.

Table 3.1 summarizes the six code classes with their degree distributions for variable and check nodes as in (2.7) and (2.8). As an example, we still use the WiMAX LDPC codes with code rates 1/2 and code length $n = 576$ ($z = 24$) mentioned both in Fig. 3.2 and (3.11). The base-matrix is 12×24, and the column-weights and row weights are $w_c = 2, 3, 6$ and $w_r = 6, 7$, respectively. The column weights are indicated in Fig. 3.2.

Table 3.1: Degree distributions of the WiMAX LDPC codes.

Code rate	Base matrix size	Column weight	Row weight	Variable-nodes $\gamma(x)$	Check-nodes $\rho(x)$
1/2	12×24	2, 3, 6	6, 7	$\gamma(x) = \frac{11}{24}x + \frac{8}{24}x^2 + \frac{5}{24}x^5$	$\rho(x) = \frac{8}{12}x^5 + \frac{4}{12}x^6$
2/3A	8×24	2, 3, 6	10	$\gamma(x) = \frac{7}{24}x + \frac{12}{24}x^2 + \frac{5}{24}x^5$	$\rho(x) = \frac{8}{8}x^9$
2/3B	8×24	2, 3, 4	10, 11	$\gamma(x) = \frac{7}{24}x + \frac{1}{24}x^2 + \frac{16}{24}x^3$	$\rho(x) = \frac{7}{8}x^9 + \frac{1}{8}x^{10}$
3/4A	6×24	2, 3, 4	14, 15	$\gamma(x) = \frac{5}{24}x + \frac{1}{24}x^2 + \frac{18}{24}x^3$	$\rho(x) = \frac{5}{6}x^{13} + \frac{1}{6}x^{14}$
3/4B	6×24	2, 3, 6	14, 15	$\gamma(x) = \frac{5}{24}x + \frac{12}{24}x^2 + \frac{7}{24}x^5$	$\rho(x) = \frac{2}{6}x^{13} + \frac{4}{6}x^{14}$
5/6	4×24	2, 3, 4	20	$\gamma(x) = \frac{3}{24}x + \frac{10}{24}x^2 + \frac{11}{24}x^3$	$\rho(x) = \frac{4}{4}x^{19}$

In summary, we note that the WiMAX LDPC codes have the following flexible characteristics:

1) Six different code types.
2) Different degree distributions of variable-nodes and check-nodes with maximum column-weight $w_c^{max} = 6$ and maximum row-weight $w_r^{max} = 20$.
3) Various sub-matrix sizes from 24×24 to 96×96.
4) Various code lengths from 576 to 2304 bits.

3.2.3 Applications of LDPC codes in other standards

Besides the WiMAX standard, next generation communications systems such as WiFi (802.11n standard) [15] and DVB-S2 (Satellite video broadcasting standard) [16] have also adopted LDPC codes as an optional error-correction coding scheme. Table 3.2 shows the design parameters of LDPC codes in different standards [37].

Table 3.2: The design parameters of LDPC codes in different standards.

Parameter \ Standard		WiMAX	WiFi	DVB-S2
Code length	#	19	3	2
	Minimum	576	648	16800
	Maximum	2304	1944	64800
Code rate	#	4	4	11
	Minimum	1/2	1/2	1/4
	Maximum	5/6	5/6	9/10
Row weight	#	7	9	11
	Minimum	6	7	4
	Maximum	20	22	30
Column weight	#	4	8	7
	Minimum	2	2	2
	Maximum	6	12	13

3.3 Performance of WiMAX LDPC codes

In this section, we will evaluate the LDPC codes specified in the WiMAX standard by performing simulations assuming binary phase-shift keying (BPSK) modulation over additive white Gaussian noise (AWGN) and flat Rayleigh fading channels. The iterative logarithmic belief-propagation (Log-BP) decoder is used for decoding. It terminates when either a valid codeword is found or the maximum of 50 iterations is reached. These simulations have been carried out using MATLAB and the parameters used in the simulation are shown in Table 3.3.

Table 3.3: Parameters used in the simulations.

Modulation	BPSK
Channel	AWGN
	Flat uncorrelated Rayleigh fading
LDPC codes	WiMAX LDPC codes (Mainly using the codes with code length 2304 and code rate 1/2)
Encoding	Richardson-Urbanke algorithm
Decoding	Logarithmic BP algorithm
Maximum number of iterations	50

3.3.1 Performance over an AWGN channel

The performance of LDPC codes for WiMAX will be analyzed and discussed through three aspects, namely number of iterations, code length and code rate.

3.3.1.1 Impact of the code rate

The performance of LDPC codes for WiMAX for all specified code rates and an input code length of 2304 bits (the maximum length specified among the WiMAX LDPC codes) is shown in Fig. 3.4. Referring to the discussion about the difference between two pairs with the same code rates, 2/3A and 2/3B, 3/4A and 3/4B, in section 3.2.2, the BER performances of 2/3A and 3/4B are slightly better than that of 2/3B and 3/4A, since the maximum column-weights w_c of 2/3B and 3/4A is 4 while that of 2/3A and 3/4B is 6, respectively. Thus, the error performance improves by increasing the column-weight accordingly.

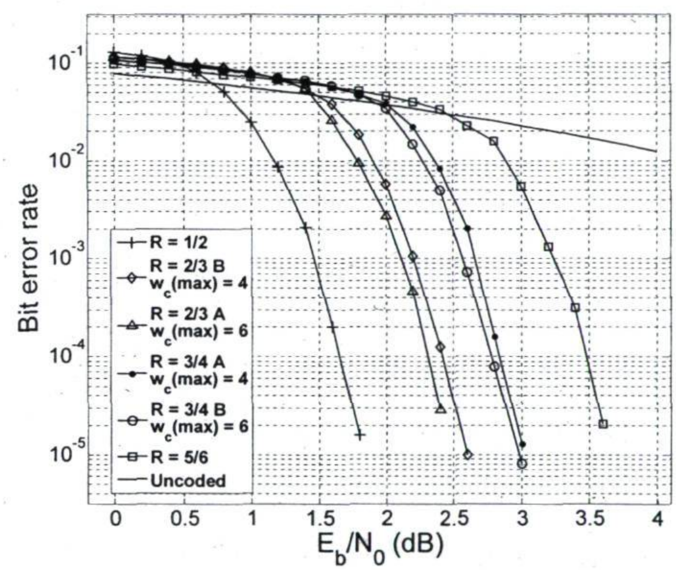

Figure 3.4: BER performances of the LDPC codes for WiMAX for all code rates with a code length of 2304 bits.

3.3.1.2 Impact of the number of iterations

The BER versus number of iterations performances for the WiMAX LDPC codes with a code length of 2304 and a code rate of 1/2 is plotted in Fig. 3.5. As can be expected, the BER decreases with increasing number of iterations and tends to converge after a certain number of iterations. The maximum number of iterations is set to 50 for this case, and the

BER converges to about $10^{-1.6}$, 10^{-3} and 10^{-5} for a signal-to-noise ratio per bit of $E_b/N_0 =$ 1.0, 1.4 and 1.8 dB, respectively. It is also clear that the greater E_b/N_0 is, the better the BER performance is. We can also see that for this case to reach a target BER of about 10^{-5}, setting the maximum number of iterations to 45 is sufficient.

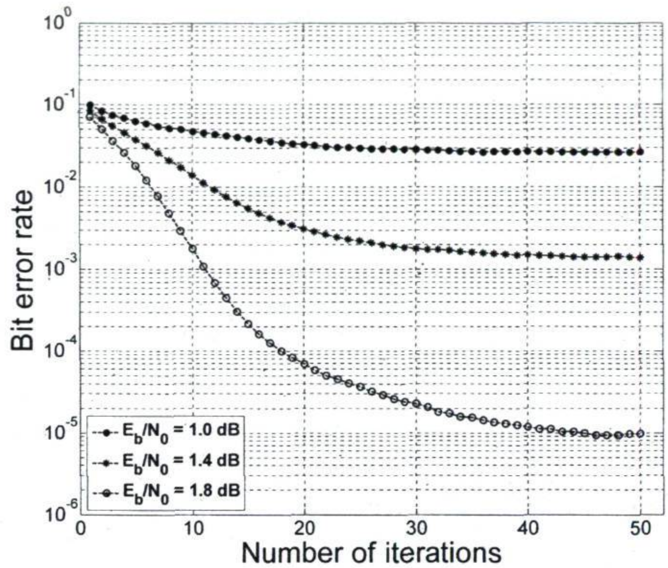

Figure 3.5: BER performance versus the number of iterations at $E_b/N_0 = 1.0$; 1.4 and 1.8 dB, with a code length of 2304 bits and a code rate of 1/2, and a maximum number of iterations of 50.

Given the fact that the Log-BP decoding algorithm will stop iterating when a legitimate codeword has been detected, the average number of iterations for the WiMAX LDPC code indicated above when the maximum number of iterations is set to 25 and 50 is shown in Fig. 3.6 (a). As we can see, the average number of iterations is almost the maximum in the low SNR region. When the SNR is increased, the actual number of iterations decreases. When employing the BP decoding algorithm, we could use a lower maximum number of iterations in comparison to other decoding algorithm such as the weighted bit-flipping (WBF) [24] and reliability ratio based weighted bit-flipping (RRWBF) [33] decoding algorithms.

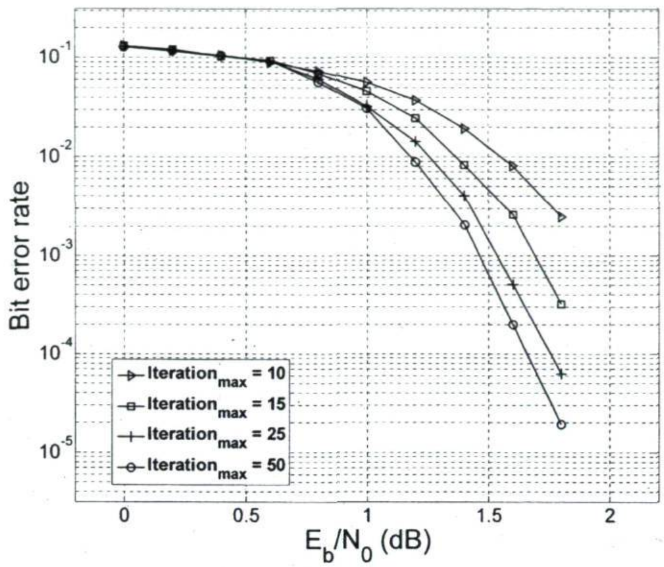

(a)

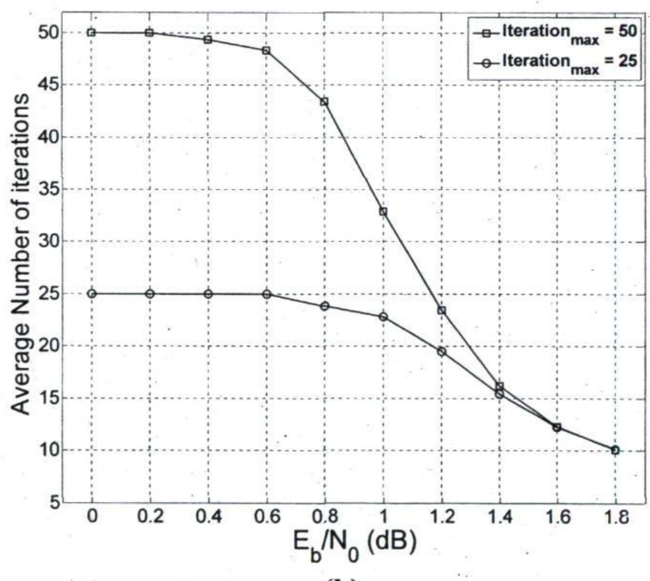

(b)

Figure 3.6: (a) BER performance of the WiMAX code for various numbers of iterations (uncoded, 10, 15, 25 and 50 iterations). (b) Average number of iterations for the LDPC code of code length 2304 and code rate 1/2 when the maximum number of iterations is set to 25 and 50.

Fig. 3.6 (a) shows that the BER performance improves by setting a larger maximum number of decoding iterations. We can obtain the best performance when the maximum number of iterations is set to 50. As shown in Fig. 3.6 (b), the average number of iterations is almost the same after $E_b/N_0 = 1.5$ while the scheme with the maximum number of iterations equal to 50 can get a little gain of BER at $E_b/N_0 = 1.8$, as shown in Fig. 3.6 (a). Thus, we can conclude that the average number of iterations is equal to the predefined maximum number of iterations at lower SNRs, and converges almost to that same number of iterations at higher SNRs using the iterative BP decoding algorithm.

3.3.1.3 Impact of the code length

As mentioned before, the code length of the WiMAX LDPC codes can be calculated via $N = 24 \cdot z$ where z is the expansion factor and all six code classes have 19 codeword sizes ranging from $N = 576$ to $N = 2304$ bits. The codeword size flexibility is the most interesting aspect of this standardized LDPC code family.

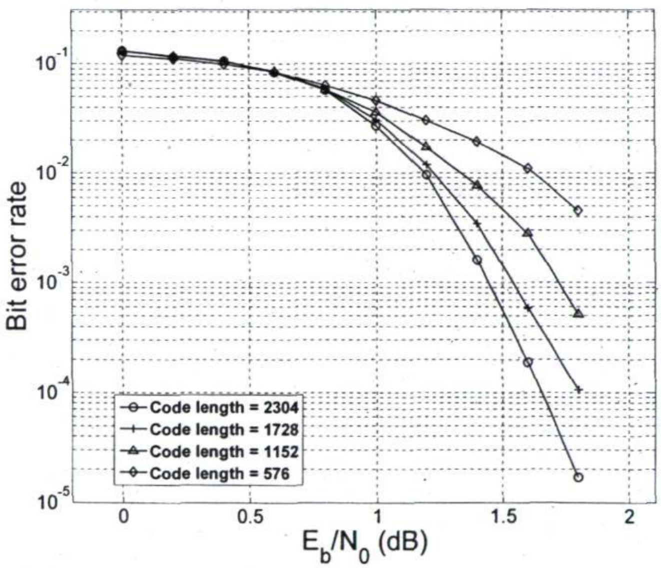

Figure 3.7: BER performance of the WiMAX LDPC codes for various code lengths and code rate $R = 1/2$.

To evaluate the influence of the code length, we select four code lengths of 576 (the minimum code length), 1152, 1728 and 2304 (the maximum code length) among the 19 code sizes for the WiMAX LDPC codes. Note that these four code lengths increase with an increment of 576 bits, meaning that the expansion factors are chosen to be 24, 48, 72 and 96. As can be expected, Fig. 3.7 shows that for a given code rate (1/2 in this case), the error performance is improved by increasing the code length. The code with a code length of 2034 bits obtains the best performance among all the code lengths in the WiMAX LDPC codes.

3.3.2 Performance over a flat Rayleigh fading channel

3.3.2.1 Rayleigh fading channel

The communications channel is the transmission medium for the signals. It can be divided into two categories: wired channels and wireless channels. In general, the former has the characteristic of being more stable and more predictable than the latter.

By contrast, wireless communications are often impacted by fading due to user mobility or the mobile environment. Fading causes variations of the received signal level and consequently of the signal-to-noise ratio (SNR).

The flat fading channel is a much used model for wireless and mobile communications. All signal frequencies are attenuated by the same factor. The received signal r can be written as

$$r = \alpha \cdot t + n \tag{3.14}$$

where α is the fading amplitude, the fading phase is uniformly distributed between 0 and 2π, t is the transmitted channel symbol and n is the AWGN. The fading amplitude α can be described as a stochastic variable. When $\alpha = 1$, there is no fading and the channel is just an AWGN channel.

The Rayleigh fading model is commonly used in mobile communications when there is no line-of-sight path between transmitter and receiver. The probability density function (PDF) of Rayleigh fading is given by [6]

$$p(\alpha) = \frac{\alpha}{\sigma^2} \cdot \exp\left(-\frac{\alpha^2}{2\sigma^2}\right), \qquad (\alpha \geq 0, \sigma \geq 0) \tag{3.15}$$

For BPSK modulation, the energy of the transmitted symbols is unitary. The fading amplitude is thus generated using [38]

$$\alpha = \sqrt{-\ln(1-b)} \tag{3.16}$$

where b is a random number uniformly distributed between 0 and 1.

3.3.2.2 Decoding analysis for uncorrelated Rayleigh fading

For uncorrelated Rayleigh fading, the conditional PDF of the receiver output r is [39]

$$P_r(r|t,\alpha) = \frac{r}{\sqrt{2\pi\sigma^2}} \exp\left(-\frac{(r - t \cdot \alpha)^2}{2\sigma^2}\right) \tag{3.17}$$

where is α the normalized Rayleigh fading factor with $E[\alpha^2] = 1$.

1) **Ideal channel state information (CSI):**

   When we have ideal CSI, the logarithmic likelihood ratio (LLR) $l(r)$ is given by [39]

$$l(r) = \log \frac{P(c=0|r,\alpha)}{P(c=1|r,\alpha)} = \frac{2}{\sigma^2} r \cdot \alpha \tag{3.18}$$

2) **No channel state information (NCSI):**

   When no CSI is available, following [39], we assume that $P(r|t,\alpha)$ has a Gaussian distribution in the region of the most probable r, and we approximate $l(r)$ as:

$$l(r) \approx \frac{2}{\sigma^2} r \cdot E[\alpha] \tag{3.19}$$

where $E[\alpha]$ is the mean of α and is equal to 0.8862.

3.3.2.3 Performance over a flat Rayleigh fading channel

In this section, we analyze the performance of the WiMAX LDPC codes with code length 2304 and code rate 1/2 transmitted using BPSK modulation over the uncorrelated Rayleigh channels with channel state information (CSI) and no channel state information (NCSI).

In Fig. 3.8, we compare the performance over the AWGN channel and uncorrelated Rayleigh fading channels with CSI and NCSI. We can observe that this LDPC code suffers a loss of nearly 2.2 dB and 3.3 dB, respectively, in the fading channels with CSI and NCSI for a BER = 10^{-5}, relative to the AWGN channel. Thus, this WiMAX LDPC code can achieve a good error performance over the fading channel.

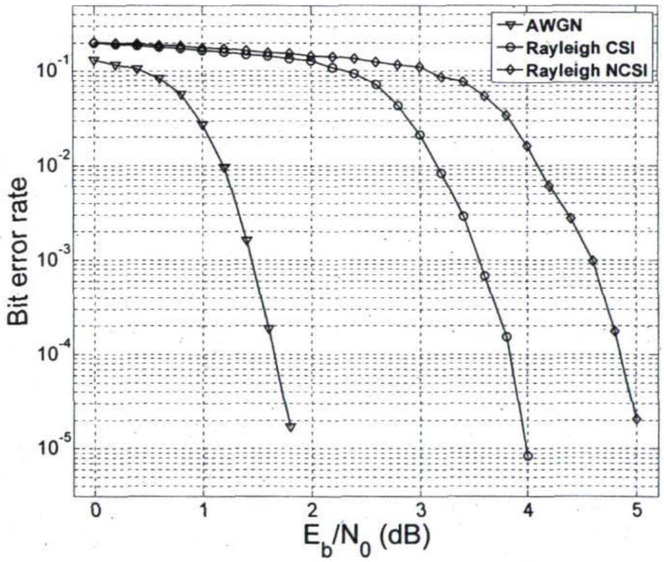

Figure 3.8: BER comparison of the WiMAX LDPC code of code length 2304 bits and code rate 1/2 over AWGN and uncorrelated Rayleigh fading channels with CSI and NCSI.

Table 3.4: Average number of decoding iterations corresponding to Fig. 3.8.

E_b/N_0 (dB)	AWGN	Rayleigh (CSI)	Rayleigh (NCSI)
0.0	50	50	50
1.0	32.9	50	50
1.8	10.1	50	50
2.0	-	50	50
3.0	-	31.2	49.1
4.0	-	10.4	28.8
5.0	-	-	11.1

For the decoding process of the above evaluation, the maximum number of iterations was set to 50. The average numbers of decoding iterations corresponding to Fig. 3.8 are given in Table 3.4. We can see that the numbers of iterations are small for high SNRs on both AWGN and Rayleigh channels. For instance, when BER = 10^{-5}, the decoding complexity is low and most codewords can be decoded in about 9-11 iterations. Also, the average number of iterations will decrease as the SNR is increased.

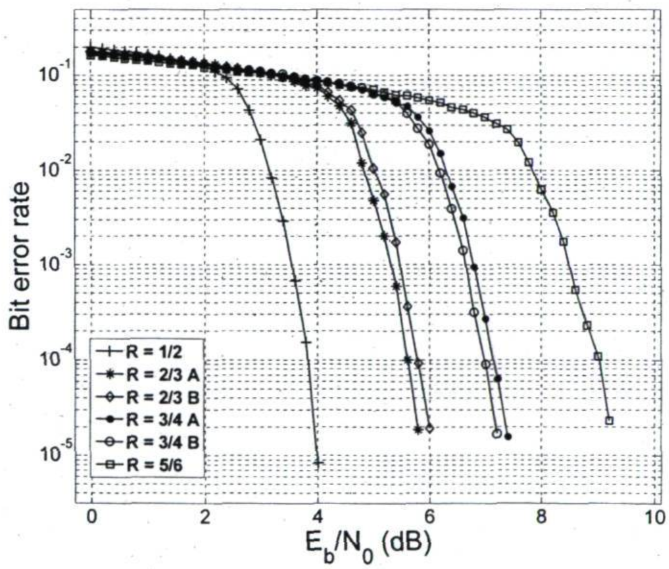

Figure 3.9: BER performance of LDPC codes for all specified code rates in the WiMAX standard with code length of 2304 bits over uncorrelated Rayleigh channel with CSI.

Fig. 3.9 shows the BER performances of the WiMAX LDPC codes with all given code rates over the uncorrelated Rayleigh fading channel with CSI. The code length is still 2304 bits. The WiMAX LDPC codes can reliably transmit over a fading channel at a proper SNR environment for all code rates.

The simulation results show that the WiMAX LDPC codes are one powerful class among the LDPC codes for FEC. We can conclude that these LDPC codes can achieve a better error performance with a greater code length and maximum number of iterations while sacrificing the output delay, since the larger the maximum number of iterations is set, the longer the decoding process will last.

In terms of modulation, WiMAX supports various modulations such as QPSK, 16-QAM and 64-QAM, but 64-QAM is optional in the uplink. We will discuss WiMAX LDPC-coded modulation in the next chapter.

Chapter 4

Spectrally-efficient LDPC-coded modulation

In 1982, Ungerböeck published his landmark paper on trellis coded modulation (TCM) [7] in which he stated that modulation and coding can be designed in a single entity for improved performance. On the other hand, as a powerful error correcting coding (ECC) technique, LDPC codes have attracted a lot of attention owing to their low decoding complexity and excellent error performance. Therefore, a promising idea that combines the functions of LDPC coding and efficient modulation has been widely considered [40]-[50].

In this chapter, we explore the use of LDPC codes in conjunction with multi-level modulation schemes to achieve both power and bandwidth efficiency for wireless communication systems. We first review the bandwidth-efficient modulation schemes and several typical coded modulation systems. Then, we present an LDPC-coded modulation system for transmission over both additive white Gaussian noise (AWGN) and uncorrelated Rayleigh fading channels. At the end, an adaptive coded modulation (ACM) scheme with LDPC coding for flat slowly-varying Rayleigh fading is proposed.

4.1 Basics of LDPC-coded modulation

In Chapter 3, we discussed and evaluated the LDPC codes specified in the WiMAX standard in conjunction with BPSK modulation for transmission over both AWGN and uncorrelated Rayleigh fading channels. We showed their excellent performance. In this section, we will focus on studying LDPC codes combined with high order multi-level modulation schemes to improve the performances of the wireless communication system.

4.1.1 Bandwidth-efficient modulation

Digital modulation is the process by which a carrier wave is able to carry the message or digital signal (series of "1"s and "0"s). There are three basic methods: amplitude, frequency and phase shift keying. For bandpass transmission such as in mobile (wireless) communications, the baseband signal needs to modulate a sinusoid which is called a carrier wave.

Since coded modulation is built upon bandwidth-efficient modulation such as M-ary phase-shift keying (M-PSK) and M-ary quadrature amplitude modulation (M-QAM), we first briefly review the concepts of power and bandwidth-limited channels. Generally, in power-limited systems, we adopt ECC techniques which can save power (minimum required transmit power) by adding redundant bits to the transmitted signals while maintaining a good performance. But this scheme has the disadvantage that the modulator operates at a higher data rate, resulting in an expanded bandwidth. By contrast, in bandwidth-limited system, a higher-order modulation scheme is required to increase the spectral efficiency while using more signal power to keep the original signal separation, or accept a loss of the error performance. Therefore, the tradeoff between bandwidth and power in a system can be a tricky problem.

To solve this conflict, trellis coded modulation (TCM) was invented by Ungerboeck [7]. His work opened the possibility to achieve both power and bandwidth efficiency in a communication system.

4.1.1.1 Quadrature amplitude modulation (QAM)

Among the family of bandwidth-efficient modulation schemes, PSK and QAM are often used to achieve high rate transmission. In particular, *M*-QAM can offer the largest spectral efficiency, since the information bits are modulated in both the amplitude and phase of the carrier wave signals. For this reason, QAM combined with Gray mapping has been widely applied over wireless links, such as in 3G and 4G mobile communication systems, broadband wireless networks (WiFi, WiMAX) and many other wireless multimedia communication systems.

The simplest method of digital signalling with a QAM system is to use one-dimensional PAM independently for each signal coordinate. Consider rectangular QAM signal constellations with $M = 2^m$, where M is the number of points. They can be represented as constellations of points in the in-phase and quadrature (I/Q) plane:

$$s(t) = A_I(t)\cos 2\pi f_c t + A_Q(t)\sin 2\pi f_c t, \qquad (0 \le t \le T\,) \tag{4.1}$$

where f_c is the carrier frequency, T is the symbol time, $A_I(t)$ and $A_Q(t)$ are the baseband signals (amplitudes) of the in-phase and quadrature components, respectively. Moreover, $A_I(t)$ and $A_Q(t)$ can be selected over the set of $\{\pm d, \pm 3d, \dots, \pm(\sqrt{M}-1)d\}$, where $2d = d_0$ is the minimum distance between signal points and can be computed using the following relationship [51],

$$d = \sqrt{\frac{3\log_2 M \cdot E_b}{2(M-1)}} \tag{4.2}$$

where E_b is the information bit energy.

Approximate bit error rate (BER) expression

The BER approximation for *M*-ary square QAM with Gray mapping is given by [51]:

$$P_b \cong \frac{\sqrt{M}-1}{\sqrt{M}\cdot\log_2\sqrt{M}}\cdot \operatorname{erfc}\left(\sqrt{\frac{3\log_2 M}{2(M-1)}\cdot\frac{E_b}{N_0}}\right) \tag{4.3}$$

where E_b/N_0 is the signal to noise ratio (SNR) per information bit and erfc$(\cdot)$ is the complementary error function. It is defined as [6]

$$\operatorname{erfc}(x) = \frac{1}{\sqrt{2\pi}}\int_x^\infty \exp\left(-\frac{u^2}{2}\right)du \tag{4.4}$$

Spectral efficiency

The spectral efficiency η (bits/symbol/Hz) of *M*-PSK and *M*-QAM schemes is the number of bits carried by each symbol. It is computed by

$$\eta = \log_2 M = m$$

4.1.1.2 Average energy of QAM constellations

Assuming the bits are identically distributed, the average symbol energy E_s is the average of the square distance of the constellation points from the origin. Figure 4.1 shows an overlay of *M*-QAM constellations, where as mentioned before, $M = 2^m$ is the size of the constellation and d_0 is the minimum distance between signal points. For even m, the constellation is a square, while for odd m, the constellation is a cross.

The average energy of *M*-QAM is defined as,

$$E_s = \frac{1}{M}\sum_{i=1}^{M} E_i \tag{4.5}$$

where, E_i is the signal energy of point i in the constellation.

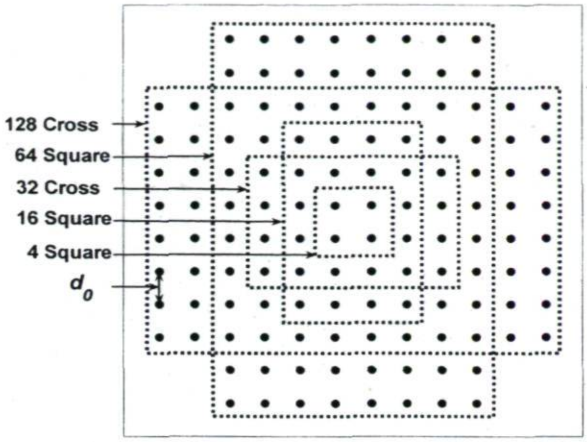

Figure 4.1: *M*-QAM signal constellations.

Square constellations

The average energy for even $k \geq 2$, i.e. for square constellations, is given by [52]

$$E_s = \frac{1}{6} d_0^2 (M - 1) \tag{4.6}$$

Cross constellations

The average energy for odd $k \geq 3$, i.e. for cross constellations, is given by [52]

$$E_s = \begin{cases} \frac{1}{6} d_0^2 \left(\frac{40}{32} M - 1\right), & m = 3 \\ \frac{1}{6} d_0^2 \left(\frac{31}{32} M - 1\right), & \text{odd } m \geq 5 \end{cases} \tag{4.7}$$

Table 4.1 lists the average energies and the spectral efficiencies of various QAM constellations. Also shown is the average energy per bit, where $E_s = \eta \cdot E_b$.

Table 4.1: Average energy for *M*-QAM constellations.

Modulation	Spectral efficiency η	Symbol energy E_s	Bit energy E_b
BPSK	1	$\frac{1}{4}d_0^2$	$\frac{1}{4}d_0^2$
QPSK	2	$\frac{1}{2}d_0^2$	$\frac{1}{4}d_0^2$
8-QAM	3	$\frac{3}{2}d_0^2$	$\frac{1}{2}d_0^2$
16-QAM	4	$\frac{5}{2}d_0^2$	$\frac{5}{8}d_0^2$
32-Cross	5	$5d_0^2$	d_0^2
64-QAM	6	$\frac{21}{2}d_0^2$	$\frac{7}{4}d_0^2$
128-Cross	7	$\frac{41}{2}d_0^2$	$\frac{41}{14}d_0^2$
256-QAM	8	$\frac{85}{2}d_0^2$	$\frac{85}{16}d_0^2$

In this thesis, without loss of generality, we set $d_0 = 2$, hence,

$$E_s = \begin{cases} \frac{2}{3}(M-1), & \text{even } m \geq 2 \\ \frac{2}{3}\left(\frac{5}{4}M-1\right), & m = 3 \\ \frac{2}{3}\left(\frac{31}{32}M-1\right), & \text{odd } m \geq 5 \end{cases} \tag{4.8}$$

4.1.2 Coded modulation techniques

As a bandwidth-efficient scheme that combines coding and modulation, coded modulation can improve performance with the same spectral efficiency compared to the scheme that treats channel coding and modulation separately.

For coded system, the spectral efficiency η (bits/symbol/Hz) of *M*-PSK and *M*-QAM schemes is the number of information bits carried by each symbol. It is computed by

$$\eta = R \cdot \log_2 M = R \cdot m \tag{4.9}$$

where R is the coding rate.

4.1.2.1 Trellis coded modulation (TCM)

The main principle of TCM [7] is based on modulation by set partitioning. More specifically, the partition of the modulating constellation in TCM is assigned based on the trellis diagram of convolutional codes in order to increase the minimum Euclidean distance of the code sequences. Various methods have been developed to improve the performance of TCM, which include multiple TCM [53] and higher dimension TCM [54]. Turbo-TCM (TTCM) [55] is a derivative of TCM and turbo coding. It increases time diversity by using a symbol interleaver between two concatenated TCM components. Moreover, an iterative technique is used at the receiver to improve error performance. TCM is used only with convolutional codes, and this technique cannot be applied to block codes such as LDPC codes.

4.1.2.2 Multilevel coded modulation (MLC)

In [56], Imai and Hirakawa proposed another coded modulation scheme, known as multilevel coded modulation (MLC). The philosophy of MLC is based on the combination of encoders at the transmitter and decoders at the receiver, as well as one signal constellation. Each level in this system can use convolutional codes or block codes. Hence, this method can be applied to block codes such as LDPC codes. However, coded modulation using the MLC scheme is less flexible and more complicated due to its parallel structure. The codewords of each component encoder are mapped into one appointed position of the constellation labels. As the constellation size increases, the number of required component codes becomes larger. For example, it is necessary to employ four encoders for a coded 16-QAM system.

4.1.1.3 Bit interleaved coded modulation (BICM)

The above two schemes can attain a good performance, but the complexity is also significantly high. More recently, another combined coding and modulation scheme which is a derivative of the MLC scheme using single binary codes, called bit interleaved coded modulation (BICM), was proposed by Caire [57]. He has shown that BICM with Gray mapping of signal points can perform very close to capacity limits. The important aspect is that a bit-wise interleaver is employed between the modulation block and the convolutional encoder. At the receiver side, a soft demodulator uses the received noisy signal to compute the log likelihood ratios (LLR) for the coded bits. These LLRs are used as the decoder input. Finally, the decoder processes the de-interleaved metrics and outputs the decisions. The decoding process is the same as for the MLC scheme. The independence of the different code bits for the BICM scheme is based on the assumption of an ideal bit interleaver.

4.1.1.4 LDPC-coded modulation

In 2001, an LDPC-coded modulation scheme based on the MLC technique was designed to achieve bandwidth-efficient transmission [41]. LDPC-coded modulation implements a serial concatenation of LDPC coding and high-level modulation mapping. Recently, various LDPC-coded modulation schemes have been proposed [42]-[50]. For example, algebraic LDPC codes is studied in [44]. Non-binary LDPC codes over GF(q) and q-ary modulations is studied in [45]. The mapping influence on LDPC-coded modulation over static and Rayleigh fading channels is evaluated in [46]. Furthermore, a bit reliability mapping strategy is discussed in [47], this strategy is only applicable to irregular LDPC codes which have unequal variable node degrees.

LDPC-coded modulation using BICM scheme is investigated in [48]. The main advantage is that a single encoder/decoder is adequate to encode/decode these multi-rate codes. Thus, it is possible to implement them in a mobile phone. Besides, another benefit for employing LDPC codes with the BICM scheme is that the interleaver can be dropped from this scheme, since LDPC codes inherently make the adjacent coded bits independent. This approach is practical but quite effective for bandwidth-efficient transmission, because only one encoder and one decoder are required. For this reason, the proposed LDPC-coded modulation system in this thesis is designed with the BICM scheme.

4.2 LDPC-coded modulation system model

We design an LDPC-coded modulation system which is shown in Fig. 4.2. We assume that after encoding, the modulated M-PSK and M-QAM signals with Gray mapping are transmitted over both AWGN and uncorrelated Rayleigh fading channels, where the LDPC encoder and M-ary modulator are designed separately in order to achieve both power and bandwidth efficiency. Especially for the Rayleigh channel, we focus on the square QAM schemes specified in the WiMAX standard [14], i.e. QPSK, 16-QAM and 64-QAM.

At the transmitter, the input bits are encoded by the LDPC encoder which was presented in Chapter 3. The encoded bits are mapped into symbols using Gray mapping constellations.

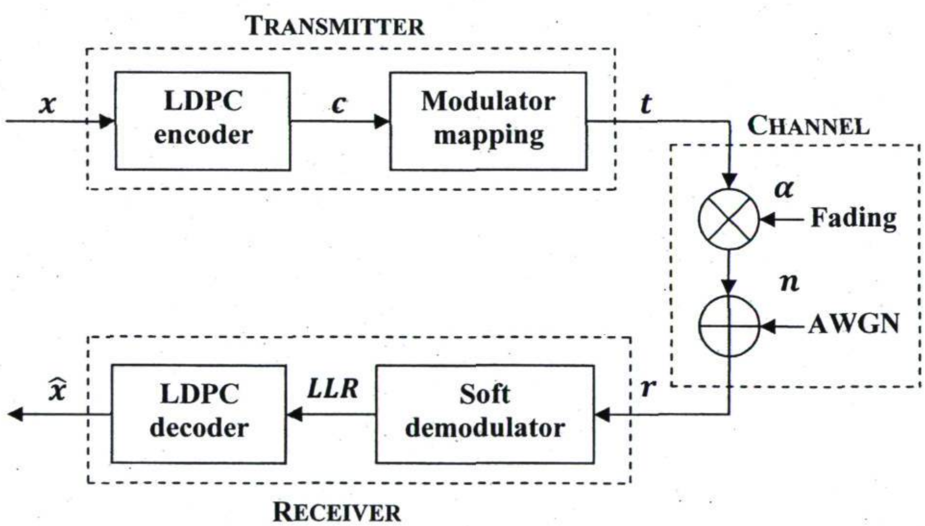

Figure 4.2: Block diagram of LDPC-coded modulation system.

At the receiver, the received signal is $\boldsymbol{r} = \boldsymbol{\alpha} \cdot \boldsymbol{t} + \boldsymbol{n}$, and $\boldsymbol{r}$ is processed in two steps as shown in Fig. 4.2. The first step corresponds to the calculation of LLR values by the soft symbol-to-bit demodulator which is based on the maximum likelihood criterion [57]. Then the LLR values are passed to the iterative Log-BP LDPC decoder at the second step.

4.2.1 Encoder and decoder

We adopt the LDPC encoder specified in the WiMAX standard. The WiMAX LDPC codes flexibly support 19 different code lengths, ranging from 576 to 2304 bits [14], and the protocol proposes four code rates, i.e. 1/2, 2/3, 3/4 and 5/6.

As mentioned above, a bit interleaver is not necessary between the LDPC encoder and the M-ary modulator. Even if the system experiences correlated fading [49], LDPC codes have a generic embedded interleaver that insures that the coded bits are nearly independent.

4.2.2 Mapping and modulator

For LDPC-coded modulation, a direct mapping scheme uses a group of $\log_2 M$ consecutive bits of LDPC codewords to select a subset in the signal constellation. Gray mapping is employed in this LDPC-coded modulation system because it is superior over partition mapping [58] or natural mapping [46].

As an example, 16-QAM can be treated as two independent 4-PAM on the in-phase and quadrature components, respectively. Each constellation point can represent $\log_2 16 = 4$ bits and take the values (-3, -1, 1, 3) on the axes as shown in Table 4.2. As can be observed from Fig. 4.3, the adjacent constellation symbols differ by only one bit in the Gray-coded mapping scheme.

Table 4.2: Gray-coded constellation mapping for 16-QAM.

$t^I = (x_1\, x_2)$	In-phase	$t^Q = (x_3\, x_4)$	Quadrature
0 0	-3	0 0	-3
0 1	-1	0 1	-1
1 1	1	1 1	1
1 0	3	1 0	3

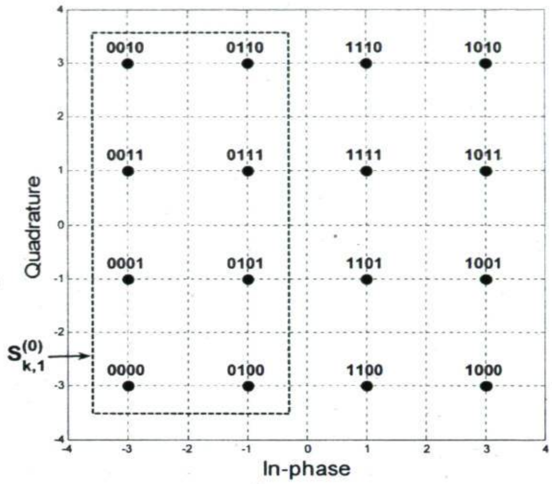

Figure 4.3: 16-QAM constellation with Gray coded mapping. $S_{k,1}^{(0)}$ comprises symbols with $x_{k,1} = 0$, which is encompassed by a dashed box.

4.2.3 Soft LLR demodulator

4.2.3.1 Exact LLR

In the LLR demodulator at the receiver side, assume a linear discrete time channel, at index k,

$$r_k = \alpha_k \cdot t_k + n_k \tag{4.10}$$

where α_k is the fading amplitude (assume α is constant over one symbol interval) and n_k is the complex AWGN. The received signal r_k will be used to produce the LLR of symbol bits as the decoder input. Let $x_{k,i}$ denote the i^{th} code bit, $(i = 1, 2, \ldots, \log_2 M)$ of the modulated symbol t_k. For example, as shown in Fig. 4.3, the coded bits in 16-QAM can be represented as $t = (x_1, x_2, x_3, x_4)$. The LLR of x_i at index k, $l(x_{k,i})$ is defined as

$$l(x_{k,i}) = \log\left(\frac{\Pr(x_{k,i} = 0 | r_k)}{\Pr(x_{k,i} = 1 | r_k)}\right) \tag{4.11}$$

The optimal decision rule is to decide, $x_{k,i} = 1$ if $l(x_{k,i}) \leq 0$, and 0 otherwise. We define that $S_{k,i}^{(0)}$ comprises symbols with $x_{k,i} = 0$ and $S_{k,i}^{(1)}$ comprises symbols with $x_{k,i} = 1$ in the constellation. Then from (4.11), we have,

$$l(x_{k,i}) = \log\left(\frac{\sum_{s\in S_{k,i}^{(0)}} \Pr(t_k = s|\, r_k)}{\sum_{s\in S_{k,i}^{(1)}} \Pr(t_k = s|\, r_k)}\right) \tag{4.12}$$

Assume that all symbols are equally likely and that fading is independent of the transmitted symbols t_k. Using Baye's rule, we have

$$l(x_{k,i}) = \log\left(\frac{\sum_{s\in S_{k,i}^{(0)}} \Pr(\, r_k | t_k = s)}{\sum_{s\in S_{k,i}^{(1)}} \Pr(\, r_k | t_k = s)}\right) \tag{4.13}$$

with the Gaussian conditional probability density function for r_k given by

$$\Pr(\, r_k | s = t_k) = \frac{1}{\sqrt{2\pi}\sigma} \exp\left(-\frac{|r_k - a_k \cdot s|^2}{2\sigma^2}\right) \tag{4.14}$$

Thus,

$$l(x_{k,i}) = \log\left(\frac{\sum_{s\in S_{k,i}^{(0)}} \exp\left(-\frac{|r_k - a_k \cdot s|^2}{2\sigma^2}\right)}{\sum_{s\in S_{k,i}^{(1)}} \exp\left(-\frac{|r_k - a_k \cdot s|^2}{2\sigma^2}\right)}\right) \tag{4.15}$$

If we assume ideal channel state information (CSI) at the receiver, and let $y_k = r_k / a_k$, we have

$$l(x_{k,i}) = \log\left(\frac{\sum_{s\in S_{k,i}^{(0)}} \exp\left(-\frac{|y_k - s|^2}{2\sigma^2}\right)}{\sum_{s\in S_{k,i}^{(1)}} \exp\left(-\frac{|y_k - s|^2}{2\sigma^2}\right)}\right) \tag{4.16}$$

4.2.3.2 Approximate LLR

We can notice that computation of (4.15) involves M exponential operations, which is complex for real applications. Therefore, to reduce the computational complexity, we use the "max-log" operation [59], i.e.

$$\log\left(\sum_j \exp\left(-f_j\right)\right) \approx \max_j\left(-f_j\right) = -\min_j\left(f_j\right) \tag{4.17}$$

Hence, (4.17) can be approximated by the following real signals,

$$\begin{aligned} l(x_{k,i}) &= \log\left(\sum\nolimits_{s\in S_{k,i}^{(0)}} \exp\left(-\frac{|r_k - a_k\cdot s|^2}{2\sigma^2}\right)\right) - \log\left(\sum\nolimits_{s\in S_{k,i}^{(1)}} \exp\left(-\frac{|r_k - a_k\cdot s|^2}{2\sigma^2}\right)\right) \\ &= \max\nolimits_{s\in S_{k,i}^{(0)}}\left(-\frac{|r_k-a_k\cdot s|^2}{2\sigma^2}\right) - \max\nolimits_{s\in S_{k,i}^{(1)}}\left(-\frac{|r_k-a_k\cdot s|^2}{2\sigma^2}\right) \\ &= -\frac{1}{2\sigma^2}\left(\min\nolimits_{s\in S_{k,i}^{(1)}}(|r_k - a_k\cdot s|^2) - \min\nolimits_{s\in S_{k,i}^{(0)}}(|r_k - a_k\cdot s|^2)\right) \\ &= -\frac{|a_k|^2}{2\sigma^2}\left(\min\nolimits_{s\in S_{k,i}^{(1)}}(|y_k - s|^2) - \min\nolimits_{s\in S_{k,i}^{(0)}}(|y_k - s|^2)\right) \end{aligned} \tag{4.18}$$

Still using 16-QAM as an example, 4 bits are transmitted by a 16-QAM symbol at each time index. The LLRs of the 4 bits, $x_{k,1}$, $x_{k,2}$, $x_{k,3}$ and $x_{k,4}$ received at time index k are calculated as follows,

$$\begin{aligned} l(x_{k,1}) &= -\frac{1}{2\sigma^2}\left(\min(\,|r_k^I + a_k|^2,\ \ |r_k^I + 3a_k|^2) - \min\,(\,|r_k^I - a_k|^2,\ |r_k^I - 3a_k|^2)\right) \\ l(x_{k,2}) &= -\frac{1}{2\sigma^2}\left(\min(\,|r_k^I - a_k|^2,\ \ |r_k^I + 3a_k|^2) - \min\,(\,|r_k^I + a_k|^2,\ |r_k^I - 3a_k|^2)\right) \\ l(x_{k,3}) &= -\frac{1}{2\sigma^2}\left(\min\left(\left|r_k^Q + a_k\right|^2,\ \left|r_k^Q + 3a_k\right|^2\right) - \min\left(\left|r_k^Q - a_k\right|^2,\ \left|r_k^Q - 3a_k\right|^2\right)\right) \\ l(x_{k,4}) &= -\frac{1}{2\sigma^2}\left(\min\left(\left|r_k^Q - a_k\right|^2,\ \left|r_k^Q + 3a_k\right|^2\right) - \min\left(\left|r_k^Q + a_k\right|^2,\ \left|r_k^Q - 3a_k\right|^2\right)\right) \end{aligned} \tag{4.19}$$

where $r_k = r_k^I + jr_k^Q$.

In summary, compared with the conventional LLR demodulator, the approximate LLR modulator can reduce the computational complexity without performance loss [60].

4.3 Adaptive LDPC-coded modulation for flat slowly-varying Rayleigh fading

With the ever-increasing demand for high speed and high quality of service (QoS) for wireless mobile devices, the radio spectrum becomes more limited and crowded. Hence, to efficiently use the available spectrum while maintaining desirable performance is an important trend for wireless communication development. As can be expected, this system is designed to be more intelligent and flexible, able to adapt and adjust the transmission parameters based on the link quality, improving the spectral efficiency, and reaching a maximum achievable throughput. Link adaptation techniques, such as adaptive coded modulation (ACM), are a good way to achieve the purpose indicated above. They are capable of tracking the channel variations, thus changing the modulation and coding schemes to yield a higher throughput by transmitting with high information rates under favorable channel conditions and reducing the information rate in response to channel degradation.

We focus on studying these techniques and design an adaptive LDPC-coded modulation system for flat slowly-varying Rayleigh fading environment with the parameters specified in the WiMAX standard. A theoretical explanation, necessary to understand the operation principles of ACM, is presented in the following.

4.3.1 Adaptive coded modulation techniques

Like we studied in Section 4.2, traditional coded modulation (non-adaptive) systems are made of fixed encoders and modulators for fading channels. But due to the time-variability of fading channels, the transmission is designed under the worst-case channel conditions to obtain acceptable transmission performance, while resulting in insufficient utilization of the radio spectrum.

Adaptive coded modulation (ACM) is designed by adapting the transmit power, coding rate (encoding) and modulation (size of the signal constellation) scheme to the corresponding channel conditions at the receiver. The basic principle of ACM is that a higher data rate is transmitted during good channel conditions, while a lower data rate is transmitted during poor channel conditions.

Based on these adaptive theories, [61] showed an adaptive variable-rate variable-power transmission scheme using uncoded *M*-QAM. Moreover, an adaptive trellis-coded PSK scheme for Rayleigh fading channels was proposed in [18]. Currently, next generation communication systems such as WiMAX [14], WiFi [15], HiperLAN/2 [62] and 4G are beginning to explore link adaptation in order to increase spectral efficiency.

4.3.2 Flat slowly-varying Rayleigh fading

Adaptive coded modulation can be applied to frequency-selective channels on each sub-channel in a multi-carrier system, i.e. an orthogonal frequency-division multiplexing (OFDM) scheme [63], or flat fading [64]. In this thesis, we consider the flat slowly-varying Rayleigh channel for the proposed ACM scheme.

For flat fading, the channel SNR is the same for all frequencies and can be regarded as nearly constant for short periods of time. This makes it possible to feed back relevant CSI to the transmitter using a feedback or return channel [65]. However, the challenge associated with adaptive coded modulation is that the mobile channel is time-varying, and thus, the feedback of the channel information becomes a limiting factor. Hence, a slowly-varying fading environment is assumed in order to achieve an accurate performance of the ACM scheme. Furthermore, no delay or transmission error can occur in the feedback channel so that no difference between the predicted and the actual SNR of the next frame appears [66].

To represent a slowly-varying fading channel, we adopt a block-fading channel model [67] to implement frame by frame adaptation, i.e., the fading amplitude remains invariant during a frame, but varies from frame to frame, as will be presented in the following.

4.3.2.1 Rayleigh block-fading channel

Block-fading channels are characterized by the fact that the noise severity remains constant in blocks of some consecutive transmitted symbols but are independent from block to block [68]. The block-fading channel can be a model for multi-carrier communication systems such as OFDM, frequency-hopped spread spectrum and also the slow fading channel we use.

Recall the flat Rayleigh fading channel modeled in section 3.3.2. The signal at the receiver is given by

$$\boldsymbol{r} = \boldsymbol{\alpha} \cdot \boldsymbol{t} + \boldsymbol{n}$$

where $\boldsymbol{\alpha}$ is the fading amplitude, $\boldsymbol{t}$ is the transmitted signal and $\boldsymbol{n}$ is the complex AWGN. The term, "flat" means that all signal frequencies are attenuated by the same fading factor and the phase of the fading signal is uniformly distributed between 0 and 2π.

For the block-fading structure, each codeword (frame) of n_{sc} symbols is split into several sub-blocks, and each sub-block of length n_{sh} is affected by the same fading factor. As shown in Fig. 4.4, we define,

- n_{sc} is the number of symbols per codeword;
- n_{bs} is the number of bits per symbol;
- n_{sh} is the number of symbols per sub-block;
- n_{hc} is the number of sub-blocks per codeword;

and all parameters are supposed integer.

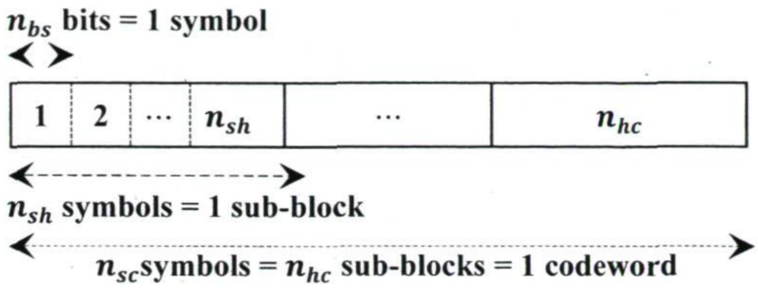

Figure 4.4: Frame structure.

We find the following special cases.

- Transmission over a slow fading channel [68], when $n_{hc} = 1$ or $n_{sh} = n_{sc}$, i.e., the entire codeword is affected by the same fading gain (used for the slow-varying fading channel in this thesis).
- Transmission over a fast fading channel, when $n_{hc} = n_{sc}$ or $n_{sh} = 1$, each symbol is affected by an independent fading amplitude (used for fast fading in the previous sections).

4.3.2.2 Error performance over a Rayleigh block-fading channel

We examine the performance of LDPC-coded modulation over a Rayleigh block-fading channel with ideal CSI. We consider an LDPC code with code length 2304 and code rate 1/2 transmitted by QPSK modulation over a flat Rayleigh block-fading channel, when varying the number of symbols per independent sub-block, n_{sh}. The number of bits per modulated symbol is $m = \log_2 4 = 2$, so that the number of symbols per codeword is $n_{sc} = 2304/2 = 1152$. For the sake of comparison, the number of symbols per sub-block is varied from $n_{sh} = 1$ (keeping constant over a symbol), to 144, 576 and 1152 (fading is constant over a frame). The corresponding number of sub-blocks per codeword n_{hc} is thus $n_{hc} = 1152, 32, 8, 4, 2$ and 1.

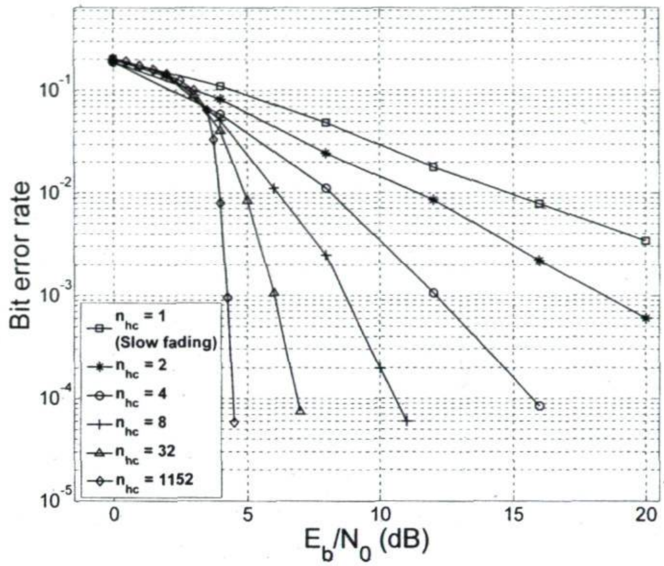

Figure 4.5: BER performance of WiMAX LDPC code with code length 2304 and code rate 1/2 transmitted using QPSK modulation over a flat Rayleigh block-fading channel.

In Fig. 4.5, the results are given in terms of BER versus the SNR per information bit. We can clearly see that the different behaviour of the code with different lengths of sub-blocks per codeword. It can be observed that the performance improves as the length of the sub-block increases, and is at best when fading is constant over the entire block. This is because the fewer the number of sub-blocks per codeword, the larger is the number of coded bits per sub-block. The fading amplitudes in a sub-block are considered correlated, thus the correlation of the probabilistic information transmitted into the LDPC decoder becomes larger.

Later, we will adopt this kind of fading channel when the number of sub-blocks per codeword n_{hc} is 1 to implement an adaptive coded scheme with frame by frame adaptation over slowly-varying Rayleigh fading channels.

4.4 Adaptive LDPC-coded modulation system model

In this section, we design an adaptive system for LDPC-coded modulation using BPSK, QPSK, 16-QAM and 64-QAM as specified in the WiMAX [14] and WiFi [15] standards, for a flat slowly-varying Rayleigh fading channel.

A simplified block diagram for this adaptive scheme is shown in Fig. 4.6. At the transmitter, LDPC ACM provides multiple transmission modes, where each mode is specified by a modulation and a FEC code pair as in WiMAX. The transmitter selects an ACM mode for transmission and adapts the transmit power on a frame-by-frame basis based on the CSI feedback from the receiver.

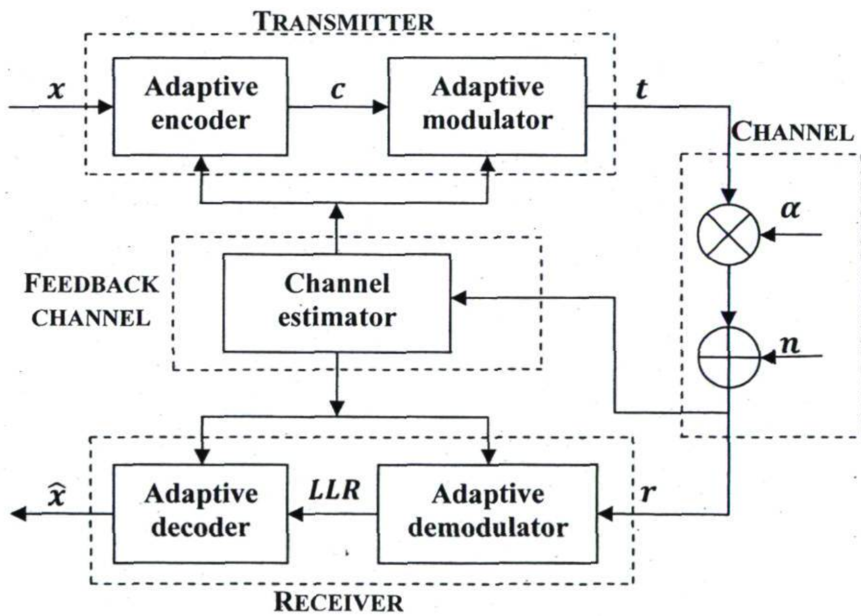

Figure 4.6: Adaptive LDPC-coded transmission system.

At the receiver, we adopt a soft ML demodulator and a Log-BP LDPC decoder. Each frame contains the number of symbols $n_{sc} = n/m$ which depends on the type of encoding and modulation, where n is the codeword length and $m = \log_2 M$ is the number of bits per modulated symbol. We assume perfect channel estimates at the receiver and perfect CSI at the transmitter.

4.4.1 Adaptation threshold

To select the appropriate mode for the ACM system, we need to know the SNR thresholds. We assume that L modulation and code pairs are candidates for the ACM system. The transmitter decides which pair should be used at the start of each transmission according to a given set of SNR thresholds. For a certain level of BER, we consider choosing $L-1$ adaption thresholds, $\gamma \in \{\gamma_1, \gamma_2, \dots \gamma_{L-1}\}$ for instantaneous SNR (E_s/N_0) for every transmitted frame. Thus, each of the L candidates is assigned to operate in a particular SNR region. When the threshold γ falls within a given SNR region, $\gamma_l \leq \gamma \leq \gamma_{l+1}$, where $l \in \{1, 2, \dots L-1\}$, the associated CSI is sent back to the transmitter to adapt its corresponding modulation and coding mode. This enables the LDPC-coded modulation system to transmit with high spectral efficiency when the SNR is high, and to reduce the spectral efficiency as the SNR decreases. The corresponding spectral efficiency of each candidate is denoted η_l, and $\eta_1 < \eta_2 < \cdots < \eta_L$.

We adapt the method in [18] to obtain the thresholds from the BER versus SNR for each candidate of coding and modulation on AWGN channels. The threshold for a given code is then found by curve fitting on the simulated BER at a specific BER_0.

Example

As an intuitive example, consider a simple adaptive uncoded modulation system with four modulation modes, i.e., BPSK, QPSK, 16-QAM and 64-QAM. As shown in Fig. 4.7, there are three SNRs, γ_1, γ_2 and γ_3 to control the selection of a proper modulation mode. Thus, when $0 \leq \text{SNR} \leq \gamma_1$, BPSK is employed, when $\gamma_1 \leq \text{SNR} \leq \gamma_2$, QPSK is adopted. Consequently, when $\text{SNR} \geq \gamma_3$, 64-QAM is used for this adaptive transmission over a fading environment.

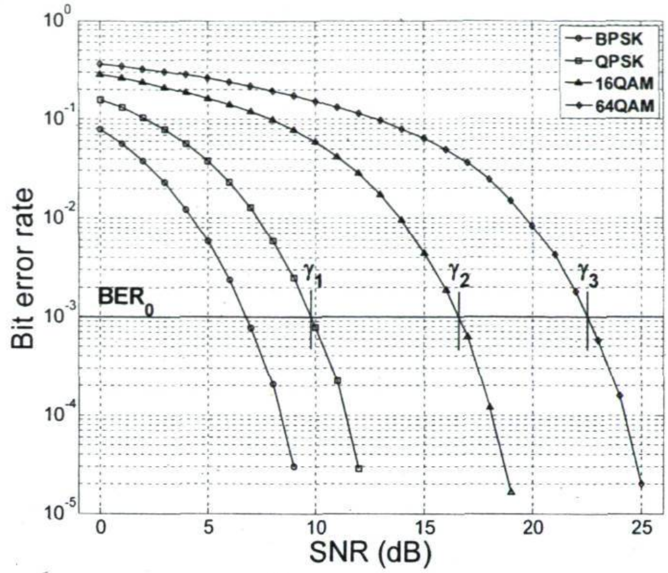

Figure 4.7: BER versus SNR relationship and corresponding SNR thresholds ($\gamma_1 = 9.7$, $\gamma_2 = 16.5$, $\gamma_3 = 22.5$ dB) for four modulation modes employed by an adaptive modulation system.

4.4.2 SNR estimation

The SNR per symbol, E_s/N_0 is evaluated by the channel estimator. The instantaneous SNR for each frame is defined as [18],

$$\gamma_w = \alpha_w^2 (E_s/N_0) \tag{4.20}$$

where w is the index of the transmitted frame.

As mentioned before, when $0 \leq \gamma_w \leq \gamma_1$, the first pair of modulation and encoding schemes is employed during the w^{th} transmitted frame. When γ_w satisfies the following inequality,

$$\gamma_l \leq \gamma_w \leq \gamma_{l+1} \qquad (l = 1, 2, \dots L-1) \tag{4.21}$$

the $(l+1)^{th}$ pair is employed. We can deduce the inequality for the instant fading amplitude, α_w, when the $(l+1)^{th}$ scheme is employed [18],

$$\sqrt{\frac{\gamma_l}{E_s/N_0}} \leq \alpha_w \leq \sqrt{\frac{\gamma_{l+1}}{E_s/N_0}} \qquad (l = 1,2, \dots L-1) \tag{4.22}$$

The adaptation thresholds for the fading amplitude are then determined by the relationship $\sqrt{\frac{\gamma_l}{E_s/N_0}} = v_l$, thus

$$v_l \leq \alpha_w \leq v_{l+1} \qquad (l = 1,2, \dots L-1) \tag{4.23}$$

4.4.3 Average spectral efficiency

The main advantage of ACM is that it can explore and make good use of the time-varying nature of the radio channel. It can not only keep the performance at an acceptable level but can also raise spectral efficiency. Thus, due to its adaptive nature, the spectral efficiency of the proposed adaptive LDPC-coded modulation scheme is varied as a function of the instantaneous SNR. The average spectral efficiency can be defined as the average number of information bits transmitted per symbol duration. As defined previously, there are L candidate pairs of modulation and code, and the corresponding spectral efficiencies are $(\eta_1, \ \eta_2, \dots \eta_L)$, respectively. The average spectral efficiency (ASE) (bits/s/Hz) $\bar{\eta}$ is defined as [69]:

$$\bar{\eta} = \sum_{l=1}^{L} \eta_l \cdot \mathrm{P}_l(\alpha) \tag{4.24}$$

where $\mathrm{P}_l(\alpha)$ is the Rayleigh probability distribution for α being in the interval $[v_l, \ v_{l+1}]$, here $v_l = \sqrt{\frac{\gamma_l}{E_s/N_0}}$, and recall that the probability density function of the Rayleigh distribution given by

$$\mathrm{P}(\alpha) = 2\alpha \cdot \exp(-\alpha^2)$$

Thus, the average spectral efficiency is expressed by,

$$\bar{\eta} = \eta_1 \cdot \mathrm{P}(0 \leq \alpha \leq v_1) + \eta_2 \cdot \mathrm{P}(v_1 \leq \alpha \leq v_2) + \cdots + \eta_L \cdot \mathrm{P}(v_{L-1} \leq \alpha \leq \infty) \tag{4.25}$$

Since

$$\mathrm{P}(v_l \le \alpha \le v_{l+1}) = \int_{v_l}^{v_{l+1}} \mathrm{P}(\alpha)d\alpha = \int_{v_l}^{v_{l+1}} 2\alpha \cdot \exp(-\alpha^2)\, d\alpha$$

$$= \exp(-{v_l}^2) - \exp(-{v_{l+1}}^2) \tag{4.26}$$

we thus have,

$$\bar{\eta} = \eta_1 \cdot [\exp(-{v_0}^2) - \exp(-{v_1}^2)] + \eta_2 \cdot [\exp(-{v_1}^2) - \exp(-{v_2}^2)] +$$

$$\cdots + \eta_L \cdot [\exp(-{v_{L-1}}^2) - \exp(-{v_L}^2)]$$

$$= \sum_{l=1}^{L} \eta_l \cdot [\exp(-\,{v_{l-1}}^2) - \exp(-\,{v_l}^2)] \tag{4.27}$$

where $v_0 = 0, v_L = \infty$.

Chapter 5

Simulation results and analysis

In the last chapter, we presented a power and bandwidth-efficient LDPC-coded modulation system for transmission over both additive white Gaussian noise (AWGN) and uncorrelated Rayleigh fading channels. In this system, the data bits are first encoded using a WiMAX LDPC encoder and then mapped into two-dimensional signal constellations, i.e., M-ary phase shift keying (M-PSK) or M-ary quadrature amplitude modulation (M-QAM) at the transmitter. At the receiver side, a soft maximum likelihood (ML) demodulator and a logarithmic belief propagation (Log-BP) LDPC decoder are employed. Furthermore, an adaptive LDPC-coded modulation system for flat slowly-varying Rayleigh channels was proposed using the method in [18].

In this chapter, numerical simulation results using MATLAB according to these proposed coded modulation systems are depicted and discussed. We first evaluate the performance of the LDPC-coded modulation system. Then, the proposed adaptive coded scheme employing LDPC codes is analyzed in detail through bit error rate (BER) and average spectral efficiency (ASE) performances.

5.1 Performances of LDPC-coded modulation

In this section, the performances of the LDPC-coded modulation scheme advocated are evaluated from three aspects, i.e., various spectral efficiencies of LDPC-coded *M*-QAM on AWGN channels, performances over uncorrelated Rayleigh fading channels and constellation rotation effects on LDPC-coded *M*-PSK modulation.

The overall simulation parameters for this section are summarized in Table 5.1. We adopt the rate-flexible WiMAX LDPC codes which have four coding rate, i.e. 1/2, 2/3, 3/4 and 5/6. The code rates are adjusted for different modulation and design purposes. Note that there are two code classes with rate 2/3, 2/3A and 2/3B, and two with rate 3/4, 3/4A and 3/4B. We select code rates 2/3A and 3/4B for the system due to their better performances as explained in section 3.1.1.1. Moreover, because performances improve with increasing code length, we choose a code length of 2304 bits (the maximum code size defined in WiMAX) to obtain the best performances.

Table 5.1: Simulation parameters used for the LDPC-coded modulation system.

LDPC codes	WiMAX LDPC codes (code length is 2304, code rates are 1/2, 2/3, 3/4 and 5/6)
Encoding	Richardson-Urbanke algorithm
Modulation	QAM, PSK, with Gray mapping
Channel	AWGN
	Uncorrelated Rayleigh fading
Demodulation	Soft ML
Decoding	Log-BP algorithm (Maximum number of decoding iterations is 30)

5.1.1 Performances over an AWGN channel

We start by discussing the performance of the proposed LDPC-coded modulation scheme transmitted over an AWGN channel. Eight levels of *M*-QAM schemes are employed, i.e., QPSK (4-QAM), 8-QAM, 16-QAM, 32-QAM, 64-QAM, 128-QAM, 256-QAM and 512-QAM, which can offer uncoded spectral efficiencies from 2 to 9 bits/s/Hz. In addition, the LDPC coding scheme uses code rates of 1/2, 2/3, 3/4 and 5/6. The corresponding coded spectral efficiencies are given in Table 5.2. The spectral efficiency (bits/s/Hz) is computed using $\eta = R \cdot \log_2 M$, where R is the coding rate and M is the constellation size. The BER performance of these eight LDPC-coded QAM schemes with coding rate of 1/2, 2/3, 3/4 and 5/6, respectively, is shown in Fig. 5.1 to Fig. 5.4.

Table 5.2: Various spectral efficiencies of LDPC-coded *M*-QAM. Note that some schemes have the same spectral efficiency (highlighted by underlines).

Modulation	Spectral efficiency (bits/s/Hz)				
	Uncoded	Code rate 1/2	Code rate 2/3	Code rate 3/4	Code rate 5/6
QPSK	2	1.0	1.3	<u>1.5</u>	1.7
8-QAM	3	<u>1.5</u>	<u>2.0</u>	2.3	<u>2.5</u>
16-QAM	4	<u>2.0</u>	2.7	<u>3.0</u>	<u>3.3</u>
32-QAM	5	<u>2.5</u>	<u>3.3</u>	3.8	4.2
64-QAM	6	<u>3.0</u>	<u>4.0</u>	<u>4.5</u>	5.0
128-QAM	7	3.5	4.7	<u>5.3</u>	5.8
256-QAM	8	<u>4.0</u>	<u>5.3</u>	<u>6.0</u>	6.7
512-QAM	9	<u>4.5</u>	<u>6.0</u>	6.8	7.5

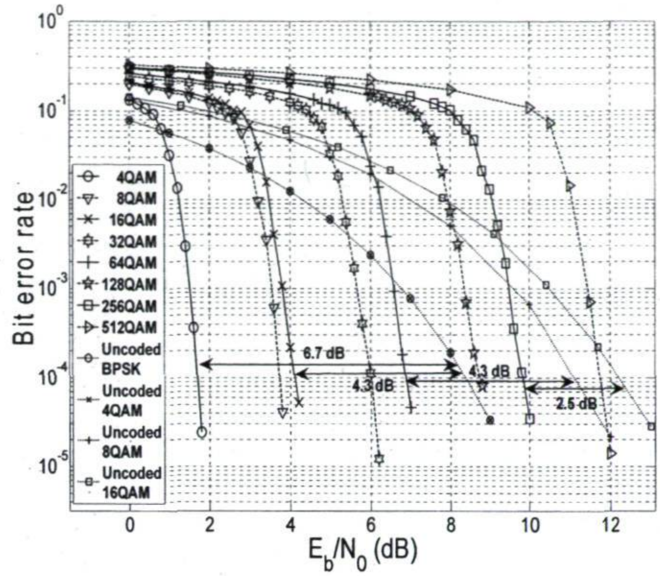

Figure 5.1: BER performances of LDPC-coded M-QAM with coding rate 1/2 transmitted over an AWGN channel.

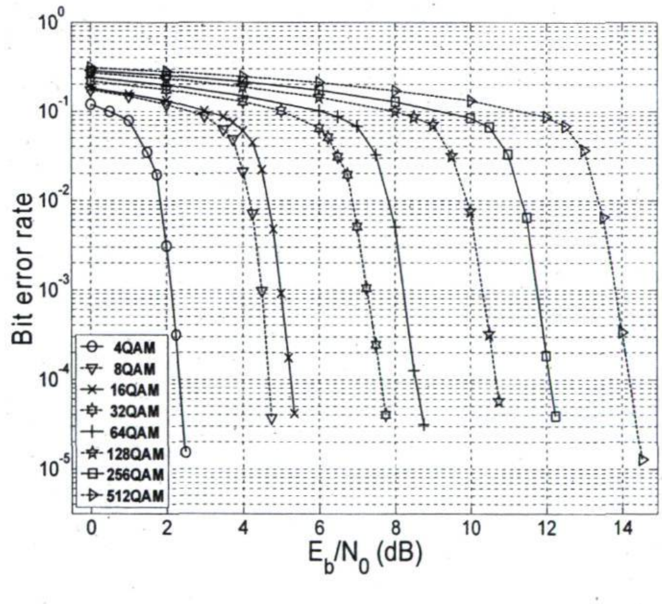

Figure 5.2: BER performances of LDPC-coded M-QAM with coding rate 2/3 transmitted over an AWGN channel.

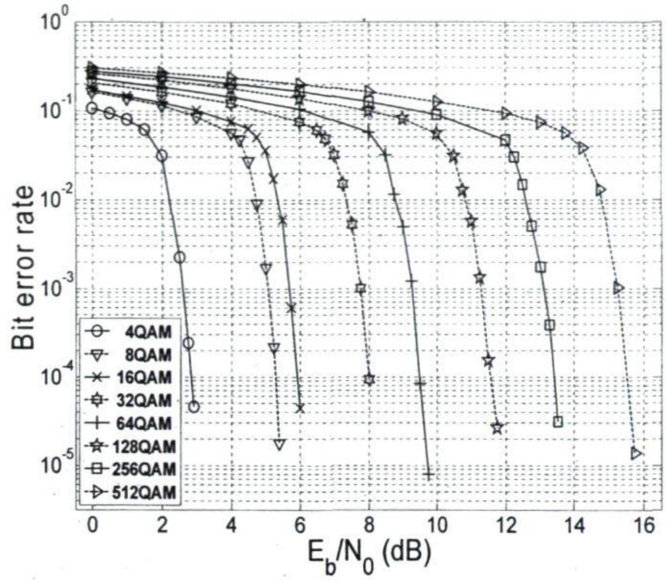

Figure 5.3: BER performances of LDPC-coded *M*-QAM with coding rate 3/4 transmitted over an AWGN channel.

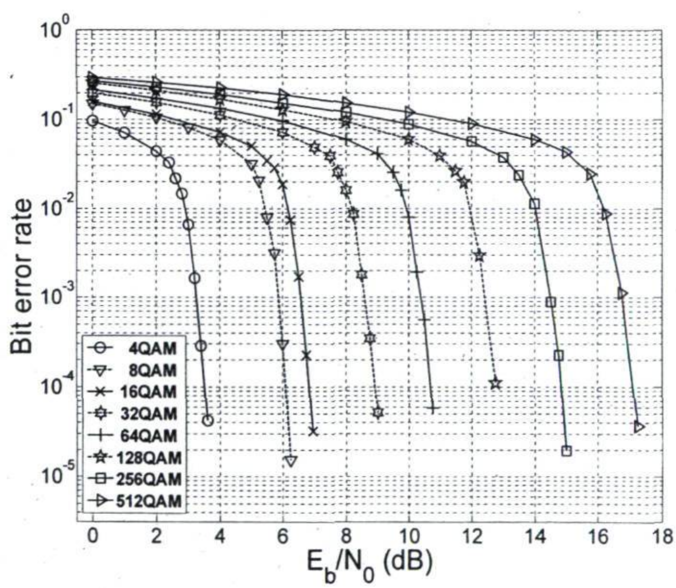

Figure 5.4: BER performances of LDPC-coded *M*-QAM with coding rate 5/6 transmitted over an AWGN channel.

5.1.1.1 Comparisons between the coded and uncoded QAM schemes

For comparison purposes, four uncoded modulations with spectral efficiencies of 1, 2, 3 and 4 bits/s/Hz, respectively, i.e., uncoded BPSK, QPSK, 8-QAM and 16-QAM are shown in Fig. 5.1. The corresponding coded QAM schemes with the same spectral efficiencies are thus coded QPSK, 16-QAM, 64-QAM, and 256-QAM, with coding rate 1/2 (see Table 5.2).

As shown in Fig. 5.1, the coding gains over the uncoded QAM schemes at a BER of 10^{-4} are 6.7, 4.3, 4.3 and 2.5 dB, respectively. We can observe that the SNR gap between different uncoded modulation schemes increases gradually (except for BPSK and QPSK) and the four corresponding coded QAM schemes have SNR gaps of 2 to 3 dB between each other; thus the coding gain decreases as the spectral efficiency increases. Therefore, coded QPSK has the maximum coding gain and the coding gains of coded 16-QAM and 64-QAM is greater than that of 256-QAM. It can be inferred from this observation that the lower and moderate-order QAM schemes (for example, coded QPSK or 16-QAM) are more efficient at improving performance as compared to high-order QAM for our LDPC-coded QAM scheme transmitted over an AWGN channel.

5.1.1.2 Various spectral efficiencies

Observing figures 5.1 to 5.4, we find that they have something in common: for coded cross 8-QAM, the BER curves are quite far from that of coded 4-QAM, and relatively close to that of coded 16-QAM. Thus, for a BER of 10^{-4}, coded 8-QAM with coding rate 1/2 has a gain of just 0.2 dB over coded 16-QAM, but with a loss of spectral efficiency of 0.5 bits/s/Hz compared to coded 16-QAM. Therefore, in practical applications, the coded cross 8-QAM scheme could be replaced by coded square 16-QAM with a little sacrifice in SNR when pursuing higher spectral efficiency. It can be explained that 8-QAM has a much larger average bit energy than QPSK while having slightly smaller average bit energy than that of 16-QAM, for a constant minimum distance between signal points in the constellations. For coded cross 32-QAM and 128-QAM, the SNR gaps to the square coded

QAM schemes on both sides are almost the same. Therefore, the trade-off described above does not apply for these two cross constellations.

Among the various spectral efficiencies of the coded *M*-QAM system which are shown in Table 5.2, there are nine pairs of coded modulation schemes with the same spectral efficiencies. We should choose one combination with better power efficiency for each code-modulation pair. The comparisons of their SNRs at a BER of 10^{-4} are given in Table 5.3, where lower order QAM schemes are placed on the left column (Scheme-1); accordingly, the lower coding rate schemes are on the right (Scheme-2).

Table 5.3: Power efficiency (SNR) comparisons between the coded modulation schemes with the same spectral efficiencies at a BER of 10^{-4}, where the smaller SNRs are highlighted by underlines.

Spectral efficiency (bits/s/Hz)	Scheme-1			Scheme-2		
	Code rate	Modulation	SNR (dB)	Code rate	Modulation	SNR (dB)
1.5	3/4	QPSK	<u>2.8</u>	1/2	8-QAM	3.8
2.0	2/3	8-QAM	4.7	1/2	16-QAM	<u>4.1</u>
2.5	5/6	8-QAM	<u>6.0</u>	1/2	32-QAM	6.1
3.0	3/4	16-QAM	<u>5.9</u>	1/2	64-QAM	6.9
3.3	5/6	16-QAM	<u>6.7</u>	2/3	32-QAM	7.6
4.0	2/3	64-QAM	<u>8.6</u>	1/2	256-QAM	9.8
4.5	3/4	64-QAM	<u>9.5</u>	1/2	512-QAM	11.6
5.3	3/4	128-QAM	<u>11.6</u>	2/3	256-QAM	12.1
6.0	3/4	256-QAM	<u>13.3</u>	2/3	512-QAM	14.2

Observe from Table 5.3 that for each coded modulation scheme with the same spectral efficiency, the schemes with lower order modulation outperform the schemes with higher order, except for the spectral efficiency of 2 bits/s/Hz, i.e., 8-QAM with code rate 2/3 versus 16-QAM with code rate 1/2. This is because cross 8-QAM is not an efficient constellation.

For instance, the spectral efficiency of coded 8-QAM with a rate of 1/2 can be achieved by employing the combination of QPSK and rate 3/4. Note that coded QPSK has a lower complexity of implementation. The performance comparison is demonstrated in Fig. 5.5. It shows that coded QPSK with rate 3/4 scheme has a gain of approximately 1 dB at a BER of 10^{-4} over coded 8-QAM with rate 1/2.

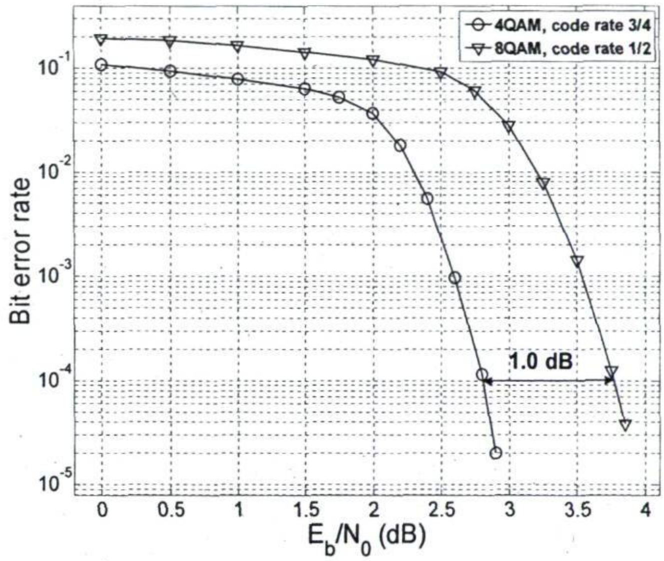

Figure 5.5: BER performance comparison of two LDPC-coded QAM schemes with the same spectral efficiency of 1.5 bits/s/Hz over an AWGN channel.

5.1.1.3 The Shannon limit gap

The performances of LDPC-coded modulation can be illustrated from the angle of spectral efficiency versus power efficiency (SNR per bit, E_b/N_0). After the selection of the best coded scheme among the code-modulation pairs with the same spectral efficiency, our coded *M*-QAM system offers a total of 23 spectral efficiencies, from 1.0 to 7.5 bits/s/Hz, in which there are 13 coded square QAM and 10 coded cross QAM schemes. We investigate the gaps between these coded QAM schemes and the Shannon limit [1] at a BER of 10^{-4}.

This is shown in Fig. 5.6 and their corresponding coded modulation schemes are highlighted by underlines given in Table 5.4. For reference, the spectral efficiency for various uncoded QAM (from BPSK, $\eta = 1$, to 128-QAM, $\eta = 7$) are also given. The derivation of the Shannon limit is shown in Appendix B.

In Fig. 5.6, we see that the gap between the Shannon capacity limit and required E_b/N_0 of coded square QAM schemes is nearly independent and becomes slightly larger with increased spectral efficiency. For the coded schemes with cross QAM constellations, the gaps is slightly larger than that of coded square QAM, especially for coded 128-QAM with coding rate 1/2 and a spectral efficiency of 3.5 bits/s/Hz. Thus, the coded cross QAM schemes are less efficient than the square QAM schemes in this LDPC-coded *M*-QAM system.

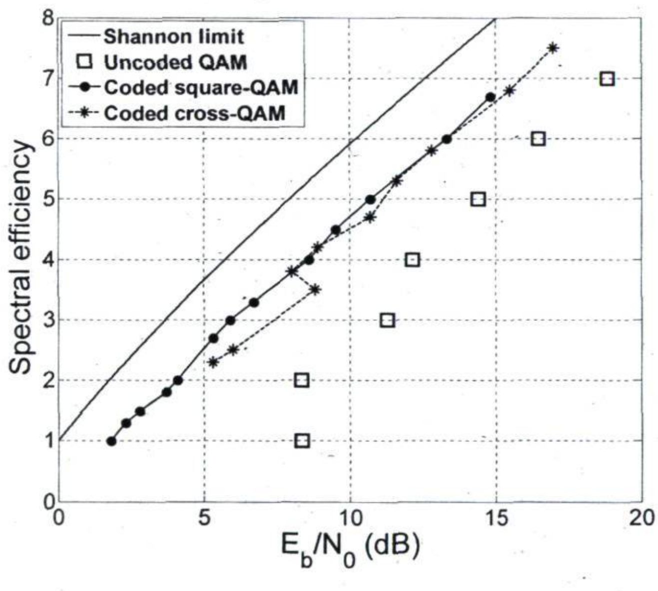

Figure 5.6: The Shannon limit gap of LDPC-coded QAM for various spectral efficiencies at a BER of 10^{-4}.

Table 5.4: All LDPC-coded and uncoded modulation schemes for each achievable spectral efficiency (from 1.0 to 7.5 bits/s/Hz), where the coded schemes selected in Fig. 5.6 are highlighted by underlines.

Uncoded schemes	Coded schemes		Spectral efficiency (bits/s/Hz)
	Coded square-QAM	Coded cross-QAM	
BPSK	QPSK, 1/2	-	1.0
-	QPSK, 2/3	-	1.3
-	QPSK, 3/4	8-QAM, 1/2	1.5
-	QPSK, 5/6	-	1.7
QPSK	16-QAM, 1/2	8-QAM, 2/3	2.0
-	-	8-QAM, 3/4	2.3
-	-	8-QAM, 5/6 32-QAM, 1/2	2.5
-	16-QAM, 2/3	-	2.7
8-QAM	16-QAM, 3/4 64-QAM, 1/2	-	3.0
-	16-QAM, 5/6	32-QAM, 2/3	3.3
-	-	128-QAM, 1/2	3.5
-	-	32-QAM, 3/4	3.8
16-QAM	64-QAM, 2/3 256-QAM, 1/2	-	4.0
-	-	32-QAM, 5/6	4.2
-	64-QAM, 3/4	512-QAM, 1/2	4.5
-	-	128-QAM, 2/3	4.7
32-QAM	64-QAM, 5/6	-	5.0
-	256-QAM, 2/3	128-QAM, 3/4	5.3
-	-	128-QAM, 5/6	5.8
64-QAM	256-QAM, 3/4	512-QAM, 2/3	6.0
-	256-QAM, 5/6	-	6.7
-	-	512-QAM, 3/4	6.8
128-QAM	-	-	7.0
-	-	512-QAM, 5/6	7.5

5.1.2 Performance over flat uncorrelated Rayleigh fading channels

Based on the analysis above, square QAM constellations are more efficient at achieving a good performance for LDPC-coded modulation. Several wireless communication systems, such as 3G and 4G mobile communication systems, wireless networks (WiMAX, WiFi, HiperLAN/2), DVB-T (Digital video broadcasting-Terrestrial) have adopted three square QAM schemes, namely QPSK, 16-QAM and 64-QAM. Hence, we employ these three square QAM schemes to evaluate the performance of LDPC-coded modulation for transmission over a flat uncorrelated Rayleigh fading channel. Also, these three QAMs with appropriate coding rates will also be used for the adaptive coded modulation system that we will present later. By combining these QAM schemes with appropriate coding rates, various spectral efficiencies from 1 to 5 bits/s/Hz are achieved as shown in Table 5.5. The simulation results for each QAM scheme with various coding rates are shown in Fig. 5.7.

Table 5.5: Various spectral efficiencies of LDPC-coded modulation used in the uncorrelated Rayleigh fading channel.

Modulation	Spectral efficiency (bits/s/Hz)			
	Code rate 1/2	Code rate 2/3	Code rate 3/4	Code rate 5/6
QPSK	1.0	1.3	1.5	1.7
16-QAM	2.0	2.7	<u>3.0</u>	3.3
64-QAM	<u>3.0</u>	4.0	4.5	5.0

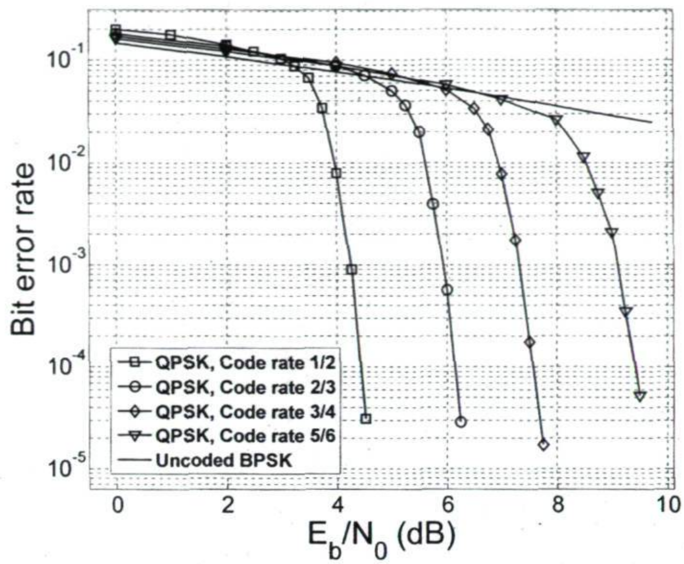
QPSK, Code rate 1/2
QPSK, Code rate 2/3
QPSK, Code rate 3/4
QPSK, Code rate 5/6
Uncoded BPSK
Bit error rate
E_b/N_0 (dB)

(a)

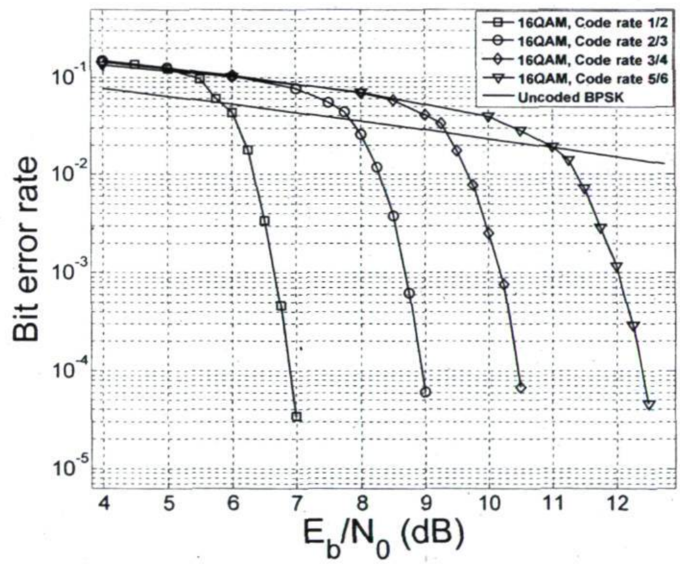
16QAM, Code rate 1/2
16QAM, Code rate 2/3
16QAM, Code rate 3/4
16QAM, Code rate 5/6
Uncoded BPSK
Bit error rate
E_b/N_0 (dB)

(b)

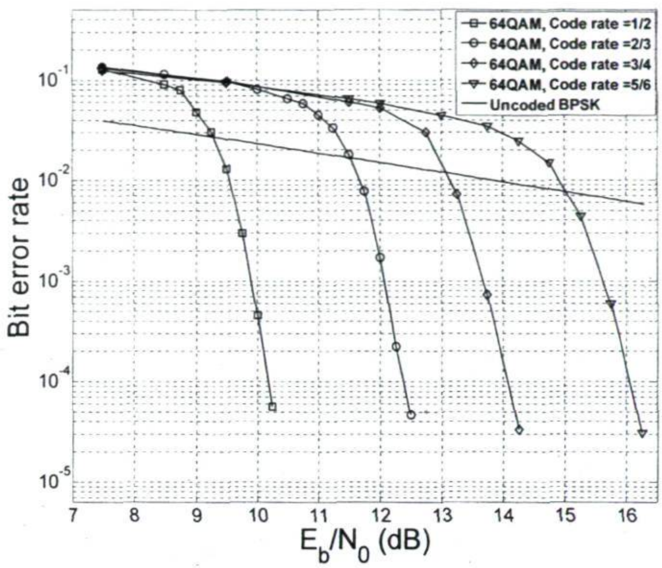

(c)

Figure 5.7: BER performances of LDPC-coded QPSK, 16-QAM and 64-QAM with various coding rates for transmission over an uncorrelated Rayleigh fading channel.

Compared to the performances of coded QAM over an AWGN channel, the LDPC-coded QAM schemes on the uncorrelated Rayleigh fading channel have much larger coding gains with respect to uncoded BPSK. For example, as shown in Fig. 5.7 (c), even coded 64-QAM, which has the maximum achievable spectral efficiency of 5 bits/s/Hz, is much better than uncoded BPSK with the minimum uncoded spectral efficiency of 1 bit/s/Hz. This is because over fading channels, code performance depends more on the minimum Hamming distance between coded symbol sequences than on the minimum Euclidean distance [57]. LDPC codes have excellent Hamming distance properties. Therefore, LDPC-coded modulation can achieve excellent performance while having a high spectral efficiency over uncorrelated Rayleigh fading channels.

The spectral efficiency versus the required E_b/N_0 at a BER of 10^{-4} for each coded QAM modulation is shown in Fig. 5.8. Uncoded QPSK and 16-QAM have spectral efficiencies of 2 and 4 bits/s/Hz, which is smaller than that of 64-QAM. Thus, for coded QPSK (squares) and 16-QAM (stars), the spectral efficiency increases slowly with increasing SNR. We notice that for a spectral efficiency of 3 bits/s/Hz, there is a pair of coded modulation schemes that have the same spectral efficiency, namely 16-QAM with rate 3/4 and 64-QAM with rate 1/2. At a BER of 10^{-4}, the latter has a small SNR gain of 0.2 dB over the former. However, since lower order modulations have lower complexity, the coded 16-QAM scheme with coding rate 3/4 is more practical.

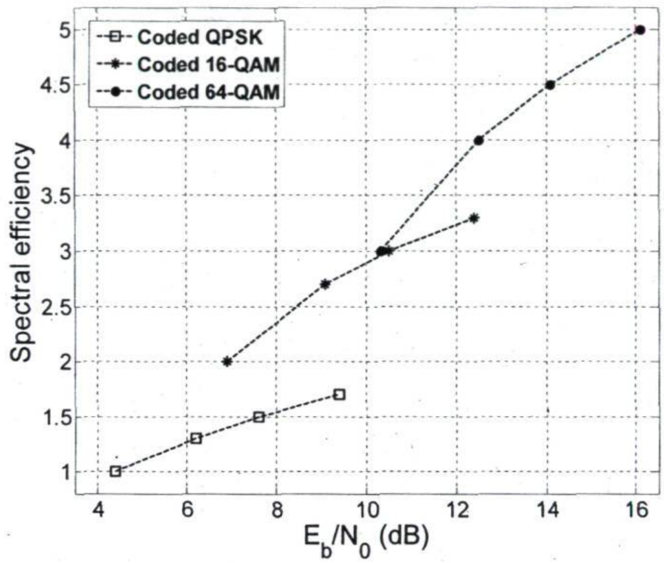

Figure 5.8: Spectral efficiency versus the required E_b/N_0 at BER = 10^{-4} for each coded QAM modulation, corresponding to Fig. 5.7.

5.1.3 Decoding complexity

To evaluate the decoding complexity and delay of our coded modulation system, we simulated the BER performance and average number of decoding iterations versus E_b/N_0 for coded QPSK and 16-QAM with a fixed coding rate of 2/3, transmitted over both AWGN and uncorrelated Rayleigh fading channels. As mentioned before, the decoding is performed using the Log-BP algorithm and the maximum number of iterations is set to 30. Fig. 5.9 shows the results.

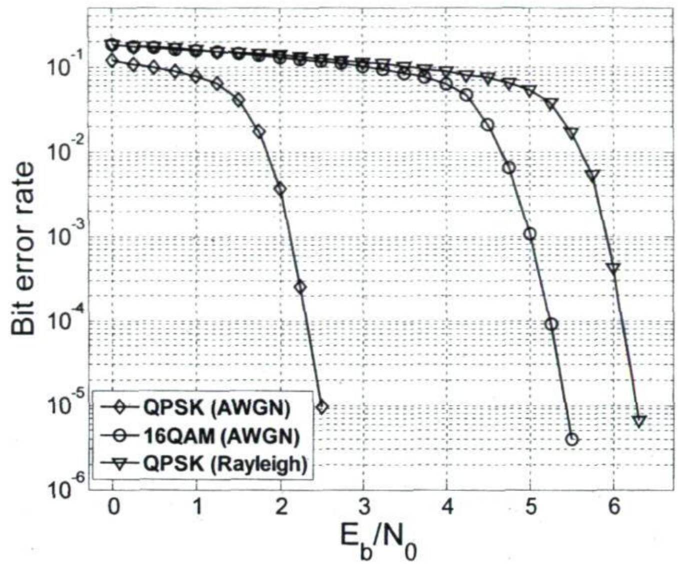

(a)

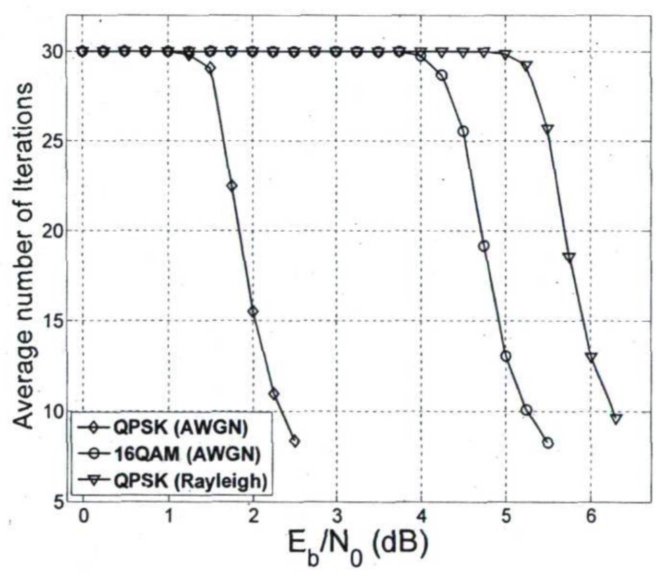

(b)

Figure 5.9: (a) BER performance of LDPC-coded QPSK and 16-QAM with a fixed coding rate of 2/3, transmitted over AWGN and uncorrelated Rayleigh fading channels. (b) The corresponding average number of decoding iterations for these three schemes.

The average numbers of decoding iterations corresponding to Fig. 5.9 are given in Table 5.6. For each coded scheme, the number of iterations is 30 for low SNRs and much smaller than 30 at high SNRs. For example, at BER = 10^{-5}, the required E_b/N_0 for each scheme is approximately 2.5, 5.5 and 6.2 dB, respectively. From Table 5.6, we can see that the corresponding average number of decoding iterations is low and between 8 to 9.5 iterations. Obviously, the decoding complexity will be lower with increasing SNR. Therefore, the LDPC-coded modulation scheme has a low decoding complexity not only when transmitting over the AWGN channel, but also over the uncorrelated Rayleigh fading channel. This is a very important benefit for the LDPC-coded modulation system.

Table 5.6: Average number of decoding iterations.

E_b/N_0 (dB)	QPSK (AWGN)	16-QAM (AWGN)	QPSK (Rayleigh CSI)
1.0	30.0	30.0	30.0
2.0	15.6	30.0	30.0
2.5	8.3	30.0	30.0
3.0	-	30.0	30.0
4.0	-	29.6	30.0
5.0	-	13.5	29.8
5.5	-	8.3	25.1
6.2	-	-	9.3

5.2 Performances of adaptive LDPC-coded modulation

Based on the principle of adaptive coded modulation (ACM) as explained in section 4.4, the performance of an ACM scheme in conjunction with LDPC coding for a flat slowly-varying Rayleigh fading channel are evaluated and discussed in this section, including the BER and spectral efficiency performance and the influence of adaptation threshold selection.

5.2.1 Candidate pairs

As mentioned before, WiMAX provides four flexible coding rates, 1/2, 2/3, 3/4 and 5/6, and four modulation schemes, BPSK, QPSK, 16-QAM and 64-QAM (optional in the uplink). We adopt six different combinations of modulation order and coding rates, as shown in Table 5.7. Since the BER performance improves with increasing code length, the longer the code length is, the steeper the BER curve is. Thus, we select LDPC codes with a code length of 576 bits in order to obtain clear SNR threshold differences under different BER levels.

Table 5.7: The spectral efficiencies and thresholds of six candidate pairs for the proposed adaptive LDPC-coded modulation scheme.

Candidate	Modulation	Coding rate	Spectral efficiency	SNR threshold
CM-1	BPSK	1/2	0.5	$0 < \text{SNR} \leq \gamma_1$
CM-2	QPSK	1/2	1.0	$\gamma_1 \leq \text{SNR} \leq \gamma_2$
CM-3	16-QAM	1/2	2.0	$\gamma_2 \leq \text{SNR} \leq \gamma_3$
CM-4	16-QAM	3/4	3.0	$\gamma_3 \leq \text{SNR} \leq \gamma_4$
CM-5	64-QAM	2/3	4.0	$\gamma_4 \leq \text{SNR} \leq \gamma_5$
CM-6	64-QAM	5/6	5.0	$\text{SNR} \geq \gamma_5$

Among the candidate pairs, the rate 1/2 scheme with BPSK is used during the worst channel conditions and the scheme with rate 5/6 and 64-QAM is for the best channel conditions. Since there are six different pairs employed for this ACM system, we define five adaptation thresholds: $\gamma_1, \gamma_2, \gamma_3, \gamma_4$ and γ_5 as in the method presented in [18]. The transmitter looks at the value of the instantaneous SNR, i.e. $\text{SNR}_w = \alpha_w^2(E_s/N_0)$, where w is the index of a transmitted frame, and determines the optimum code-modulation pair. Hence, CM-1 (rate 1/2 BPSK) is employed if $0 < \text{SNR} \leq \gamma_1$, otherwise, CM-2 (rate 1/2 QPSK) is chosen if $\gamma_1 \leq \text{SNR} \leq \gamma_2$, and so on. The spectral efficiency can vary from 0.5 to 5.0 bit/s/Hz during transmission.

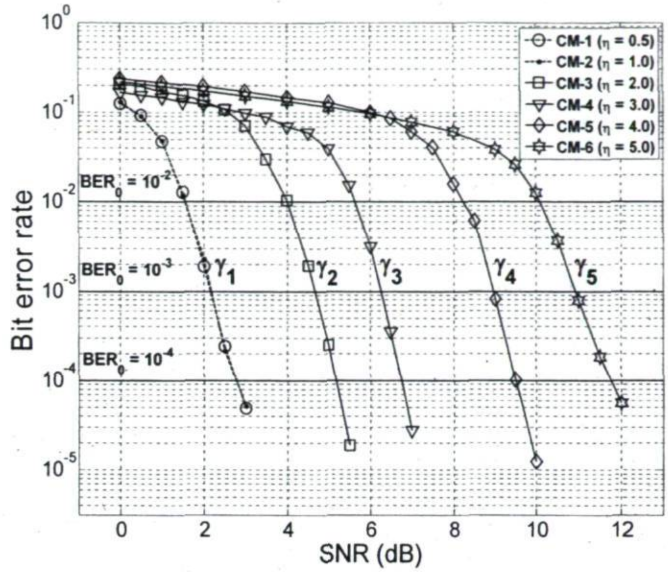

Figure 5.10: BER performance for each candidate pair transmitted over an AWGN channel.

Fig. 5.10 shows the BER performance as a function of the SNR per bit (E_b/N_0) for each candidate pair transmitted over an AWGN channel. The SNR thresholds (see Table 5.8) are found from curve fitting on the simulated BER curve of each candidate pair and by setting $BER_0 = 10^{-2}$, 10^{-3} and 10^{-4} (also called error roof in [18]), respectively.

Table 5.8: The SNR thresholds under different BER levels, obtained from curve fitting in Fig. 5.10.

Thresholds (dB) / BER_0	γ_1	γ_2	γ_3	γ_4	γ_5
$BER_0 = 10^{-2}$	1.5	4.0	5.6	8.3	10.1
$BER_0 = 10^{-3}$	2.2	4.6	6.4	9.0	11.0
$BER_0 = 10^{-4}$	3.0	5.0	7.0	10.0	12.0

5.2.2 BER and spectral efficiency performances

The numerical results for the BER and spectral efficiency performance of the proposed adaptive LDPC-coded modulation scheme are presented and analyzed. All simulations assumed that the signal attenuation due to fading is kept constant during a frame transmission period in order to model a slowly-varying fading channel, corresponding to the case when $n_{hc} = 1$, as explained in section 4.3.2.

The BER performance of the proposed ACM scheme obtained with $BER_0 = 10^{-3}$ is given in Fig. 5.11. For comparison, the performance of three code-modulation pairs used in a non-adaptive scheme, CM-1, CM-4 and CM-6 (indicated in Table 5.6) are also plotted. CM-1 has the best BER performance but the lowest spectral efficiency, 0.5 bit/s/Hz, among the six candidate pairs. Conversely, CM-6 has the highest spectral efficiency, 5 bits/s/Hz, but the worst BER performance.

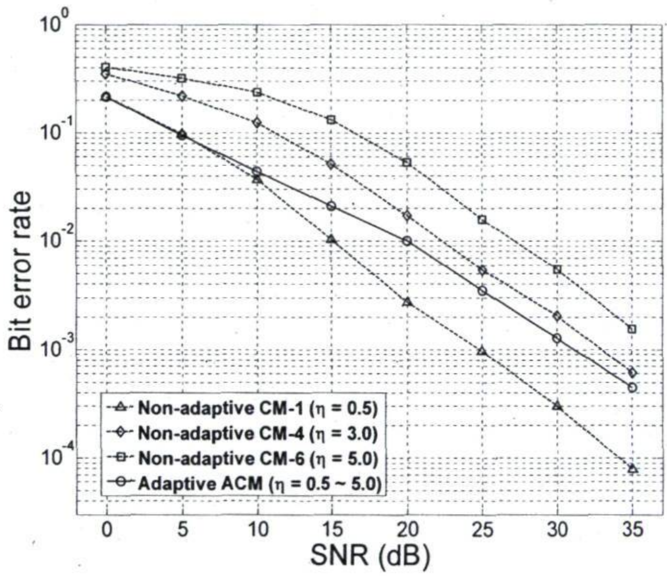

Figure 5.11: BER performances of adaptive LDPC-coded modulation for $BER_0 = 10^{-3}$.

The BER curve of ACM is between that of CM-1 and CM-4. We can observe that ACM can have a coding gain between 5 to 10 dB over CM-6, between 2 to 6 dB over CM-4, respectively, and a loss of about 6 dB for large SNRs compared with CM-1. This is because to improve spectral efficiency, ACM tends to adopt the code-modulation pair with higher spectral efficiency as the SNR is increased. With the SNRs increase, the BER curve of ACM tends to CM-6.

The spectral efficiency of the adaptive system varies as a function of the SNR. We can compute the theoretical average spectral efficiency (ASE) using (4.26) as follows,

$$\begin{aligned}\bar{\eta} &= 0.5 \cdot \mathrm{P}(0 \leq \alpha \leq v_1) + 1 \cdot \mathrm{P}(v_1 \leq \alpha \leq v_2) + 2 \cdot \mathrm{P}(v_2 \leq \alpha \leq v_3) \\ &\quad +3 \cdot \mathrm{P}(v_3 \leq \alpha \leq v_4) + 4 \times \mathrm{P}(v_4 \leq \alpha \leq v_5) + 5 \cdot \mathrm{P}(v_5 \leq \alpha \leq \infty) \\ &= 0.5 + 0.5 \cdot \exp(-{v_1}^2) + \exp(-{v_2}^2) + \exp(-{v_3}^2) + \exp(-{v_4}^2) + \exp(-{v_5}^2) \\ &= 0.5 + 0.5 \cdot \exp\left(-\frac{\gamma_1}{E_s/N_0}\right) + \exp\left(-\frac{\gamma_2}{E_s/N_0}\right) + \exp\left(-\frac{\gamma_3}{E_s/N_0}\right) + \exp\left(-\frac{\gamma_4}{E_s/N_0}\right) \\ &\quad + \exp\left(-\frac{\gamma_5}{E_s/N_0}\right) \end{aligned} \tag{5.1}$$

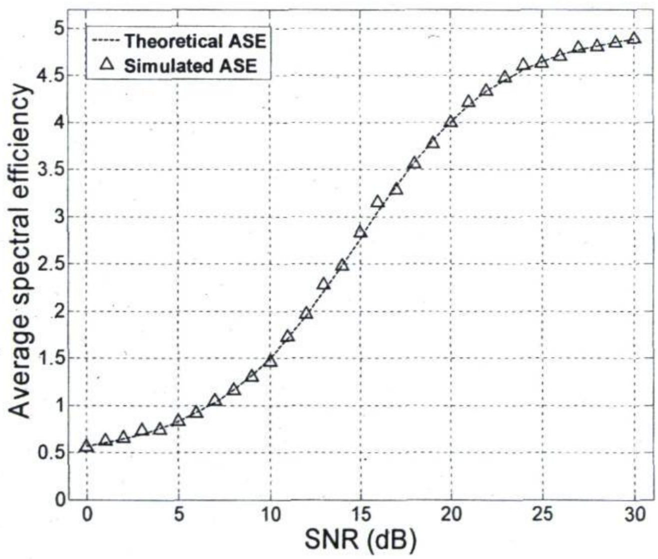

Figure 5.12: Theoretical and simulated spectral efficiency of the proposed ACM system for $\mathrm{BER}_0 = 10^{-3}$.

Fig. 5.12 presents the theoretical and simulated average spectral efficiencies. We can see that both curves are quite close. It shows an increase of the average spectral efficiency for this ACM scheme as the SNR is increased. As seen in Fig. 5.11, at BER = 10^{-3}, the required SNR for ACM is 31 dB, and the corresponding spectral efficiency is approximately 4.8 bits/s/Hz (shown in Fig. 5.12). For that same BER, the SNRs of CM-1, CM-4 and CM-6 are about 25, 35, 40 dB, respectively, with fixed spectral efficiencies of 0.5, 3 and 5 bits/s/Hz. Thus, the ACM scheme can outperform CM-4 and CM-6 while having almost the maximum spectral efficiency for large SNRs. Although it requires about 6 dB more in SNR, ACM has almost ten times the spectral efficiency of CM-1.

As shown in Fig. 5.12, when ACM attains the spectral efficiency of 3 bits/s/Hz, its SNR is approximately 16 dB. The corresponding BER is about 10^{-2} as found in Fig. 5.11. At the same BER of 10^{-2}, CM-4 has an SNR of 20 dB. Thus, ACM has a gain of 4 dB compared to CM-4 while attaining the same spectral efficiency of 3 bits/s/Hz. The SNRs (E_s/N_0) needed for a given spectral efficiency for both adaptive and non-adaptive schemes at the same BER are given in Table 5.9. The required SNRs for the non-adaptive schemes are obtained from the simulation results for the code-modulation pairs, CM-3, CM-4 and CM-5. We see that the adaptive scheme outperforms all the non-adaptive schemes for a given spectral efficiency at the same BER.

Table 5.9: Comparison of the adaptive and non-adaptive schemes for the same spectral efficiency.

Spectral efficiency (bits/s/Hz)	SNR (dB)		BER level
	Adaptive	Non-adaptive	
2 (CM-3)	12.2	15.4	5.1×10^{-2}
3 (CM-4)	15.5	20.7	2.3×10^{-2}
4 (CM-5)	20.0	24.6	1.1×10^{-2}

5.2.3 Influence of the adaptation threshold

To see the influence on the BER performance of different adaptation thresholds, the BER curves with the thresholds defined for $BER_0 = 10^{-2}$, 10^{-3} and 10^{-4} are given in Fig. 5.13. From Fig. 5.10, we know that as BER_0 is lowered, the SNR thresholds for all schemes move to the right (higher SNRs). Thus, as shown in Fig. 5.13, the BER performance is improved by decreasing BER_0, since the corresponding lower efficiency code-modulation pair is used more often. The SNR gap between schemes under different BER_0 is approximately 2.5 dB.

The influence of different error roofs and adaptation thresholds on the spectral efficiency performance is demonstrated in Fig. 5.14. As expected, the spectral efficiency of the schemes using a higher error roof ($BER_0 = 10^{-2}$) have a gain of approximately 0.5 to 1 bits/s/Hz for the same SNR, compared to those with $BER_0 = 10^{-4}$. We see that at high SNRs (after 30 dB), the spectral efficiencies for the same SNR tend to converge, while the BER performances are still different (see Fig. 5.13). This is because after a certain SNR (in this case 30 dB), the spectral efficiency reaches the maximum achievable value. Thus, if the adaptive system is to operate at high SNRs, it is recommended to use a relatively lower error roof. Therefore, schemes with better BER performances are employed while having a good spectral efficiency at large SNRs.

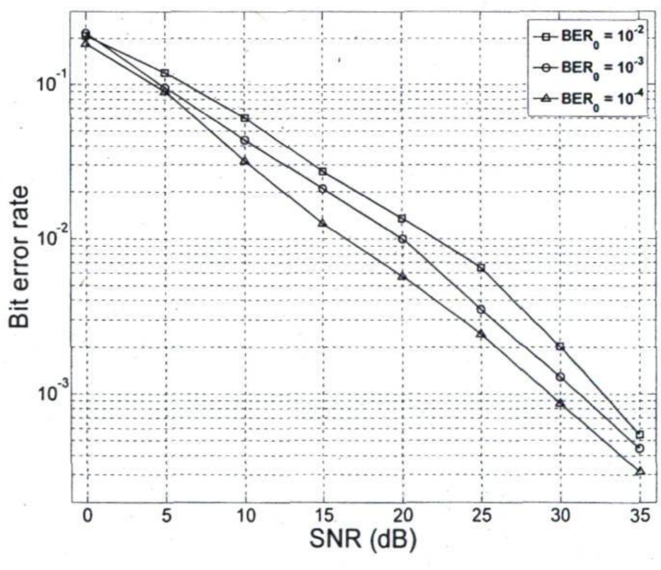

Figure 5.13: The effect of the adaptation threshold on the BER performances of ACM.

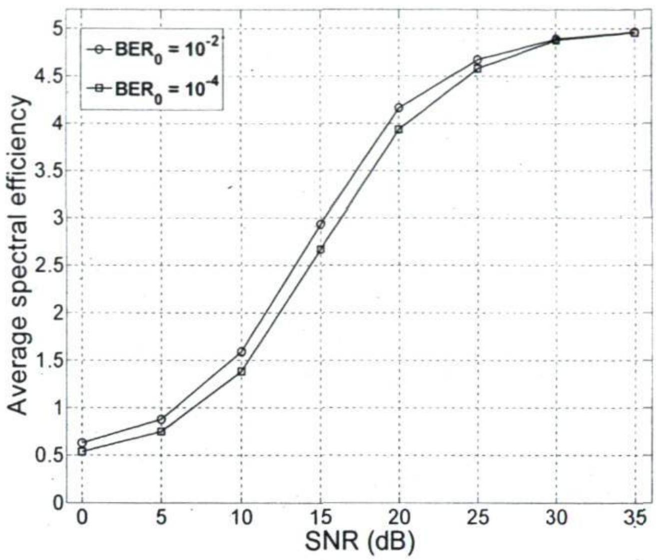

Figure 5.14: The influence of the error roof on the BER performance of the proposed adaptive coded modulation system.

The selection of the optimum adaptation thresholds for an adaptive system depends on the practical situation. Because of the tradeoff between BER and spectral efficiency performances, it is difficult to say which one is the best among schemes using different error roofs BER_0. However, we can consider choosing one scheme that is more suitable for the requirement of the practical application. A possible way of improving BER performance which would not reduce the average spectral efficiency might be to add an interleaver. But as shown in [49], the BER performance of LDPC-coded modulation in a correlated Rayleigh fading channel improves only slightly using an interleaver.

Chapter 6

Conclusions and suggestions for future works

In this thesis, we studied the principles of LDPC codes and designed a power and bandwidth-efficient coded modulation system based on WiMAX LDPC codes for wireless communications. The conclusions and suggestions for future studies are discussed in this chapter.

6.1 Thesis conclusions

6.1.1 LDPC codes with low complexity and fast encoding

The most difficult part in the implementation of LDPC codes is code construction and encoding. We studied a class of irregular LDPC codes with small to moderate lengths which are defined in the WiMAX standard. These codes have fast encoding and lower construction complexity, owing to the structure of their parity-check matrices. These codes are constructed by a parity-check matrix in an approximate triangular dual-diagonal form and encoded using the Richardson-Urbanke encoding algorithm.

6.1.2 LDPC-coded modulation

A coded modulation scheme using the WiMAX LDPC codes was presented for wireless communication systems. This approach is pragmatic but quite effective for bandwidth efficient transmission, because only one encoder and one decoder are employed and it does not require an interleaver. This is an advantage over other coded modulation schemes such as Turbo coded modulation for reducing the associated complexity.

It is difficult to analytically evaluate LDPC-coded modulation schemes, so we investigated and discussed their performances via computer simulations. The results show that the performance of LDPC-coded M-QAM scheme with Gray mapping on the AWGN channel is close to the Shannon limit, when using the LDPC codes with a length of 2304 bits and a maximum of 30 decoding iterations. Furthermore, this coded system can also achieve excellent performance over the flat uncorrelated Rayleigh fading channel. The performance can also be improved using a larger maximum number of decoding iterations and longer LDPC codes.

6.1.3 Adaptive LDPC-coded modulation

Another bandwidth efficient scheme was developed based on LDPC-coded modulation for flat slowly-varying Rayleigh fading channels. In this scheme, six combinations of encoding and modulation pairs are employed for frame by frame adaptation with various spectral efficiencies, varying between 0.5 and 5.0 bits/s/Hz, and resulting in several dB of gains in BER performance when compared to non-adaptive coded modulation schemes. The simulation results confirm that adaptive LDPC-coded modulation has the benefit of offering better spectral efficiency under a slowly-varying fading environment while maintaining acceptable BER performance. The adaptation thresholds are determined using the method presented in [18]. The use of adaptive coded modulation in wireless communications improves spectral efficiency, yielding higher throughputs. Therefore, it is suited for next generation wireless systems, such as WiMAX and 4G, for transmission in a relatively slowly-varying fading environment.

6.2 Future works

Based on the studies in this thesis, several future researches are suggested as follows:

- Consider combining LDPC codes of sufficient length with much higher-order QAMs to achieve near-capacity performances. Possible candidates are the standardized LPDC codes in DVB-S2, whose lengths are 16800 bits and 64800 bits.
- We have only investigated the performance of our proposed coded modulation scheme over flat Rayleigh fading channels. We could employ this scheme in a variety of channels such as correlated Rayleigh and Rician fading channels.
- The LDPC-coded modulation system we designed in this thesis can be combined with MIMO-OFDM to enable higher throughput communications.
- Adaptive LDPC-coded modulation techniques can be applied to MIMO systems in a slowly-varying fading environment.

Appendix A

Parity-check matrices of WiMAX LDPC codes

A base model matrix of the WiMAX LDPC codes is defined in the IEEE 802.16e standard [14] for the largest code length ($n = 2304$) of each code rate. The set of shifts $\{p(i,j)\}$ in the base model matrix are used to determine the shift sizes for all other code lengths of the same code rate. Each base model matrix has $n_b = 24$ columns, and the expansion factor z_f is equal to $n/24$ for code length n. Here f is the index of the code lengths for a given code rate, $f = 0, 1, 2, \ldots 18$. For code length $n = 2304$, the expansion factor is set to $z_0 = 96$.

For code rates 1/2, 3/4 A and B, 2/3 B and 5/6, the shift sizes $\{p(f,i,j)\}$ for a code size corresponding to expansion factor z_f are derived from $\{p(i,j)\}$ by scaling $p(i,j)$ proportionally,

$$p(f,i,j) = \begin{cases} p(i,j), & p(i,j) \le 0 \\ \left\lfloor \frac{p(i,j)\, z_f}{z_0} \right\rfloor, & p(i,j) > 0 \end{cases} \tag{A.1}$$

where $\lfloor x \rfloor$ denotes the flooring function that gives the nearest integer towards $-\infty$.

For code rate 2/3 A, the shift sizes $\{p(f,i,j)\}$ for a code size corresponding to expansion factor z_f are derived from $\{p(i,j)\}$ by using a modulo function, i.e.

$$p(f,i,j) = \begin{cases} p(i,j), & p(i,j) \le 0 \\ \mathrm{mod}\big(p(i,j),\ z_f\big), & p(i,j) > 0 \end{cases} \tag{A.2}$$

Code rate 1/2

$$\begin{bmatrix}
 & 94 & 73 & & & & & & 55 & 83 & & & 7 & 0 & & & & & & & & & & \\
 & 27 & & & & 22 & 79 & 9 & & & & 12 & & 0 & 0 & & & & & & & & & \\
 & & & 24 & 22 & 81 & & 33 & & & & 0 & & & 0 & 0 & & & & & & & & \\
61 & & 47 & & & & & & 65 & 25 & & & & & & 0 & 0 & & & & & & & \\
 & & 39 & & & & 84 & & & 41 & 72 & & & & & & 0 & 0 & & & & & & \\
 & & & & 46 & 40 & & 82 & & & & 79 & & & & & & 0 & 0 & & & & & \\
 & & 95 & 53 & & & & & & 14 & 18 & & & & & & & & 0 & 0 & & & & \\
 & 11 & 73 & & & & 2 & & & 47 & & & & & & & & & & 0 & 0 & & & \\
12 & & & & 83 & 24 & & 43 & & & & 51 & & & & & & & & & 0 & 0 & & \\
 & & & & & 94 & & 59 & & & 70 & 72 & & & & & & & & & & 0 & 0 & \\
 & & 7 & 65 & & & & & 39 & 49 & & & & & & & & & & & & & 0 & 0 \\
43 & & & & & 65 & & 41 & & & & 26 & & & & & & & & & & & & 0
\end{bmatrix}$$

Code rate 2/3 A

$$\begin{bmatrix}
3 & 0 & & & 2 & 0 & & 3 & 7 & & & & & & & & 1 & 0 & & & & & & \\
 & & 1 & & 36 & & & 34 & 10 & & & 18 & 2 & & 3 & 0 & & 0 & 0 & & & & & \\
 & & 12 & 2 & & 15 & & 40 & & 3 & & 15 & & 2 & 13 & & & & 0 & 0 & & & & \\
 & & 19 & 24 & & 3 & 0 & & 6 & & 17 & & & & 8 & 39 & & & & 0 & 0 & & & \\
20 & & 6 & & & 10 & 29 & & & 28 & & 14 & & 38 & & & 0 & & & & 0 & 0 & & \\
 & & 10 & & 28 & 20 & & & 8 & & 36 & & & & 21 & 45 & & & & & & 0 & 0 & \\
35 & 25 & & 37 & & 21 & & & 5 & & & 0 & 9 & 4 & 20 & & & & & & & & 0 & 0 \\
 & 6 & 6 & & & & 4 & & 14 & 30 & & 3 & 36 & & 14 & & & & & & & & & 0
\end{bmatrix}$$

Code rate 2/3 B

$$\begin{bmatrix}
2 & & 19 & & 47 & & 48 & & 36 & & 82 & & 47 & & 15 & & 95 & 0 & & & & & & \\
& 69 & & 88 & & 33 & & 3 & & 16 & & 37 & & 40 & & 48 & & 0 & 0 & & & & & \\
10 & & 86 & & 62 & & 28 & & 85 & & 16 & & 34 & & 73 & & & & 0 & 0 & & & & \\
& 28 & & 32 & & 81 & & 27 & & 88 & & 5 & & 56 & & 37 & & & & 0 & 0 & & & \\
23 & & 29 & & 15 & & 30 & & 66 & & 24 & & 50 & & 62 & & & & & & 0 & 0 & & \\
& 30 & & 65 & & 54 & & 14 & & 0 & & 30 & & 74 & & 0 & & & & & & 0 & 0 & \\
32 & & 0 & & 15 & & 56 & & 85 & & 5 & & 6 & & 52 & & 0 & & & & & & 0 & 0 \\
& 0 & & 47 & & 13 & & 61 & & 84 & & 55 & & 78 & & 41 & 95 & & & & & & & 0
\end{bmatrix}$$

Code rate 3/4 A

$$\begin{bmatrix}
6 & 38 & 3 & 93 & & & & 30 & 70 & & 86 & & 37 & 38 & 4 & 11 & & 46 & 48 & 0 & & & & \\
62 & 94 & 19 & 84 & & 92 & 78 & & 15 & & & 92 & & 45 & 24 & 32 & 30 & & & 0 & 0 & & & \\
71 & & 55 & & 12 & 66 & 45 & 79 & & 78 & & & 10 & & 22 & 55 & 70 & 82 & & & 0 & 0 & & \\
38 & 61 & & 66 & 9 & 73 & 47 & 64 & & 39 & 61 & 43 & & & & & 95 & 32 & 0 & & & 0 & 0 & \\
& & & & 32 & 52 & 55 & 80 & 95 & 22 & 6 & 51 & 24 & 90 & 44 & 20 & & & & & & & 0 & 0 \\
& 63 & 31 & 88 & 20 & & & & 6 & 40 & 56 & 16 & 71 & 53 & & & 27 & 26 & 48 & & & & & 0
\end{bmatrix}$$

Code rate 3/4 B

$$\begin{bmatrix}
& 81 & & 28 & & & 14 & 25 & 17 & & & 85 & 29 & 52 & 78 & 95 & 22 & 92 & 0 & 0 & & & & \\
42 & & 14 & 68 & 32 & & & & & 70 & 43 & 11 & 36 & 40 & 33 & 57 & 38 & 24 & & 0 & 0 & & & \\
& & 20 & & & 63 & 39 & & 70 & 67 & & 38 & 4 & 72 & 47 & 29 & 60 & 5 & 80 & & 0 & 0 & & \\
64 & 2 & & & 63 & & & 3 & 51 & & 81 & 15 & 94 & 9 & 85 & 36 & 14 & 19 & & & & 0 & 0 & \\
& 53 & 60 & 80 & & 26 & 75 & & & & & 86 & 77 & 1 & 3 & 72 & 60 & 25 & & & & & 0 & 0 \\
77 & & & & 15 & 28 & & 35 & & 72 & 30 & 68 & 85 & 84 & 26 & 64 & 11 & 89 & 0 & & & & & 0
\end{bmatrix}$$

Code rate 5/6

$$
\begin{bmatrix}
 & 25 & 55 & & 47 & 4 & & 91 & 84 & 8 & 86 & 52 & 82 & 33 & 5 & 0 & 36 & 20 & 4 & 77 & 80 & 0 & & \\
 & 6 & & 36 & 40 & 47 & 12 & 79 & 47 & & 41 & 21 & 12 & 71 & 14 & 72 & 0 & 44 & 49 & 0 & 0 & 0 & 0 & \\
51 & 81 & 83 & 4 & 67 & & 21 & & 31 & 24 & 91 & 61 & 81 & 9 & 86 & 78 & 60 & 88 & 67 & 15 & & & 0 & 0 \\
50 & & 50 & 15 & & 36 & 13 & 10 & 11 & 20 & 53 & 90 & 29 & 92 & 57 & 30 & 84 & 92 & 11 & 66 & 80 & & & 0
\end{bmatrix}
$$

where unmarked positions are zero matrices, "0" is the identity matrix and a number represents a right cyclic-shift $z_f \times z_f$ identity matrix by this number.

Appendix B

Calculation of Shannon limit on AWGN channels

The Shannon limit is derived as follows. Let the channel capacity C of an AWGN channel (Shannon-Hartley theorem) [1] be stated as

$$C = B \log_2 \left(1 + \frac{S}{N}\right) \tag{B.1}$$

where B denotes the bandwidth, $S = E_b R_b$ (Watt) denotes the average received signal power with E_b the energy per bit, R_b the transmission bit rate and $N = N_0 B$ (Watt) is the average noise power. Thus we have,

$$\frac{S}{N} = \frac{E_b}{N_0} \cdot \frac{R_b}{B} \tag{B.2}$$

Substituting (B.2) into (B.1) and rearranging terms yields,

$$\frac{C}{B} = \log_2 \left(1 + \frac{E_b}{N_0} \cdot \frac{R_b}{B}\right) \tag{B.3}$$

For the case where the transmission bit rate is equal to the channel capacity, $R_b = C$. Hence, we modify (B.3) as follows:

$$\frac{E_b}{N_0} = \left(2^{\frac{C}{B}} - 1\right) \cdot \left(\frac{C}{B}\right)^{-1} \tag{B.4}$$

Therefore, as shown in Fig. 5.4, C/B, i.e. the spectral efficiency (bits/s/Hz) versus E_b/N_0 in accordance with (B.4) is plotted. As $B \to \infty$ or $C/B \to 0$, we get the Shannon capacity limit,

$$\frac{E_b}{N_0} \to \frac{1}{\log_2 e} = 0.693 \approx -1.6 \text{ (dB)} \tag{B.5}$$

Bibliography

[1] C. E. Shannon, "A mathematical theory of communication", *Bell System Technical Journal*, Vol. 27, pp. 379-423, 623-657, Oct. 1948.

[2] R. Hamming, "Error detecting and error correcting codes", *Bell System Technical Journal*, Vol. 29, pp. 147-160, Apr. 1950.

[3] P. Elias, "Coding for noisy channels", *Institute of Radio Engineers Convention Record*, Vol. 4, pp. 37-46, Sep. 1955.

[4] A. Viterbi, "Error bounds for convolutional codes and an asymptotically optimum decoding algorithm", *IEEE Transactions on Information Theory*, Vol. IT-13, no. 2, pp. 260–269, Apr. 1967.

[5] I. Reed and G. Solomon, "Polynomial codes over certain finite fields", *Society for Industrial Applied Mathematics Journal*, Vol. 8, no. 2, pp. 300-304, Jun. 1960.

[6] B. Sklar, *Digital communications: Fundamental and applications*, 2nd edition. Prentice Hall, Jan. 2001.

[7] G. Ungerbock, "Channel coding with multilevel/phase signals", *IEEE Transactions on Communications*, Vol. IT-25, pp. 55-67, Jan. 1982.

[8] C. Berrou, A. Glavieux and P. Thitimajshima, "Near Shannon limit error-correcting coding and decoding: Turbo-codes", *Proceedings of IEEE International Conference on Communications*, Vol. 2, pp. 1064–1070, May 1993.

[9] D. J. C. Mackay and R. M. Neal, "Near Shannon limit performance of low density parity check codes", *IEEE Transactions on Information Theory*, Vol. 32, no. 18, pp. 1645-1646, Aug. 1996.

[10] R. G. Gallager, "Low-density parity-check codes", *IEEE Transactions on Information Theory*, Vol. IT-8, no. 1, pp. 21-28, Jan. 1962.

[11] R. G. Gallager, "Low-density parity-check codes", *Ph.D. dissertation*, Department of Electrical Engineering, M.I.T., Cambridge, Mass., Jul. 1963.

[12] S. Y. Chung, G. D. Forney, T. J. Richardson, and R. L. Urbanke, "On the design of low-density parity check codes within 0.0045 dB of the Shannon limit", *IEEE Communications Letters,* Vol. 5, pp. 58–60, Feb. 2001.

[13] R. McEliece, D. Mackay and J. Cheng, "Turbo decoding as an instance of Pearl's belief propagation algorithm", *IEEE Journal on Selected Areas of Communications*, Vol. 16, no. 2, pp. 140-152, Feb. 1998.

[14] IEEE 802.16e. Air Interface for Fixed and Mobile Broadband Wireless Access System. IEEE P802.16e/D 12 Draft, Oct. 2005.

[15] IEEE 802.11.n. Wireless LAN Medium Access Control and Physical Layer specifications: Enhancements Higher Throughput. IEEE P802.16n/D1.0, Mar. 2006.

[16] European Telecommunications Standards Institute (ETSI). Digital Video Broadcasting (DVB) Second generation framing structure, channel coding and modulation systems for Broadcasting; EN 302 307 V1.1.1. www.dvb.org.

[17] A. H. Khan, M. A. Qadeer, J. A. Ansari, and S. Waheed, "4G as a Next Generation Wireless Network", *Future Computer and Communication, 2009. ICFCC*, pp. 334-338, Apr. 2009.

[18] S. M. Alamouti and S. Kallel, "Adaptive trellis-coded multiple-phase-shift keying for Rayleigh fading channels", *IEEE Transactions on Communications*, Vol. 42, No. 6, pp. 2305-2314, Jun. 1994.

[19] C. M. Jorge and G. F. Patric, *Essentials of error-control coding*, John Wiley and Sons, Ltd, Chichester, UK, 2006.

[20] R. M. Tanner, "A recursive approach to low complexity codes", *IEEE Transactions on Information Theory*, Vol. IT-27, no. 5, pp. 533–547, Sep. 1981.

[21] D. J. C. Mackay, S. T. Wilson and M. C. Davey, "Comparison of construction of irregular Gallager codes", *IEEE Transactions on Communications*, Vol. 47, pp. 1449–1454, Oct. 1999.

[22] M. G. Luby, M. Mitzenmacher, M. A. Shokrollahi, and D. A. Spielman, "Improved low-density parity check codes using irregular graphs," *IEEE Transactions on Information Theory*, Vol. 47, pp. 585–598, Feb. 2001.

[23] T. J. Richardson, M. A. Shokrollahi, and R. L. Urbanke, "Design of capacity-approaching irregular low-density parity-check codes," *IEEE Transactions on Information Theory*, Vol. 47, pp. 619–637, Feb. 2001.

[24] Y. Kou, S. Lin and M. P. C. Fossorier, "Low-density parity-check codes based on finite geometries: a rediscovery and new results", *IEEE Transactions on Information Theory,* Vol. 47, no. 7, pp. 2711–2736, Nov. 1981.

[25] Z. He, S. Roy and P. Fortier, "FPGA Implementation of LDPC Decoders Based on Joint Row-column Decoding Algorithm", *IEEE International Symposium on Circuits and Systems*, pp. 1653–1656, May 2007.

[26] N. Wiberg, "Codes and Decoding on General Graphs", *Ph.D. dissertation*, Linkoping University, Sweden, 1996.

[27] T. J. Richardson and R. L. Urbanke, "Efficient encoding of low-density parity-check codes", *IEEE Transactions on Information Theory*, Vol. 47, no. 2, pp. 638-656, Feb. 2001.

[28] S. Myung, K. Yang and J. Kim, "Quasi-cyclic LDPC codes for fast encoding", *IEEE Transactions on Information Theory*, Vol. 51, no.8, pp. 2894- 2900, Aug. 2004.

[29] W. E. Ryan, "An introduction to LDPC codes", Department of Electrical and Computer engineering, University of Arizona, Aug. 2003.

[30] M. P. C. Fossorier, "Quasi-cyclic low-density parity-check codes from circulant permutation matrices", *IEEE Transactions on Information Theory*, Vol. 50, no. 8, pp. 1788-1794, Aug. 2004.

[31] LDPC Code using MATLAB, http://sites.google.com/site/bsnugroho/ldpc.

[32] J. Zhang, M. P. C. Fossorier, "A modified Weighted Bit-flipping decoding of Low-density parity-check codes", *IEEE Communications Letters,* Vol. 8, pp. 165–167, Mar. 2004.

[33] F. Guo and L. Hanzo, "Reliability ratio based Weighted Bit-flipping decoding for LDPC codes", *IEEE Communications Letters,* Vol. 40, pp. 1356–1358, Oct. 2004.

[34] R. Lucas, M. Fossorier, Y. Kou, and S. Lin, "Iterative decoding of one-step majority logic decodable codes based on belief propagation", *IEEE Communications Letters*, Vol. 48, pp. 931–937, Jun. 2000.

[35] T. Brack, M. Alles, F. Kienle, and N. When, "A synthesizable IP core for WiMAX 802.16e LDPC code decoding", *IEEE 17th International Symposium Personal, Indoor and Mobile Radio Communications (PIMRC)*, pp. 1-5, 2006.

[36] X. Y. Shih, C. Z. Zhan, C. H. Lin, and A. Y. Wu, "A 19-mode 8.29 mm^2 52 mW LDPC decoder chip for IEEE 802.16e system", *2007 Symposium on VLSI Circuits*, Jun. 2007.

[37] T. Brack, M. Alles, T. Lehnigk-Emden, F. Kienle, N. When, N. E. L'Insalata, F. Rossi, M. Rovini, and L. Fanucci, "Low complexity LDPC code decoder for next generation standards", *Design, Automation & Test in Europe Conference & Exhibition, 2007. DATE '07*, pp. 1-6, Apr. 2007.

[38] H. G. Zhang, D. F. Yuan, P. M. Ma, and X. M. Yang, "Performance of LDPC-coded BICM with low complexity decoding", *Personal, Indoor and Mobile Radio Communications, PIMRC 2003. 14th IEEE Proceeding*, Vol. 2, pp. 1570-1582, Sep. 2003.

[39] J. Hou, P. H. Siegel, and L. B. Milstein, "Performance analysis and code optimization of low density parity-check codes on Rayleigh fading channels", *IEEE Journal on Selected Areas in Communications*, no. 15, pp. 924–934, May. 2001.

[40] J. Hou. P. H. Siegel, L. B. Milstein, and H. D. Pfister, "Multilevel coding with low-density parity-check component codes", *IEEE Globecom '01.* (San Antonio, Taxes, Nov. 25-29), 2001.

[41] J. Hou, P. H. Siegel, L. B. Milstein, H. D. Pfister, "Design of low-density parity-check codes for bandwidth efficient modulation", *IEEE Information Theory Workshop*, pp. 24 – 26, 2001.

[42] T. Wadayama, "A coded modulation scheme based on low density parity check codes", *IEICE Transactions on Fundamentals*, Vol. E84-A, no. 10, Oct. 2001.

[43] D. Sridhara, T. E. Fuja, "Bandwidth efficient modulation based on algebraic low density parity check codes", *IEEE International Symposium on Information Theory*, pp.165, 2001.

[44] Y. Yi, J. Hou, M. H. Lee, "Design of semi-algebraic low-density parity-check (SA-LDPC) codes for multilevel coded modulation", *4th International Conference on Parallel and Distributed Computing, Applications and Technologies*, pp. 931-934, 2003.

[45] X. Li, M. R. Soleymani, J. Lodge, P. S. Guinand, "Good LDPC codes over GF(q) for bandwidth efficient transmission", *4th IEEE Workshop on Signal Processing Advances in Wireless Communications*, pp. 95-99, 2003.

[46] J. Wu and H. N. Lee, "Best mapping of LDPC-coded modulation on SISO, MIMO and MAC channels", *IEEE WCNC 2004*, Atlanta, GA, Vol. 4, pp. 2428-2431, Mar. 2004.

[47] Y. Li and W. E. Ryan, "Bit-reliability mapping in LDPC-coded modulation systems", *IEEE Communications Letters*. Vol. 9, no. 1, pp. 1-3. Jan. 2005.

[48] J. Hou, P. H. Siegel, L. B. Milstein, and H. D. Pfister, "Capacity-approaching bandwidth-efficient coded modulation schemes based on low-density parity-check codes", *IEEE Transactions on Information Theory*. Vol. 49, no. 9, pp. 2141-2155. Sep. 2003.

[49] F. Guo, S. X. Ng and L. Hanzo, "LDPC assisted block coded modulation for transmission over Rayleigh fading channels", *Vehicular Technology Conference, VTC 2003-Spring*, Jan. 2003.

[50] D. Hamdani, W. Endemann, R. Kays, "Enhancing performance of high-order Modulation with LDPC codes using feedback mechanism", *Proceeding of International Conference on Electrical Engineering and Informatics*, Institut Teknologi Bandung, Indonesia, Jun. 2007.

[51] K. Cho, D. Yoon, W. Jeong, and M. Kavehrad, "BER analysis of arbitrary rectangular QAM", *IEEE Transactions on Communications*, Vol. 28, pp. 55-67, Jan. 1982.

[52] H. Holm, "Adaptive coded modulation performance and channel estimation tools for flat fading channels", *Ph.D. dissertation*, Department of Telecommunications, Norwegian University of Science and Technology, 2002.

[53] D. Divsalar and M. K. Simon, "Multiple trellis coded modulation (MTCM)," *IEEE Transactions on Communications*, Vol. 36, pp. 410–419, Apr. 1988.

[54] A. R. Calderbank and N. J. A. Sloane, "New trellis codes based on lattices and cosets", *IEEE Transactions on Information Theory*, Vol. 36, pp. 177–195, Mar. 1987.

[55] P. Robertson and T. Worz, "Bandwidth-efficient turbo trellis-coded modulation using punctured component codes," *IEEE Journal on Selected Areas in Communications*, Vol. 16, pp. 206–218, Feb. 1998.

[56] H. Imai and S. Hirakawa, "A new multilevel coding method using error correcting codes", *IEEE Transactions on Communications*, Vol. 23, pp. 371-377, May 1977.

[57] G. Caire, G. Taricco and E. Biglieri, "Bit-interleaved coded modulation", *IEEE Transactions on Communications*, Vol. 44, pp. 927-946, May 1998.

[58] E. Zehavi, "8-PSK trellis coded for Rayleigh channel", *IEEE Transactions on Communications*, Vol. 40, pp. 873-884, May 1992.

[59] A. J. Viterbi, "An intuitive justification and a simplified implementation of the MAP decoder for convolutional codes", *IEEE Journal on Selected Areas in Communications*, Vol. 7, No. 50, pp. 1074-1080, 1998.

[60] F. Tosato and P. Bisaglia, "Simplified soft-output demapper for binary interleaved COFDM with application to HIPERLAN/2", *Proceedings of 2002 IEEE International Conference on Communications*, Vol. 2, pp. 664-668, 2002.

[61] A. J. Goldsmith and S. G. Chua, "Variable-rate variable-power MQAM for fading channels", *IEEE Transactions on Communications*, Vol. 45, pp. 1218-1230, Oct. 1997.

[62] A. Doufexi, S. Armour, M. Butler, A. Nix, D. Bull, J. McGeehan, and P. Karlsson, "A comparison of the HiperLAN/2 and IEEE 802.11 a wireless LAN standards", *IEEE Transactions on Communications*, Vol. 40, pp. 172-180, May 2002.

[63] G. L. Stuber, "*Principle of Mobile Communication*", Kluwer Academic Publishers, 2nd edition, 2001.

[64] G. E. Oien, H. Holm, and K. J. Hole, "Channel prediction for adaptive coded modulation in Rayleigh fading", *Proceeding of European Signal processing Conference (EUSIPCO)*, (Toulouse, France), Sep. 2002.

[65] B. Myhr, V. Markus and G. E. Oien, "LDPC-coded adaptive modulation on slowly varying Nakagami-fading channels", *Proceeding of European Wireless 2002, (Florence, Italy)*, pp. 822-828, Feb. 2002.

[66] A. Roca, "Implementation of a WiMAX simulator in simulink", *Master's thesis*, Department of Electrical Engineering, Institut für Nachrichtentechnik und Hochfrequenztechnik, Feb. 2007.

[67] E. Biglieri, G. Caire, and G. Taricco, "Limiting performance of block fading channels with multiple antennas", *IEEE Transactions on Information Theory*, Vol. 47, pp. 1273-1289, May. 2001.

[68] M. Chiani, "Error probability for block codes over channels with block interference", *IEEE Transactions on Information Theory*, Vol. IT 44, No. 7, Nov. 1998.

[69] Y. Zhang, D. Yuan, and H. Zhang, "Adaptive LDPC for Rayleigh fading channel", *Computers and Communication, 2004. Proceeding ISCC 2004. 9th International Symposium on*, Vol. 2, pp. 651– 656, Jul. 2004.